Development and Prototyping of a Point Coupled Linear Transformer (PCLT) Displacement Sensor

MICHAEL WALTON

Supervisor: J. Tapson

Submitted: May 2005

Submitted to the Faculty of Electrical Engineering, University of Cape Town in fulfillment of the requirements for the Degree Masters of Science in Engineering.

Declaration

The content of this dissertation is my own work unless otherwise referenced. It has not been submitted for any other academic qualification or examination.

signature removed

M. WALTON
26/4/2005

Abstract

The main aims of this project were to develop and prototype a Point Coupled Linear Transformer (PCLT) displacement sensor, and to perform a general exploration of the PCLT technology. The PCLT is a recent invention that has planar PCB windings and a non-contacting movable core, and relies on variable induction to detect displacement.

Different core materials and shapes are investigated. The transformer windings layout is optimized for symmetrical response and high primary to secondary voltage coupling.

Frequency is identified as a critical factor in PCLT performance. Investigation is done into the resonant properties of the PCLT, and series and parallel capacitors are used to control the resonant frequency and alter the shape of the coupling peaks that occur at said resonance. Advantages and disadvantages of operating the PCLT at resonance are identified. The groundwork is laid for further investigation into this aspect of the PCLT.

The magnetic field strength around the sensor is tested, and 3D graphs are presented. Various prototypes of a 1-Dimensional PCLT are developed that utilize different methods of signal conditioning to extract core position from the detected secondary signals. The prototypes' performance is tested and comparisons are made. The prototypes using synchronous demodulation outperform the ones using passive demodulation. A ratio-metric calculation carried out on the detected signals is found to improve sensor linearity.

Results from the best 1D prototype are:

- **Linearity** of 1% FS (64mm stroke) and 0.18% FS (32mm stroke)
- **Output noise** of 2 mV (peak-peak) and **drift** of 0.5mV over 12 hours
- **Resolution** of *at least* 8.3µm or 0.013% FS
- **Repeatability** of 3.2µm or 0.005% FS

Recommendations are made to: increase the stroke-to-length ratio (currently at 68% max), increase the operating frequency (currently at 20 KHz), and use synchronous demodulation in conjunction with a ratiometric calculation, in future versions of the PCLT.

Methods and circuits developed for the 1D PCLT are used to create a 2-Dimensional PCLT. This sensor shows poor results, due to a lack of magnetic flux in the central region of the sensing area. Recommendations are made to redesign the primary coil with a spiral one such that a constant magnetic field is generated over the entire sensing area. Passive demodulation (which is phase insensitive) is found to be better suited to 2D PCLT signal conditioning due to the large phase changes that occur between the secondary signals as the core position changes.

Table of Contents

1 Introduction

1.1. Project description

The aim of this project is to develop and prototype a Point Coupled Linear Transformer (PCLT), which is a type of linear distance transducer, using the "point coupled induction sensor" [1] and PCLT patent application [2] as starting points. Identifying the circuit methodology (demodulation method) best suited to PCLT operation is an important goal in this project. In addition, this project will include a general exploration of the aspects relating to the PCLT technology.

1.2. Background

In 2002 J. Tapson suggested a possible method of object position sensing using point coupled induction, as part of a ball-on-beam balance undergraduate thesis [1]. A ball-on-beam balance is a toy that uses feedback control to balance a ball at a specific position along a beam. The control mechanism needs to know the ball position at all times (feedback). For the above mentioned project, point coupled induction was used to detect ball position. The project was a success, and proved that point coupled induction sensing is a viable option for position sensing, and thus the point coupled induction ball position sensor was born.

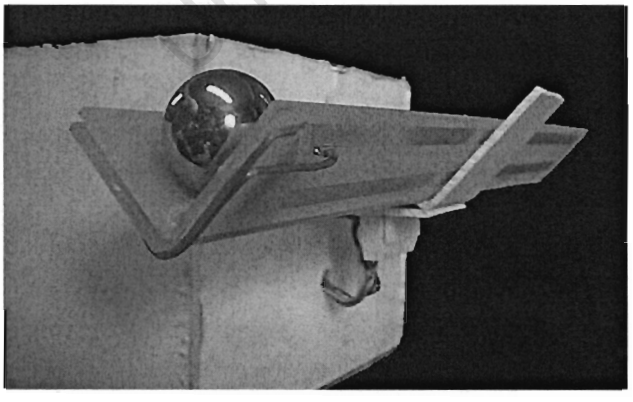

Figure 1 Ball-on-beam balance using point coupled induction to sense the ball position.

This project aims to draw on and develop further the principles used in the point coupled induction sensor, to produce a general purpose linear distance transducer with applications similar to the industry standard Linear Variable Differential Transformer (LVDT).

1.3. Scope and limitations

Signal processing, sensor excitation, windings layout, circuit design and layout, core materials and other factors affecting the performance of the sensor were investigated. Time and cost restraints meant that some areas were investigated more extensively than others.

The performance of the PCLT is heavily dependant on the signal conditioning circuitry which a) excites the primary windings and b) translates the induced secondary waveforms into a DC voltage. This project placed more emphasis on the signal conditioning than on the physical layout and structure. Aspects of signal conditioning include the frequency of operation, the demodulation technique, and the excitation waveform.

1.4. Approach/Methodology

A starting point for this project was the point coupled induction ball position sensor. This was analyzed for weaknesses and limitations. The weak points were then either improved upon or completely reworked. Similarities between the PCLT and the well-established LVDT were identified, and LVDT methods were used to aid in development. A test rig was built to evaluate and test the sensor for sensitivity, repeatability, responsiveness, stability and linearity.

2. Literature Review

The desired outcome of this research project is to develop a working linear displacement sensor; specifically using the point coupled induction method, as first developed and demonstrated in "Ball on Beam Balance Using a Point Coupled Induction Sensor" [1]. This inductive method of measurement has been named the PCLT [2].

2.1. Displacement sensors

A displacement sensor is a device used to measure the position of an object relative to a reference point, in a quantitative manner. An electromechanical measuring system is one which converts a mechanical or physical measurand, in this case distance, into a representative electrical signal. The electronic output of this type of sensor is useful for recording purposes, and is necessary for electronic feedback control. The PCLT is one of many different types of electromechanical position sensors. Others include varying resistance, digital probe and varying differential inductance sensors. The PCLT operates on a principle similar to the industry standard LVDT, a varying inductance transformer, and so the LVDT is analysed in detail.

2.2. Review of the LVDT

The LVDT is an electromagnetic transducer that produces an electrical signal proportional to the displacement of the 'core' relative to the 'body'. The body consists of three transformer coils wound co-axially on a central cylindrical former. The primary winding is placed in the centre, with the two secondary windings placed on either end. The core, usually made from a 50% nickel-iron alloy [3], is slightly longer than the primary winding and is positioned inside the coil former.

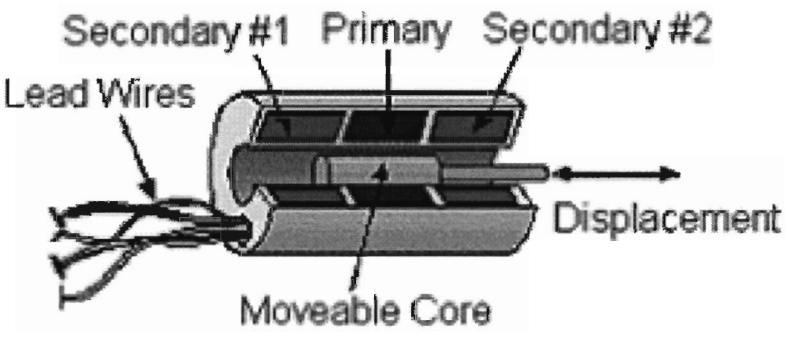

Figure 2 Picture of cut-away LVDT showing windings and core positions.

As in a conventional transformer, magnetic flux is produced by an alternating current applied to the primary winding. This flux is channelled through the core (which has a high magnetic permeability) and is coupled to the secondary windings where a voltage is induced, in accordance with Faraday's Law [4].

The LVDT differs from a conventional transformer in that the core is movable. When the core is centrally placed, flux is equally coupled to both secondary windings, resulting in identical induced secondary voltages. As the core moves off centre, more flux is coupled to the secondary coil that encompasses more of the core, resulting in a larger induced secondary voltage in that coil, and a smaller induced secondary voltage in the other coil encompassing less of the core. Normally, the secondary windings are connected series opposing, such that the induced voltages are 180 degrees out of phase. At the centre (null) position, the voltages are of equal magnitude and opposing phase, resulting in a null output. As the core moves off centre, one of the secondary voltages becomes dominant, and the LVDT output reflects a voltage proportional to the core's displacement from the null position [5]. The phase of the output changes by 180 degrees as the core moves from one side of the null position to the other [6].

Signal conditioning (consisting mainly of demodulation, filtering and scaling) applied to the LVDT output will reveal the displacement amount and direction as a DC voltage. A DC-LVDT is a device which generates the primary excitation and carries out secondary signal conditioning on-board, such that the device is DC powered and gives a DC position output [6]. The advantage of the DC-LVDT over conventional LVDTs is that the end user can avoid issues like signal conditioning and calibration [7].

The fact that the LVDT is a transformer with a non-contacting moving core makes the sensor capable of features that most other displacement sensors cannot offer, including [6]:

1) Frictionless measurement, critical, for example, in creep or tensile testing of elastic materials.

2) Infinite mechanical lifespan, as there is no wear on moving parts, an important feature in high-reliability mechanisms like aircraft.

3) Coil-core separation, allowing pressurised or corrosive fluids to be separated from the body by a non-magnetic barrier between the coil and core, for example in hydraulic systems.

4) Infinite resolution. The inductive principle is continuous and combined with frictionless operation allows for infinite resolution, only limited by the capabilities of the external interface electronics.

The PCLT is also a transformer with a non-contacting moving core, suggesting that it will share these same features with LVDTs.

2.3. Other sensors based on the LVDT

A range of different LVDT based variable inductance sensors have been developed. An LVDT with rectangular coils and secondary windings placed obliquely to the primary winding offers a stroke to length ratio of 90% with 0.5% FS accuracy [8]. A Flat Inductive Sensor (FIS) exists which has square coils and no core [9], where changes in induced voltages come from the primary winding being moved relative to the secondary windings [10]. This sensor achieved 0.4% FS non-linearity over a very short range of 10mm, which is a stroke-to-length ratio of 10%, and a repeatability of 5 μm standard deviation.

Schaevitz engineering produced a planar version of an LVDT with windings laid on Printed Circuit Board (PCB) named the LVIT [11]. It is DC operated and offers 1% FS linearity.

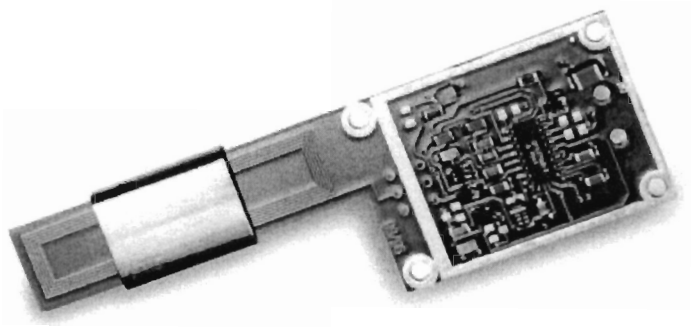

Figure 3 LVIT produced by Schaevitz Engineering, windings are printed onto PCB [11].

A Non Contact Angular Position Sensor (NCAPS) extended to become a linear displacement sensor, utilises an interesting technique for varying the inductance between primary and secondary windings [12]. An attenuating coupler mask is inserted between the primary and secondary coils, such that as the mask is moved, the amount of flux that is coupled varies.

2.4 The first PCLT sensor

The first implementation of the PCLT was in a ball-on-beam apparatus where it was used to sense the relative position of the ball on the beam [1]. One of the starting points for this project was to identify the strengths and weaknesses of the ball position sensor. The details and findings of that investigation appear in Chapter 3.

2.5 Similarities between the PCLT and the LVDT

The PCLT and the LVDT utilise the same principles of operation to detect displacement. The position of a moveable "core" relative to the body of the sensor influences the inductive process that occurs between the primary and secondary windings of an AC transformer arrangement. The changing induced voltages in the transformer windings are converted to a position-representative electrical signal through manipulation and conditioning of the detected signals. The "Handbook of measurement and control" [6], generally accepted to be the standard reference on LVDTs, gives details on the theory and application of the LVDT, and is used

extensively for investigating the finer points of LVDT operation that are relevant to optimizing the PCLT sensor. These details are included in the chapters where the findings are relevant.

2.6. What distinguishes the PCLT from the LVDT

The main difference between the LVDT and the PCLT is in the core and windings arrangement. An LVDT has two uniformly wound secondary coils that each cover about one third of the core stroke path. The core is normally longer than one secondary winding and can move along the axis of the windings, in the interior space of the coil former. With the PCLT, the secondary windings cover the full stroke length of the core and are wound in a taper fashion such that the coils are dense at one end and sparse at the other. The two secondary coils are positioned in opposition so that as the windings of one secondary get more densely wound, the windings of the other secondary become sparser.

The PCLT core can be small, such that magnetic flux is *coupled* at one *point*. The core moves perpendicularly to the axis of the windings. This arrangement allows that the windings be laid in a single plane, resulting in a physically flat transducer, as opposed to the cylindrical shape of LVDTs.

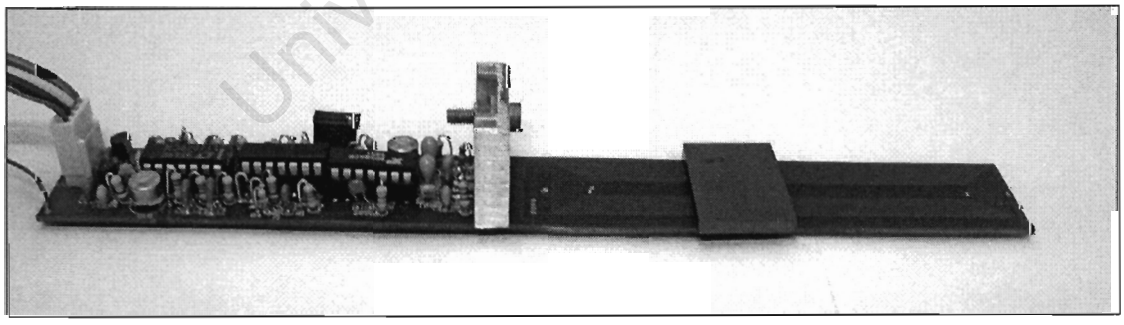

Figure 4 Photograph of PCLT prototype, showing flat windings and core.

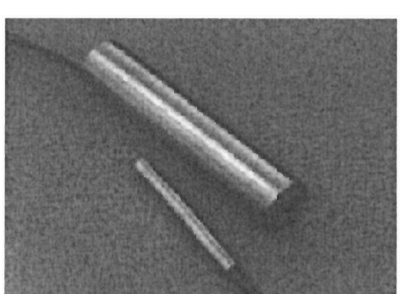

Figure 5 Photograph of LVDT, showing cylindrical body and long core.

2.7 Economic viability of the PCLT

The motivation behind this project lies in the economic potential of a sensor that can challenge existing displacement sensors in either performance or production cost. The flat nature of windings of the PCLT allows the windings to be laid out in copper tracks on a single, multi-layer PCB. This eliminates the manual winding process required by LVDTs, and its associated problems, such as labour costs, non-identical batches and difficult quality control [13].

2.7.1 Light weight

The PCB windings and small core of the PCLT make it desirable for its comparably flatter and more lightweight structure than that of LVDTs.

2.7.2 Large stroke-to-length ratio

The conventionally wound LVDT achieves a stroke-to-length ratio of about 30%. Stroke-to-length ratio is the ratio of a sensor's stroke (measurement range) over the sensor's physical length. There also exists a tapered winding LVDT, patented by J. Lipshutz in U.S. Patent 3054976 (September 1962) which can achieve a stroke-to-length ratio of about 80% [14]. The full length secondary windings and point coupling core of the PCLT offer the desirable property of an extremely good stroke-to-length ratio. Results achieved in the ball-on-beam project suggest a stroke-to-length ratio of as much as 90%.

2.8 Mathematical analysis of the PCLT

The PCLT windings are modeled as a set of parallel conductors [2], located atop each other as in Figure 6.

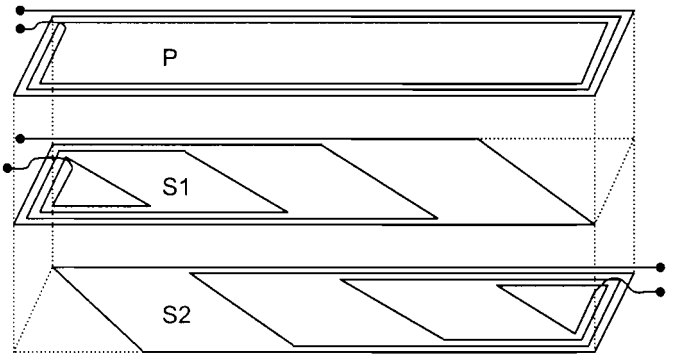

Figure 6 Exploded view of PCLT windings. P is the primary winding, S1 and S2 are the secondary windings.

X is the length of the longest conductor, and the turns of one secondary coil, S1, run from x = 0 to iX/n, where i is the endpoint of the ith of n conductors. The turns of the other secondary coil, S2, run from x = (n-i)X/n to X. The primary voltage V_P across the m turns of the primary winding induces secondary voltages V_{S1} and V_{S2} across the secondary windings. A is the coupling factor between the primary and secondary windings. The magnitudes of the induced secondary voltages are calculated as:

$$V_{S1} = \frac{V_P mA}{X}\left(\frac{X}{n} + \frac{2X}{n} + \cdots + \frac{(n-1)X}{n} + X\right) \qquad (1)$$

$$V_{S2} = \frac{V_P mA}{X}\left(1 + \frac{(n-1)X}{n} + \cdots + \frac{2X}{n} + \frac{X}{n}\right) \qquad (2)$$

With the introduction of a core, the coupling between primary and secondary windings changes, in the region around that core, as the core has a higher magnetic permeability than the air over the rest of the sensor area. The permeability non-uniformity is modeled as a slice perpendicular to the x axis, of width x_2-x_1.

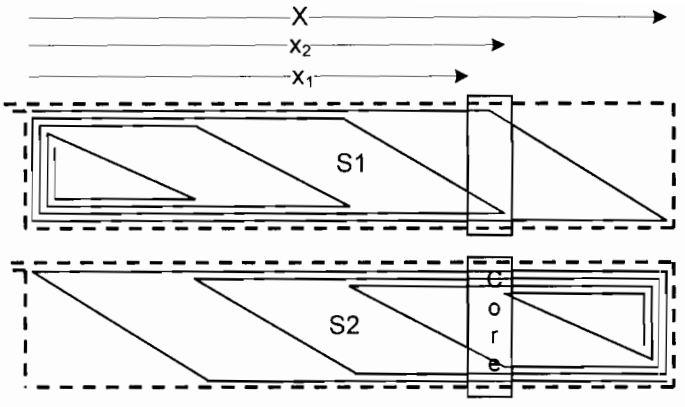

Figure 7 Secondary windings with core, showing distances x_1, x_2 and X.

A_0 is the permeability of air over the ranges $0<x<x_1$ and $x_2<x<X$, and A_1 is the permeability of the core, over the range $x_1<x<x_2$. If the number of secondary windings, n, is large, the summations in (1) and (2) can be expressed as integrals. With the core affecting the permeability, the induced secondary voltages become:

$$V_{S1} = V_P \frac{mn}{X^2}\left(A_0 \int_0^{x_1} x dx + A_1 \int_{x_1}^{x_2} x dx + A_0 \int_{x_2}^{X} x dx \right) \qquad (3)$$

$$V_{S2} = V_P \frac{mn}{X^2}\left(A_0 \int_0^{x_1} (X-x) dx + A_1 \int_{x_1}^{x_2} (X-x) dx + A_0 \int_{x_2}^{X} (X-x) dx \right) \qquad (4)$$

The difference between the secondary voltages reduces to:

$$V_{S2} - V_{S1} = \frac{V_P mn}{X^2}(A_0 - A_1)(x_2 - x_1)(X - x_1 - x_2) \qquad (5)$$

The first expression in (5) is constant for a constant magnitude primary voltage, the second represents the difference in permeability between the core and air, the third represents the width of the core, and the final component represents the position of the core along the x axis. This mathematical model indicates that the difference between the secondary voltages is linearly proportional to the core position.

3 Analysis of the Ball-on-Beam Ball Position Sensor

The PCLT is a new technology sensor which has hardly been investigated. One of the main sources of background information relating to the PCLT was found in analysis of the 'Point Coupled Induction Sensor' used as a ball position sensor in a ball-on-beam apparatus [1]. The PCLT developed in this project was based on the same operating principles as the ball position sensor. This chapter gives a review of the most relevant findings from analysis of the ball-on-beam project.

3.1 Theory of operation of the ball position sensor

The primary coil is excited by a sinusoidal voltage. This produces a band of magnetic flux along the length of the coil. Two secondary coils detect the flux. The physical arrangement is illustrated in the figure below.

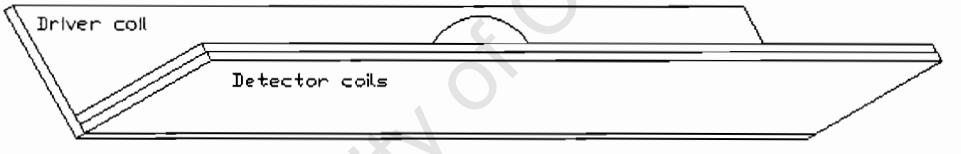

Figure 8 Arrangement of coils for the ball position sensor [1]. This sensor is 200mm long and 25mm wide, a 12mm diameter steel ball acts as the transformer core. The driver coil is the primary, and the detector coils the secondaries.

The ball is made of steel, which has a much higher (approximately 5000 times) magnetic permeability than air, so the magnetic flux produced by the primary coil is effectively only coupled to the secondary windings at the point where the ball is positioned. Hence the name "point coupled".

The voltage induced in the detector coils is a function of the magnetic flux density, the number of windings that encompass that flux and the impedance of the coil [15]. Thus, as more turns of the secondary winding encompass the high density magnetic flux path created by the ball, the induced voltage in that secondary winding increases.

Similarly, as fewer turns of the secondary winding encompass the point coupled flux the induced voltage decreases. The secondary coils are taper-wound, and positioned such that as the windings of one secondary become denser, the windings of the other secondary become sparser.

3.2 Positive aspects of the ball position sensor

The sensor performed adequately for the ball-on-beam project. The circuitry is simple, uses cheap components, and has a low component count. Circuit layout was not critical to circuit stability, and no shielding from external EMI was used. The output was approximately linear, as indicated in Figure 9.

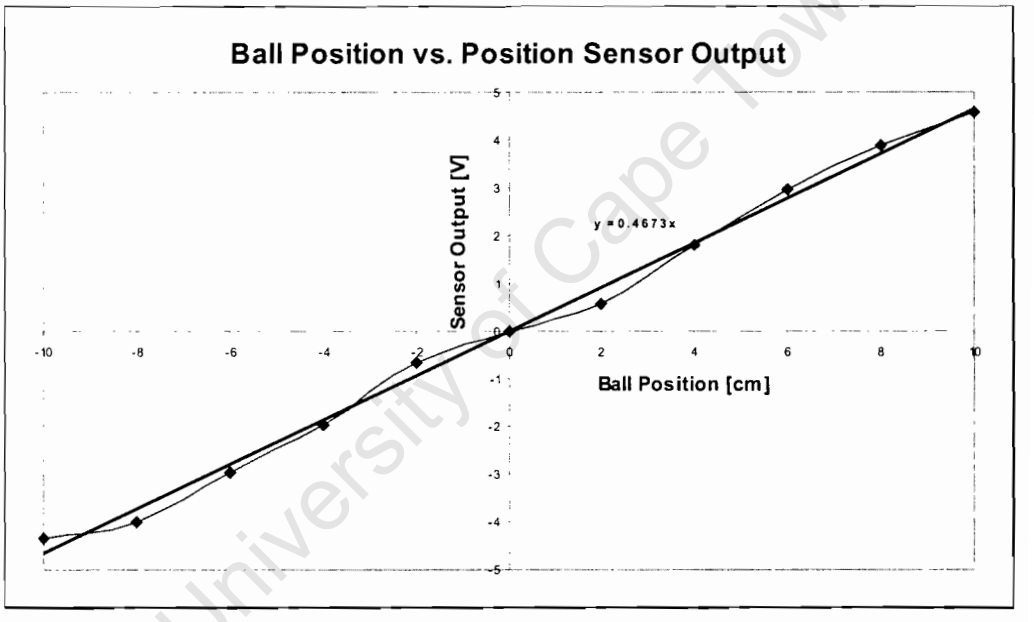

Figure 9 Graph of actual ball position versus position sensor output [1]. The output is symmetrical about the midpoint, and reasonably linear as compared to the linear trend line.

3.3 Negative aspects of the ball position sensor

The sensor was very sensitive to knocks and bumps, which would cause the output voltage to shift, and the sensor would require recalibration. The output was not perfectly linear. The three different windings, one primary and two secondary coils, were each printed on individual single sided PCBs, and the output was affected

whenever the separation gaps between the windings changed. Thus the sensor often required recalibration of the null-point. The output signal had $40mV_{pk-pk}$ of noise, and with static ball position the output slowly drifted by as much as 100mV.

3.4 Major areas for improvement

The ball position sensor's above mentioned flaws are attributed to the following reasons, which in turn suggest the solutions they require, and thus provide direction for tackling this project.

3.4.1 Primary coil excitation

The primary winding was excited by a $5V_{pk-pk}$ 20 KHz sine wave produced by an ICL8038 signal generator and boosted by an LM380 audio amplifier. The excessive noise and drift on the output signal could be due to the non-fundamental harmonics and voltage spikes induced on the secondary windings. These harmonics were caused by a distorted excitation signal. The audio power amplifier became unstable when loaded with the low impedance inductive primary coil, resulting in high frequency oscillations being superimposed on the negative half cycle of the excitation waveform. A clean excitation waveform is desired [5].

3.4.2 Signal conditioning

The sensor drift was probably due to the fluctuations in the magnitude and frequency of the excitation signal [1]. This suggests using a more complex and accurate signal conditioning approach that takes into consideration the excitation signal, as synchronous demodulation would, or ratio-metric division of the secondary voltage by the primary voltage.

3.4.3. Windings layout

A possible reason for the non-linearity of the sensor is that the secondary windings only run half of the length of the sensor. This was non-standard according to the PCLT principle of design, but was done to increase the length to width ratio of the windings. Ideally, the secondary windings would run the entire length of the sensor, and this should improve linearity. The PCB layouts are shown in Figure 13, Chapter 6.

Placing all the windings onto one multilayered PCB should solve the problem of susceptibility to bumps as this will keep the separation gaps between windings layers constant.

4. Development Approach

The PCLT is in principle an infinite resolution sensor. The physical properties that are exploited to determine core position are continuous, meaning that even the most infinitesimal of core position changes will affect the induced voltages. The limiting factor is the electrical circuitry that detects these voltage changes. Thus the performance of the PCLT is hugely dependant on the signal conditioning circuitry used, and this is where the major emphasis in this project was placed.

Analysis of the ball-on-beam induction sensor confirms that the most apparent areas for improvement fall under the electronic circuitry. It also suggests that there is room for improvement to the windings layout, which is addressed in Chapter 6.

The three main categories of the sensor's electronic circuitry are: 1) the primary excitation stage, which produces the signal to drive the sensor, 2) the secondary signals conditioning stage, where the two secondary signals are manipulated to give a DC output representative of core position, 3) the frequency at which the sensor operates, which influences both the excitation and the signal manipulation stages.

Four different prototypes were developed for comparison:

Prototype 1 – Discrete component passive demodulation
Prototype 2 – AD598 passive demodulation LVDT signal conditioner
Prototype 3 – Discrete component self-synchronous demodulation
Prototype 4 – AD698 synchronous demodulation LVDT signal conditioner

Chapter 5 is an investigation into the effect of the core shape and material on PCLT performance. Chapter 6 gives details of the windings layout and electrical characteristics.

4.1. Excitation of the primary winding

In Chapter 7, consideration is given to the following:

- The shape of the excitation waveform
- Excitation waveform generation
- Amplification of the excitation signal
- Effects of excitation amplitude on detected signals

4.2. Frequency of operation

Frequency is identified as a vital component in LVDT operation [6]. The similarities between the LDVT and the PCLT suggest that it will bear equal importance in PCLT performance and operation. A brief literature review on the effects of frequency on LVDTs is presented in Chapter 8. The relationship between frequency and indicators of performance like 'Coupling Ratio' are investigated. It is found that the PCLT has a natural resonant frequency which exhibits promising performance characteristics. Appendix A contains an investigation into the resonant properties of the PCLT.

4.3. Secondary signals conditioning

In Chapter 9 the four prototype sensors are described in detail. Two use passive demodulation and two use synchronous demodulation. Of each pair, one is made up of low cost discrete components, and the other uses an off-the-shelf LVDT signal conditioning chip modified to suit the PCLT.

4.4. Testing the prototypes

The prototypes needed to be analysed and compared to identify the strengths and weaknesses of the various signal conditioning approaches. A test rig capable of precisely controlling the core position was developed and constructed, as described in Chapter 10. A variety of tests were carried out on each of the four prototypes to

identify critical performance characteristics such as linearity, resolution and repeatability.

Chapter 10 is an investigation into the magnetic field produced by the primary winding, and Chapter 11 contains the results from linearity, repeatability, steady state and resolution tests.

A two dimensional version of the PCLT was built using principles and circuit design developed for the one dimensional PCLT. This is reported on in Appendix B.

4.5. Definition of terms

Some terms and ratios are introduced for reference later. Figure 10 shows where certain potential differences are measured across the PCLT windings. These are combined into useful ratios as defined in the equations that follow.

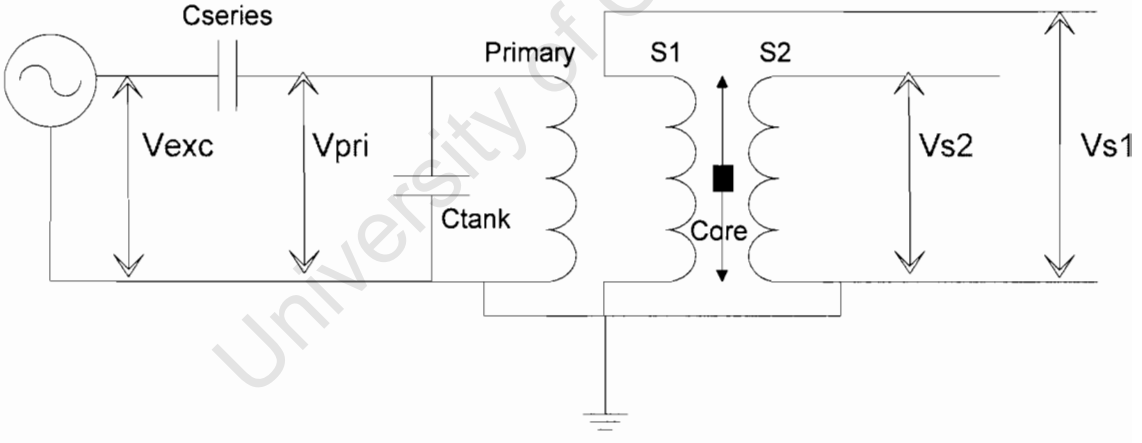

Figure 10 Indication of terms including Vpri, Vexc, Vsec (Vs1 and Vs2).

$$CouplingRatio = {V_{Secondary}^{centre}}/{V_{Primary}} \qquad (6)$$

$$ApparentCouplingRatio = {V_{Secondary}^{centre}}/{V_{Excitation}} \qquad (7)$$

$$\Delta V_{Secondary} = V_{Secondary}^{Maximum} - V_{Secondary}^{Minimum} \quad (8)$$

The coupling ratio (CR) is an important indicator, as it expresses how much of the primary signal is coupled to the secondary coils, V_{sec} measured with core at centre. The higher the coupling ratio the better, as this means a larger secondary signal is received for a certain magnitude of primary excitation, and increased secondary signals mean improved sensitivity and an increased signal-to-noise ratio.

The Apparent Coupling Ratio (APR) includes a series capacitor in the primary coil, thus indicating a relationship between the voltage applied by the primary drive circuit (V_{exc}) and the secondary voltages.

The change in secondary voltage (ΔV_{sec}) is an important term to consider as a change in core position produces a change in secondary voltage, and thus a large ΔV_{sec} is more useful than a large magnitude V_{sec} that does not vary much with core position change.

5. Core Material and Shape

The core of the PCLT couples magnetic flux from the primary coil to the secondary coils, a process fundamental to this displacement measurement technology. Initially, a soft iron core was used. Investigation into high frequency transformers, especially planar ones, revealed that iron core saturation occurs around 1 KHz. For higher frequency transformers, ferrite cores are used. A $MnZnFe_2O_4$ (3C90) ferrite core from Ferroxcube, suitable for power transformers operating up to 200 KHz, was selected for performance comparison with the soft iron core.

5.1. Dimensions of cores used

The following cores were tested:

	L x B x H
1) Soft Iron Core:	*30 x 16 x 16 mm*
2) Ferrite Slab Core:	*20 x 30 x 3 mm*
3) Ferrite Surround Core	*20 x 34 x 14 mm*

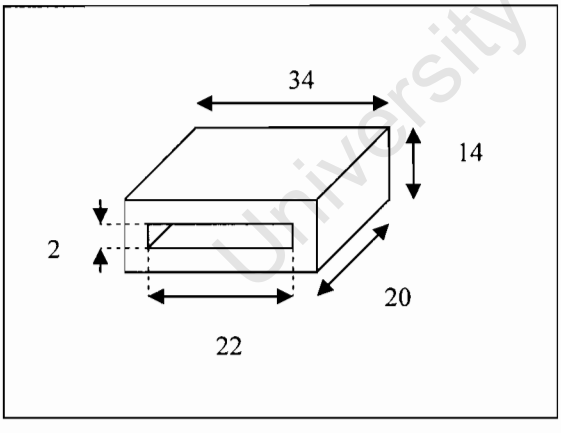

Figure 11 Surround ferrite core with dimensions in mm. The core encompasses the windings.

5.2. Change in secondary voltage with different cores

A comparison of the cores' performance, in terms of maximum change in secondary voltage with the same excitation, is shown in Table 1 below.

Core Type	Vs1 min (mVrms)	Vs1 max (mVrms)	ΔVs1 (mVrms)
Iron Slab	620	680	**60**
Ferrite Slab	650	760	**110**
Ferrite Surround	800	1420	**620**

Table 1 The maximum change in secondary voltage with different cores. The ferrite surround core developed about 10 times as much voltage change as the iron core did, for the same excitation applied.

An investigation into core performance with different coupling methods and various excitation voltages revealed the same trend as identified in Table 1. The results, presented in Figure 12, also show that ΔV_{sec} is directly proportional to the excitation voltage.

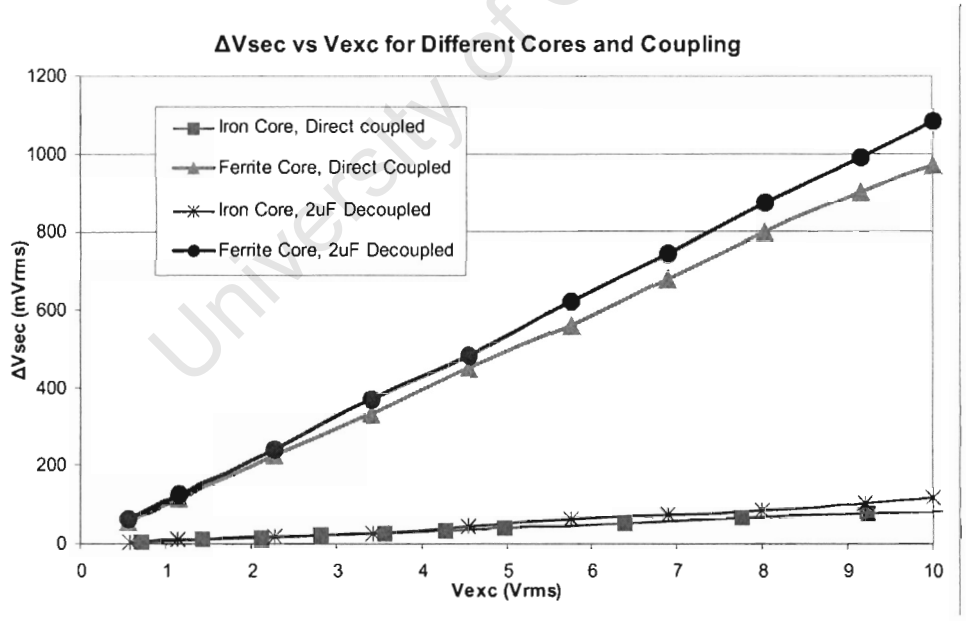

Figure 12 Comparison of maximum change in secondary voltage with ferrite and iron cores. Test carried out at 20 KHz. The ferrite core shows approximately 10 times the response of the iron core, direct coupled or 2μF decoupled. There is a slight increase in ΔVsec when the primary winding is decoupled from the power amp with a 2μF capacitor.

6. PCLT Windings

The layout of the windings for the ball-on-beam induction sensor is shown in Figure 13. The ball-on-beam apparatus required long thin sensor elements to make up the trough that the ball rolled along. Two main problems with this layout were that a) the secondary windings were on different PCBs that were laid adjacent to each other, and b) the tapered secondary windings did not run all the way from end to end.

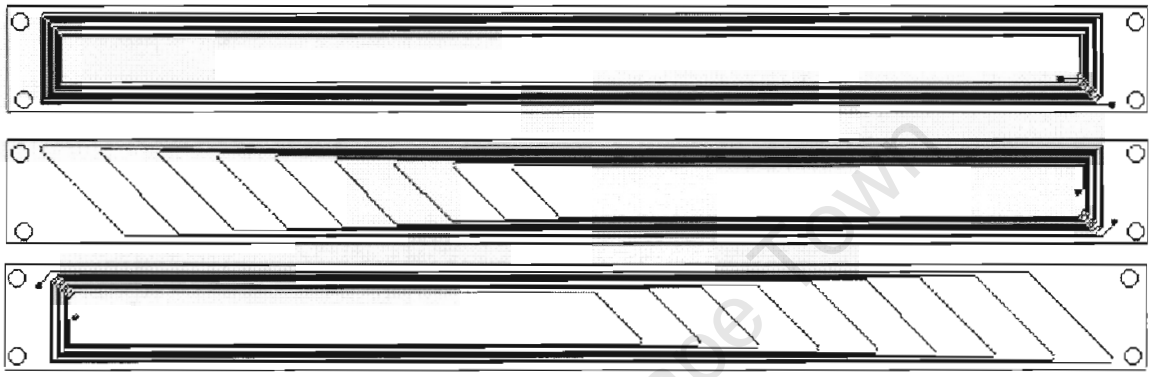

Figure 13 Ball-on-Beam Windings Layout. The tapered secondary windings only run half of the length of the sensor, because of the large length and narrow width.

The problem with the windings being on separate boards is that as soon as they move relative to each other the coupling is altered and the sensor needs to be re-calibrated, thus making the sensor extremely non-robust. With the tapered windings not overlapping, the sensor loses sensitivity as only one of the secondary voltages changes with the core position.

6.1. Version 1 windings layout

A new set of windings were laid out by J. Tapson. This design had the improvement that the tapered secondary coils ran the full length of the sensor. This sensor still suffered from reduced robustness as the primary and secondary windings were on different boards, and thus the separation gap between windings could change.

6.2. Version 2 windings layout

For this project another design of windings layout was created. All of the windings were etched on the same PCB to eliminate the problems associated with multiple board configurations. Another improvement over Version 1 was to change the order of the layers so that both secondary windings were placed equidistant from the primary coils. Figure 14 shows the Version 2 windings layout.

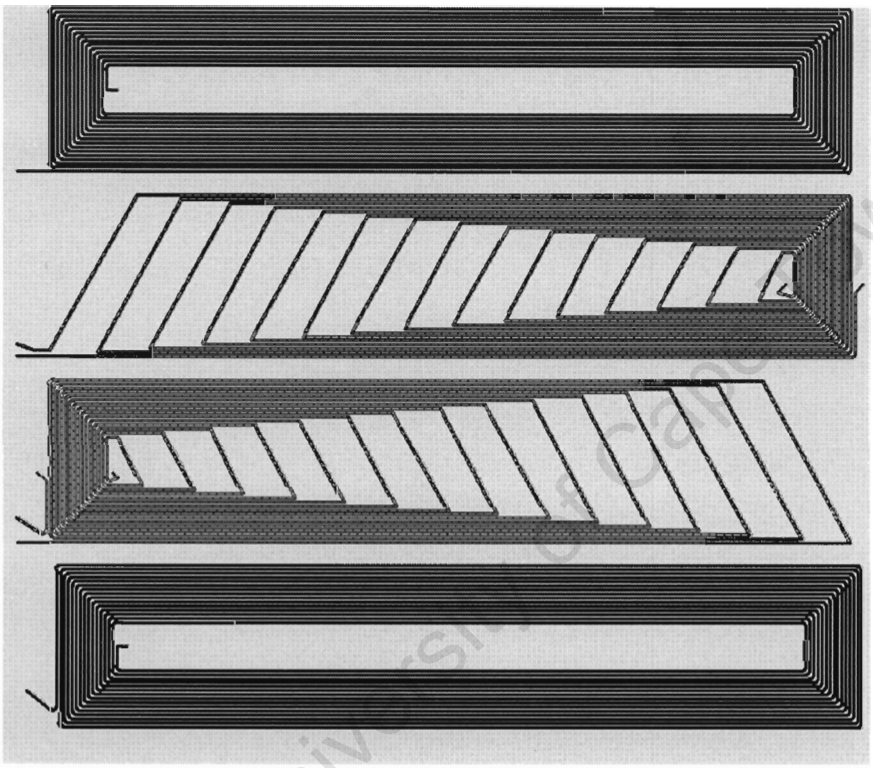

Figure 14 Version 2 windings layout. Layer 1 at the top, secondaries at 2 and 3 and layer 4 at the bottom

The number of turns in each winding was increased from 10 in Version 1 to 15 in Version 2. The primary is made up of two layers connected in series to increase the overall inductance, and thus make its excitation less difficult (as the power amplifier struggled to excite a very low impedance load). A cross-section of the 4 layer Version 2 PCB is shown to illustrate how each winding is positioned relative to the others on the PCB.

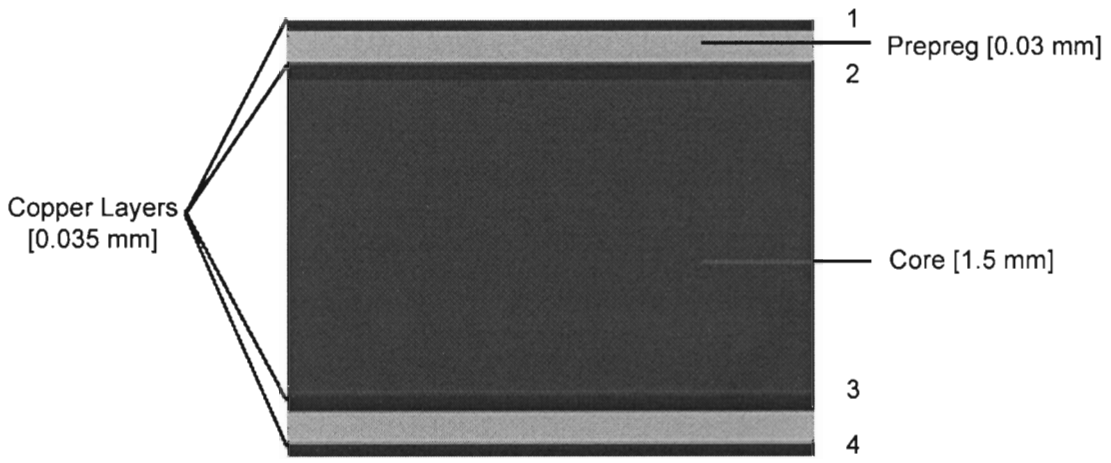

Figure 15 Version 2 PCB cross-section showing layer positions and thicknesses.

In Figure 15, layers 2 and 3 are the secondary windings, layers 1 and 4 are the two series connected halves of the primary winding. This configuration meant that with a double sided core, the secondaries were identical distances from the core, and primary windings, resulting in improved symmetry in secondary response.

6.3. *Electrical characteristics of primary windings*

Some of the electrical properties of PCB layout Versions 1 and 2 were measured for comparison. Measurements were made using an ESCORT 2260 RCL meter. The results are summarized in Table 2.

	Resistance (Ω)	Inductance (μH)	Capacitance (μF)	No. of Turns
Version 1 (no core)	8.81	38.8	0	20
Version 1 (with ferrite core)	8.81	73.8	0	20
Version 2 (no core)	9.39	60.1	0	30
Version 2 (with ferrite core)	9.39	176.2	0	30

Table 2 The characteristics of the different versions of the PCLT primary coils, with and without a ferrite core.

The core had no effect on the resistance of the primary winding, but caused a large change in the inductance of the primary. The inductance of Version 1 doubled when the core was present, and the inductance of Version 2 almost tripled. This is because the core increased the mutual inductance between the primary and secondary windings. The capacitance of the windings was too small to be measured by the RCL meter.

6.3.1. Change in primary inductance with core position

The inductance of the primary winding was strongly influenced by the presence of the core, but the resistance and capacitance were unaffected. The results of an investigation into the effect of core position on primary inductance are illustrated in Figure 16 and Figure 17.

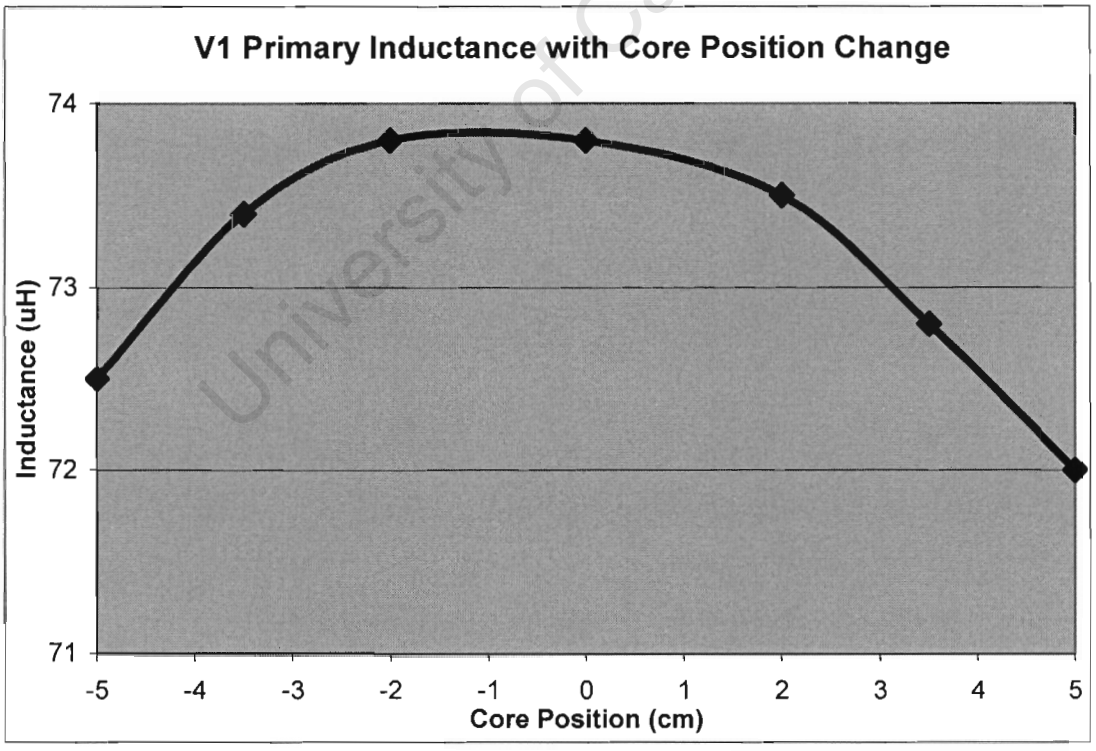

Figure 16 Effect of core position on the inductance of layout Version 1 primary winding. As the core moved towards the ends of the sensor, the inductance decreased by up to 1.8 µH.

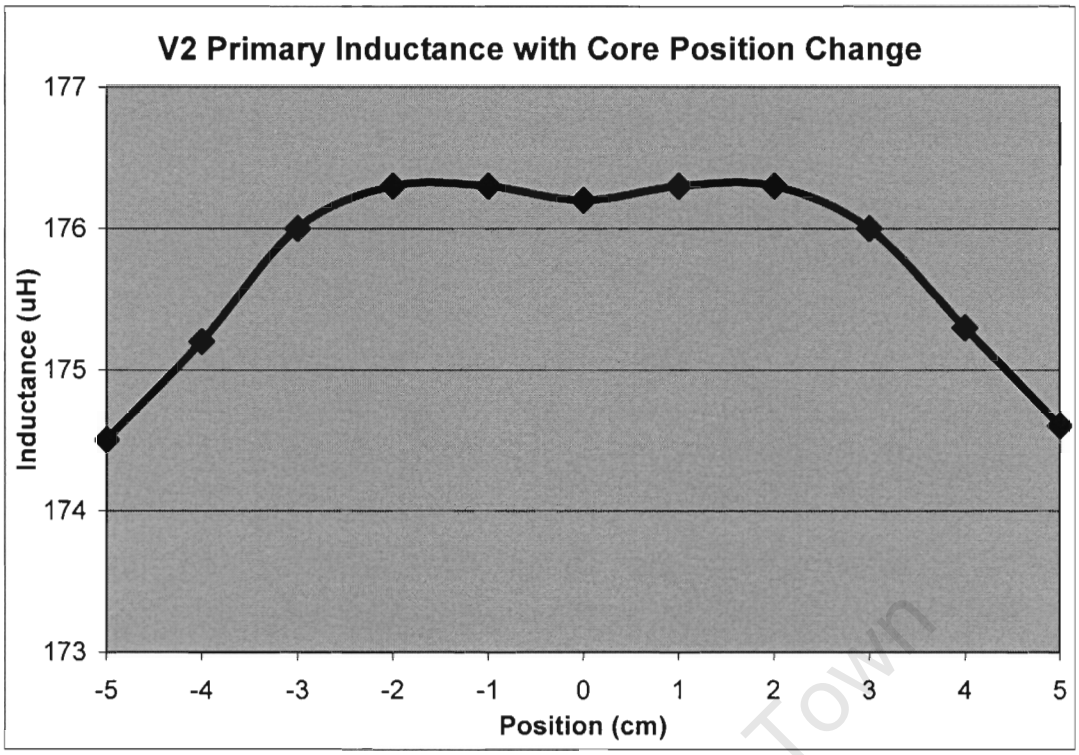

Figure 17 With PCLT layout Version 2, the primary inductance showed improved symmetry of response as the core position was changed, but the inductance did decrease by 1.8 µH at the core end points.

The above results are expressed, as a percentage change from the primary inductance with a centered core for both versions of windings, in Figure 18.

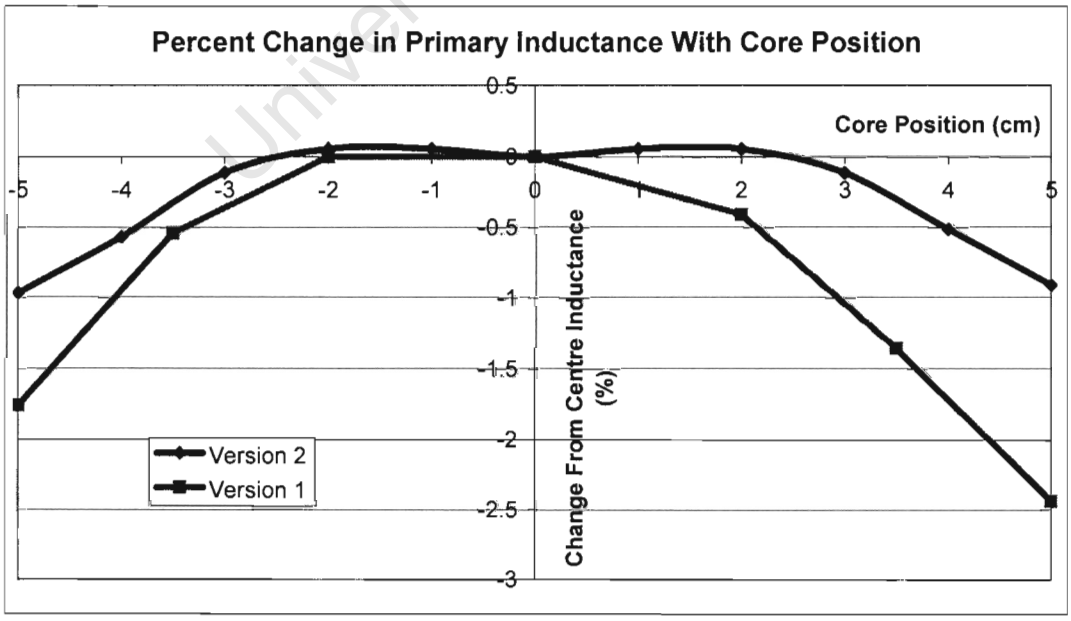

Figure 18 Percentage Change in Primary Inductance of both layout versions. Version 2 exhibits superior behavior in both symmetry and maximum inductance change.

The graphs above show that the inductance varies with core position by as much as 2.5% with Version 1 and 1% with Version 2. This could contribute to PCLT non-linearity, as the amplitudes of the secondary waveforms are dependant on primary voltage, which is in turn dependant on the inductance of the primary winding. The two LVDT signal conditioning prototypes (Prototypes 2 and 4) detailed in Chapter 9 should show better immunity to fluctuations in primary excitation amplitude than the discrete circuit prototypes (Prototypes 1 and 3), as they use a ratiometric calculation to reduce the effects of variance in the excitation signal.

6.3.2. Effect of windings layout on primary to secondary coupling

The different windings layouts responded differently to the same excitation waveform. The primary and secondary voltages were monitored for different excitation voltages applied to the two layout versions. The coils were driven with a 20 KHz sine wave from a 2 µF decoupled OPA541 power amplifier. V_{exc} is measured on the output of the op-amp, V_{pri} across the primary winding and V_{sec} across the secondary windings. A ferrite core fixed at the centre of the windings was used in all of these tests.

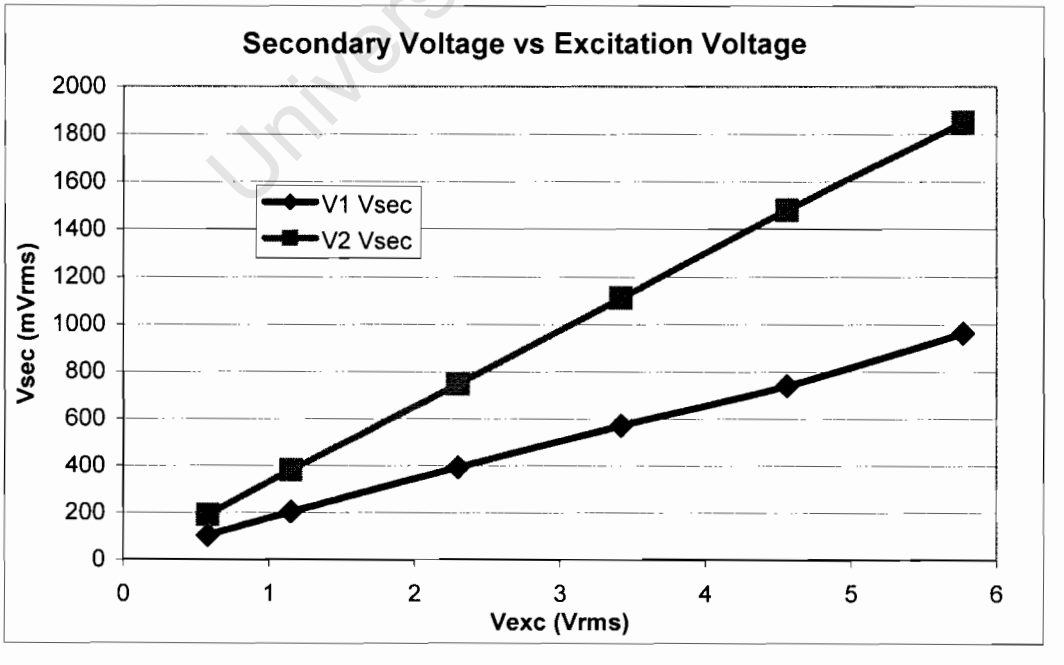

Figure 19 The secondary voltage of layout V2 is almost double that of V1 for the same excitation voltage applied.

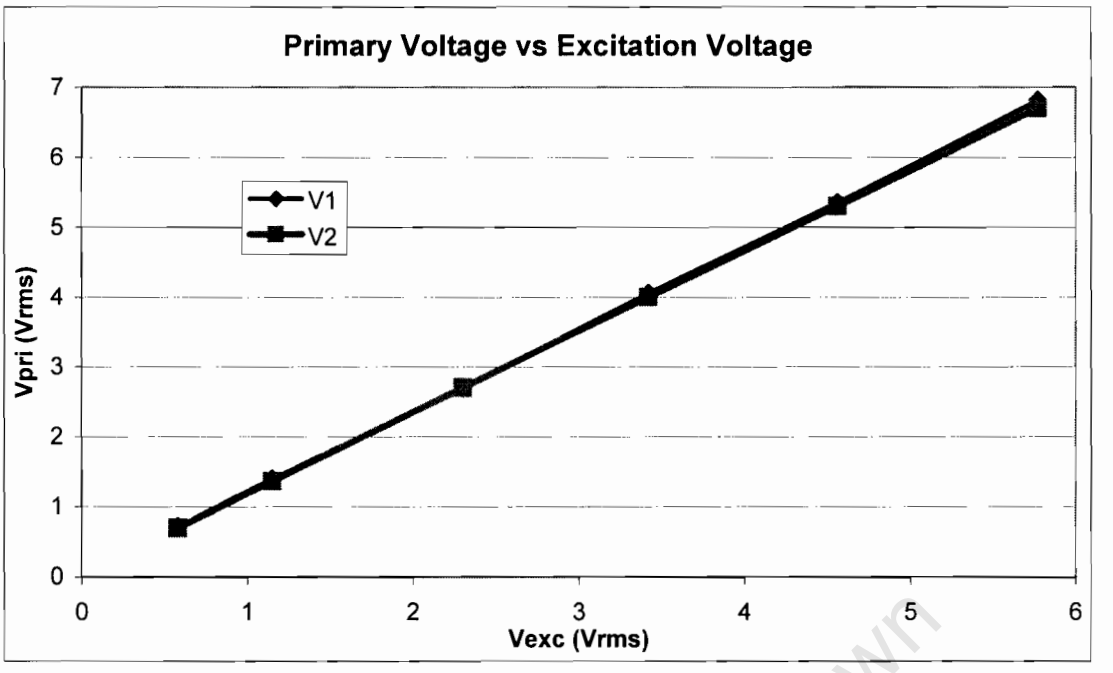

Figure 20 The primary voltages of the two windings versions are almost identical for the same excitation applied.

The above graphs indicate that for the same applied voltage the two layout versions exhibit similar primary voltages but largely different secondary voltages. This shows that layout Version 2 couples voltage to the secondary windings more effectively than does layout Version 1. Increased coupling is a desirable feature as it means increased sensitivity of the sensor. The Version 2 windings are used for all of the prototypes, as they exhibit superior coupling and symmetry of response and have a larger inductance.

7. Primary Excitation

The reason for exciting the primary winding of the PCLT is to produce a band of magnetic flux along the length of the sensor. This flux is detected in the secondary windings by the principle of induction. There are two stages to exciting the primary coil; producing the excitation waveform, and amplifying the waveform.

7.1. Producing the excitation signal

The amount of magnetic flux produced by the primary coil is proportional to the current in the coil, and the magnitude of the EMF induced in the secondary coils is proportional to the rate of change of the magnetic flux that the coils encompass [15]. Thus, a continuously changing current in the primary winding is required to continuously induce an EMF in the secondary windings. Any form of alternating current will satisfy this condition, however a sinusoidal waveform is preferable for reasons of avoiding distortion and non-fundamental harmonics [5].

The distortion to a sinusoidal wave is appreciably less than any other waveform when applied to an inductor (which a coil essentially is) because the rate of change of the current is not as large or dramatic (no instantaneous changes) in a sinusoidal wave as it is with say, a square or triangular wave. Inductors inhibit change in the current through them. Sinusoidal waves consist solely of a fundamental frequency, whereas composite waves consist of harmonics at a myriad of frequencies. Harmonic components are the cause of quadrature null voltages in LVDT's [16].

7.1.1. Prototype 1 and 3 excitation waveform

An ICL8038 precision function generator is used to generate the excitation sine wave in Prototypes 1 and 3. The frequency range of the device is 1 Hz to 300 KHz. Advantages to using the ICL8038 include; low cost, compact 14 pin package, and maximum sine wave distortion of 1%.

7.1.2. Prototype 2 and 4 excitation waveform

Prototypes 2 and 4 use off-the-shelf LVDT signal conditioning chips AD598 and AD698 respectively. Both of these devices have onboard sine wave oscillators with differential outputs, which can be configured for frequencies in the range 20 Hz to 20 KHz.

7.2. Amplifying the excitation signal

The AD598 and AD698 devices have an on-board excitation amplifier to drive an LVDT, but this is not powerful enough to drive the primary winding of the PCLT. The PCLT primary winding consists of only twenty turns, and thus has a very low resistance and inductance, specifically 8Ω and 40uH in the case of the first windings layout version. The LM380 audio amplifier that was used in the ball-on-beam sensor managed to excite the primary coil, but would burst into 8 MHz oscillations on the negative half cycle. This was the suspected reason for the large output signal drift in the ball-on-beam sensor.

An amplifier with the ability to drive a reactive load was required. LVDT's typically use a class-A power amplifier for minimum distortion [17]. A power op-amp was used for ease of implementation, precise and adjustable gain control and extremely low distortion (especially cross over distortion). After assessing many of the different power amplifiers available, the OPA 548 T was chosen, for its sample availability, relatively low cost, large power bandwidth, high current capacity and good stability with reactive loads [18]. The OPA 561 appears to be a good choice for a surface-mount equivalent.

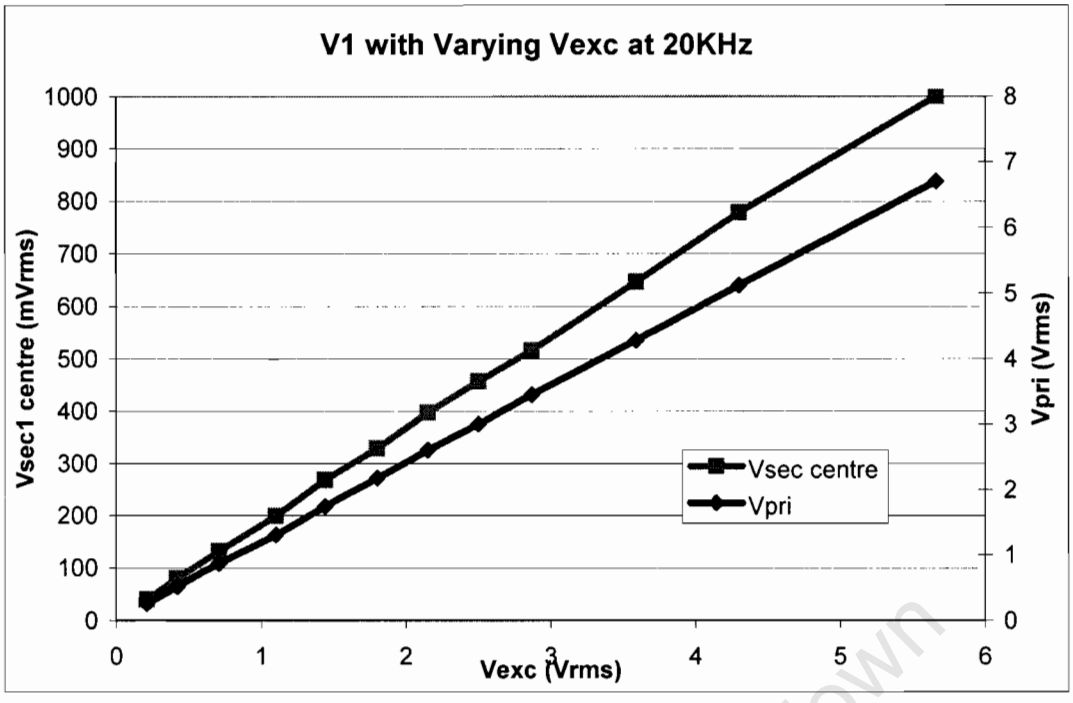

Figure 21 Effect of Excitation voltage (V_{exc}) on the primary (V_{pri}) and secondary (V_{sec}) voltages. Results show that the primary and secondary voltages are directly proportional to the excitation voltage.

8. Frequency of Operation

The excitation frequency plays a critical role in the performance of the PCLT. This chapter opens with a look at how frequency affects LVDT operation, and moves on to analyze the PCLT's frequency dependant characteristics. The PCLT is similar to the LVDT in many ways. Understanding LVDT operation gives insight into what to expect and what to look out for in analysis of the PCLT.

8.1. Effects of frequency on LVDT operation

Industry standard LVDTs operate with excitation frequency in the range 50 Hz to 25 KHz, but in special circumstances can be excited up to several MHz [6].

8.1.1. Efficiency

LVDT efficiency increases with higher excitation frequency, as the impedance of the inductive primary coil is the product of its inductance and the frequency. Higher impedance results in lower primary current and hence better efficiency. The decrease in primary current also means that a larger excitation voltage can be applied without exceeding the maximum power rating of the LVDT.

8.1.2. Sensitivity

Increasing the excitation frequency of an LVDT also results in an increase in sensitivity. Sensitivity is defined as the full scale output divided by the stroke length, divided by the excitation voltage.

8.1.3. Temperature stability

Excitation frequency affects the temperature stability of an LVDT. The primary winding is made of copper, so resistance increases with temperature. At lower

frequencies, the resistance makes up a tangible part of the primary winding impedance, and an increase in this resistance causes the excitation voltage to drop, ultimately affecting secondary voltage levels and sensor output. At higher frequencies the reactance of the primary winding becomes the dominant element of the winding's impedance, i.e. the change in resistance has a negligible effect on the overall impedance of the primary winding. The reactance is not affected by temperature changes. Summarily, adverse temperature effects are decreased at higher excitation frequencies.

8.1.4. Distortion

Excessive increase in excitation frequency leads to an increase in the Total Harmonic Distortion (THD) of the primary and, consequently, secondary waveforms. This is due to: excitation circuit components approaching their speed-of-operation limits (slew rates, bandwidth), the more noticeable effects of stray capacitance, and core material saturation.

8.2. Relationship between coupling ratio and frequency

A test to determine how the excitation frequency affects the coupling ratio was carried out using an HP33120A function generator as the excitation source. The primary winding of layout Version 1 was directly coupled to the function generator with no core present, and the Coupling Ratio was recorded for frequencies up to 15 MHz, the upper frequency limit of the function generator. The response over the first 500 KHz is shown separately in Figure 22, as this is likely to be the region of realizable operation. Figure 23 shows the results over the full frequency range.

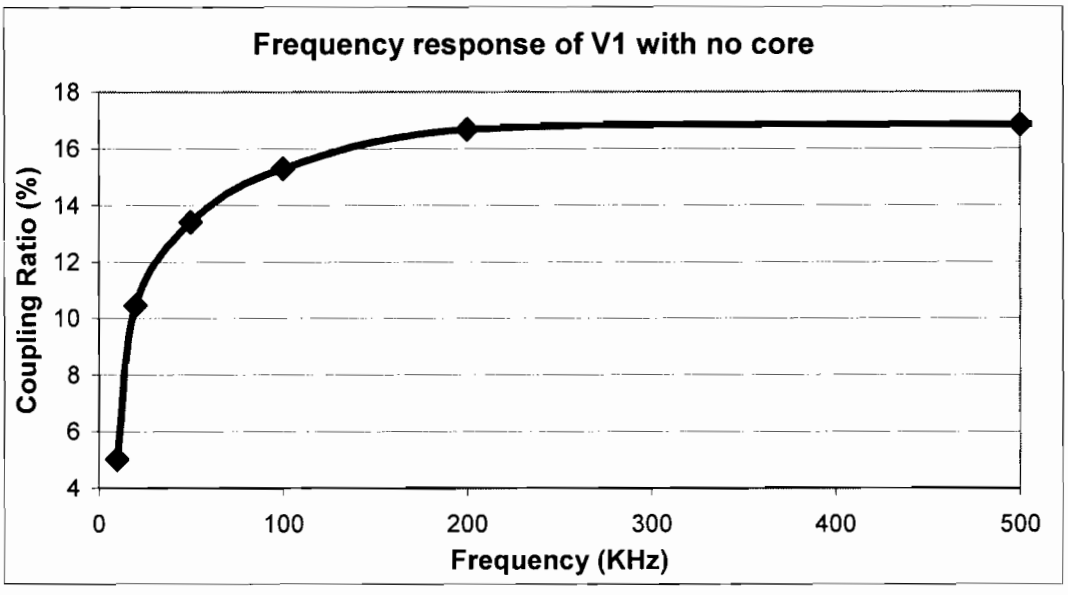

Figure 22 Coupling Ratio with frequency up to 500 KHz. The CR was immeasurably low for frequencies less than 10 KHz, but rose rapidly to 17 % by 200 KHz, where it leveled out.

The Coupling Ratio increased rapidly at first, leveling off to a steady 17 % by 200 KHz. The function generator was not powerful enough to induce a secondary voltage discernable from the background noise for frequencies lower than 10 KHz.

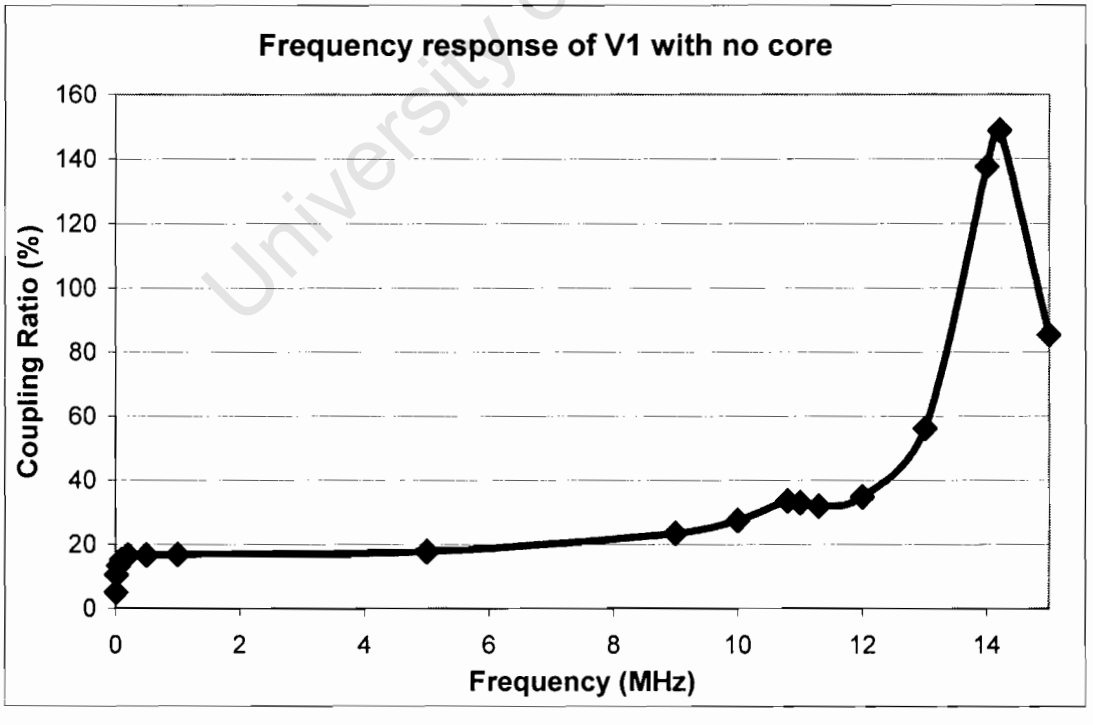

Figure 23 Relationship between Coupling Ratio and excitation frequency with Version 1 windings. There is a peak at 14 MHz where the coupling ratio exceeds 100 %, i.e. the induced secondary voltages are larger than the primary voltage applied to the sensor.

The CR remained at a steady 17 % until about 6 MHz, and then started to increase with frequency again. A slight peak occurred at 11 MHz, and a more prominent peak occurred at 14 MHz. This response suggested some form of resonance was occurring in the windings.

8.3. Natural resonant frequency

A 4195A HP Network/Spectrum Analyzer was used to test the impedance of the primary coil in an attempt to confirm that the V1 PCLT windings indeed had a resonant mode at 14MHz, as suggested by the previous test. Figure 24 shows the relevant section of the results obtained from the spectrum analyzer.

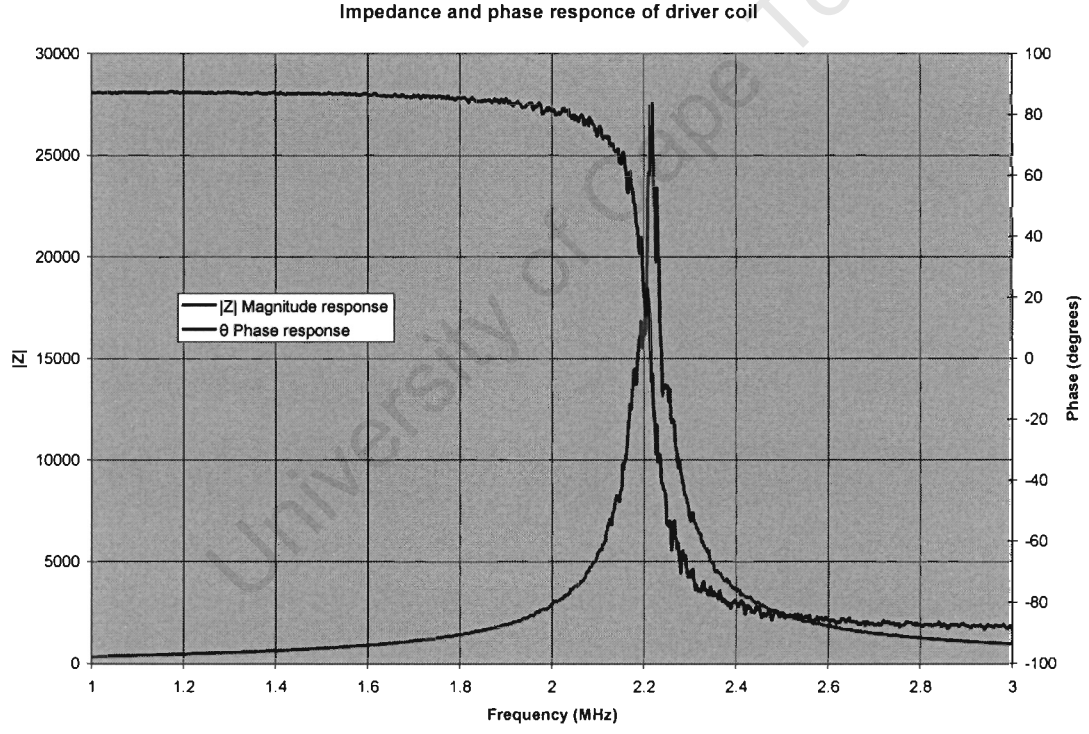

Figure 24 Spectrum analyzer results showing a natural resonant mode at 2.22 MHz. A definite inversion of phase and sharply peaking magnitude identify the resonant mode.

A frequency sweep from 10 KHz to 100 MHz revealed only one pole, occurring at 2.22 MHz. This differs hugely from the 14 MHz mode revealed in Figure 23. It is possible that the connecting leads influenced the results, or that the function generator in combination with the coil was resonating.

8.4. Altering the resonant frequency

It is not convenient to drive the circuit at such a high frequency as 2.2 MHz, as sine wave distortion and stray capacitance have detrimental effects, and circuit complexity increases as gain bandwidth products and slew rates of components become critical. Also, the AD598 and AD698 cannot operate above 20 KHz.

When an RCL circuit is driven at its resonant frequency the current and the voltage are in phase, and thus the load appears to be purely resistive. Theory suggested that introducing series capacitance would transform the primary winding into an RCL circuit with a natural resonant frequency determined by the inductance and capacitance of the circuit [19].

$$f_{resonance} = \frac{1}{2\pi\sqrt{LC}} \qquad (9)$$

As the capacitive component in the circuit can be chosen, it follows that the resonant frequency of the circuit can be controlled, in accordance with the relationship defined in (9).

8.4.1. 200 KHz resonant point

It was calculated that a capacitance of 17 nF in series with the V1 primary winding would cause the RCL combination to have a natural resonant frequency of 200 KHz. An impedance test was done with the 17 nF capacitor in series with the primary winding; the result is shown in Figure 25.

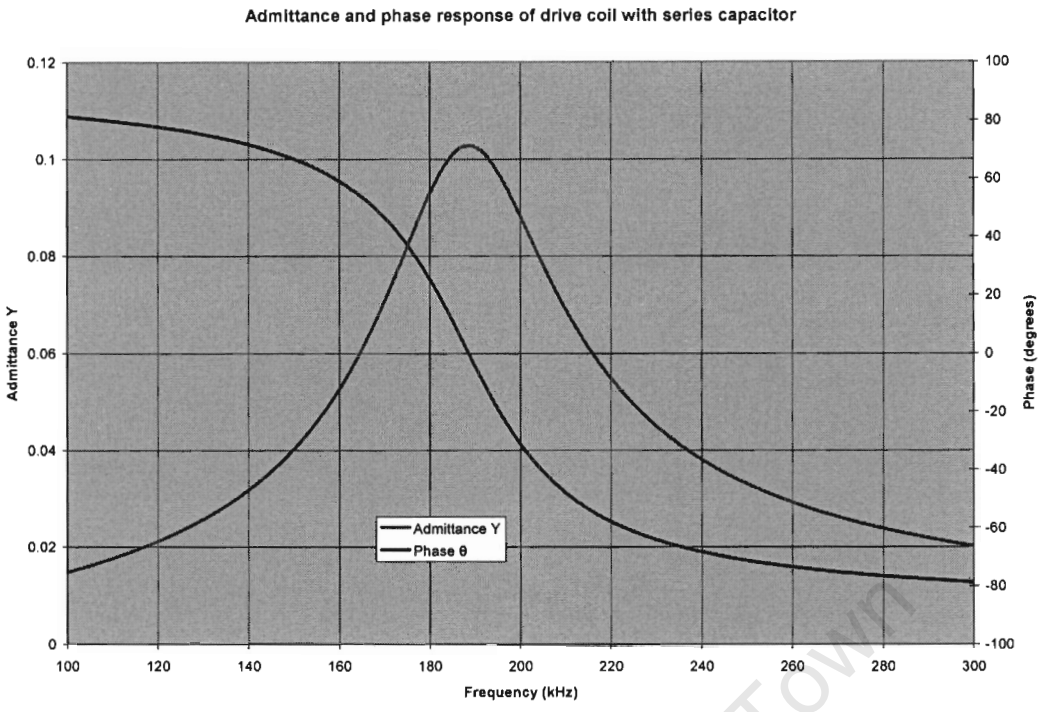

Figure 25 Impedance and phase response with 17 nF series capacitance. The resonant peak shifted to 190 KHz.

This confirms that the resonant frequency of the PCLT windings can be adjusted to the desired frequency with the introduction of a capacitor in series with the primary winding. Further investigation into the resonant properties of the PCLT is detailed in Appendix A.

8.5. Choice of frequency for the PCLT operation

A high operating frequency offers improvements in PCLT operation. These include increased coupling (and therefore increased sensitivity), reduced temperature effects, and better power efficiency. The AD 598 and AD698 LVDT signal conditioning circuits (Prototypes 2 and 4, explained in detail in Chapter 9) can be configured to operate between 20 Hz and 20 KHz. The maximum operating frequency of 20 KHz was chosen, to exploit the advantages of a high operating frequency.

The discrete component circuits (Prototypes 1 and 3) are capable of operating at much higher frequencies. The instrumentation amplifier used in Prototype 3 is the

frequency limiting component, with an upper frequency limit of 100 KHz, and Prototype 1 is limited by the sine wave generators maximum frequency of 300 KHz. It would be desirable to operate these prototypes at close to their maximum frequency capability to further exploit the advantages offered by increased frequency of operation. However, in accordance with a primary aim in this project, which is to determine which of the circuit methodologies (passive or synchronous demodulation of the detected signals) is best suited to PCLT operation, all of the prototypes were operated at the same frequency of 20 KHz. Having all the prototypes operate at the same frequency allows for a more accurate comparison of their demodulating performance. Future work should aim towards increasing the frequency of operation into the hundreds of KHz range.

In accordance with the findings in Appendix A, and the fact that all prototypes operate at 20 KHz, 2 μF of series capacitance was used with all four of the prototypes.

9. Secondary Signal Conditioning

The PCLT requires signal conditioning to change the two varying amplitude sine wave secondary signals into a DC signal which is a linear representation of the core position. The amplitude and phase of the secondary voltages vary with core position, while their frequency remains constant. Thus, the secondary waveforms are effectively amplitude-modulated signals where the excitation signal is the carrier waveform. Demodulation is required to extract the desired information. Similarly, LVDTs use demodulation of the secondary signals to determine the core position [6].

9.1. Different methods of demodulation

There are two main categories of demodulation, passive demodulation and synchronous demodulation [6]. With passive demodulation, the secondary signals are separately rectified (either half or full wave) and filtered, such that two DC voltages are obtained. The difference of these two voltages represents the core position. With synchronous demodulation, the two secondary signals are added (series opposing) and then multiplied by the carrier waveform and low pass filtered to obtain a DC voltage representing core position.

9.2. Existing LVDT signal conditioners

There are a large number of signal conditioning units for LVDTs available on the market, most of which are large, complex and expensive precision devices. Many of these are built around an analogue LVDT signal conditioning chip. The NE5521 made by Phillips [5] was the first of its kind, but is rather crude and outdated. Analogue Devices makes two different versions, the AD598 and AD698. They have slightly different characteristics, as the former uses precision rectification and the latter synchronous demodulation to create the DC position output. Both use ratio-metric division of the secondary signals to improve on temperature stability and immunity against fluctuations in the excitation voltage.

9.3. Four different approaches to signal conditioning

There are many possible methods of performing either passive or synchronous demodulation. Not knowing which would yield the best results, four different prototypes were developed; two of them using passive demodulation and two using synchronous demodulation. In each category, one would use the more expensive precision industry standard LVDT signal conditioning electronics, modified as necessary, and the other would be built from low-cost discrete components.

9.4. Prototype 1 – discrete component passive demodulation

The first prototype is similar in design to the signal conditioning circuitry that was used in the ball-on-beam project. Changes were made to improve on the weaknesses of the sensor as identified in Chapter 3. Improvements in Prototype 1 over the ball-on-beam version include: a more powerful excitation power amplifier, precision rectification [5] to eliminate errors introduced by diode turn-on voltage, second order low-pass filtering for reduced ripple, and controlled high frequency roll-off points of op-amps to eliminate unwanted high frequencies at every stage.

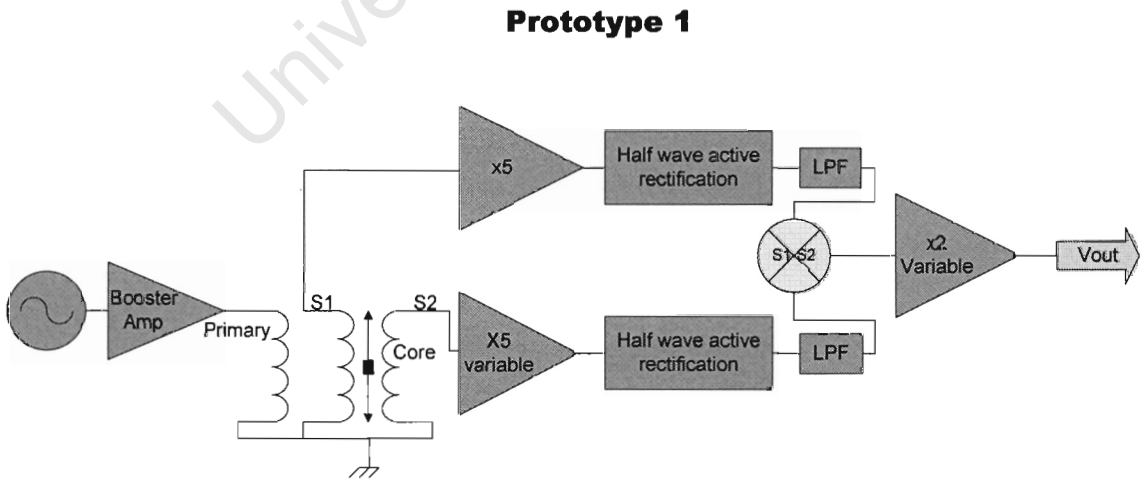

Figure 26 Functional block diagram of P1.

9.4.1. Description of operation

The magnitudes of the secondary signals are indicative of the core position. At the null point they have equal magnitude, to the left S1 is larger than S2, and to the right of null S2 is larger than S1. Figure 26 is a block diagram representation of the circuitry operation. The 'x5' stages simply magnify the secondary signals for increased sensitivity, and one is variable to allow null point adjustment by changing the point where the two secondary signals have equal magnitude.

The precision rectification and low pass filter stages extract the magnitude of the sine wave secondary signals as DC voltages. Rectification is active, or op-amp assisted, to overcome diode voltage drops [5]. The difference of the magnitude voltages gives the core position, and a final magnification stage allows for full scale adjustments. Full scale output is -10 to 10 V.

9.4.2. Prototype 1 circuit diagram

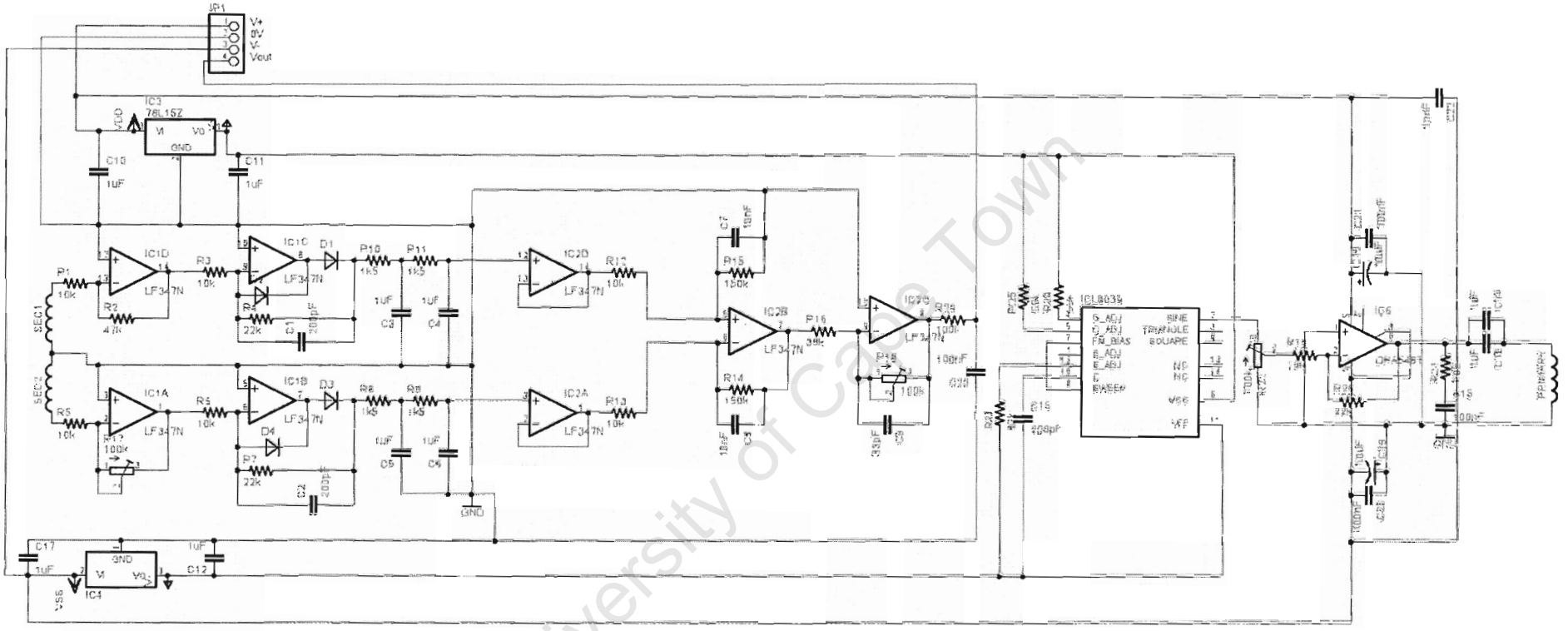

Figure 27 Prototype 1 circuit diagram.

9.5. Prototype 2 – modified LVDT AD598 signal conditioner

The circuitry of P2 is built around an off-the-shelf LVDT signal conditioning subsystem, AD598. The AD598 operates with passive demodulation by means of two precision rectifiers, one for each secondary signal. The difference between the rectified secondary signals is divided by the sum of the secondaries. This requires that the sum of the secondary signals is constant over the full range of the sensor, which is the case with the PCLT Version 2 windings operating at 20 KHz. This division improves temperature stability and immunity from fluctuations in the excitation waveform.

Two modifications had to be made for the LVDT signal conditioning subsystem to enable it to work with PCLT windings: a pre-amp stage was added between the secondary windings and the AD598 inputs, and a booster amplifier was used to excite the primary winding.

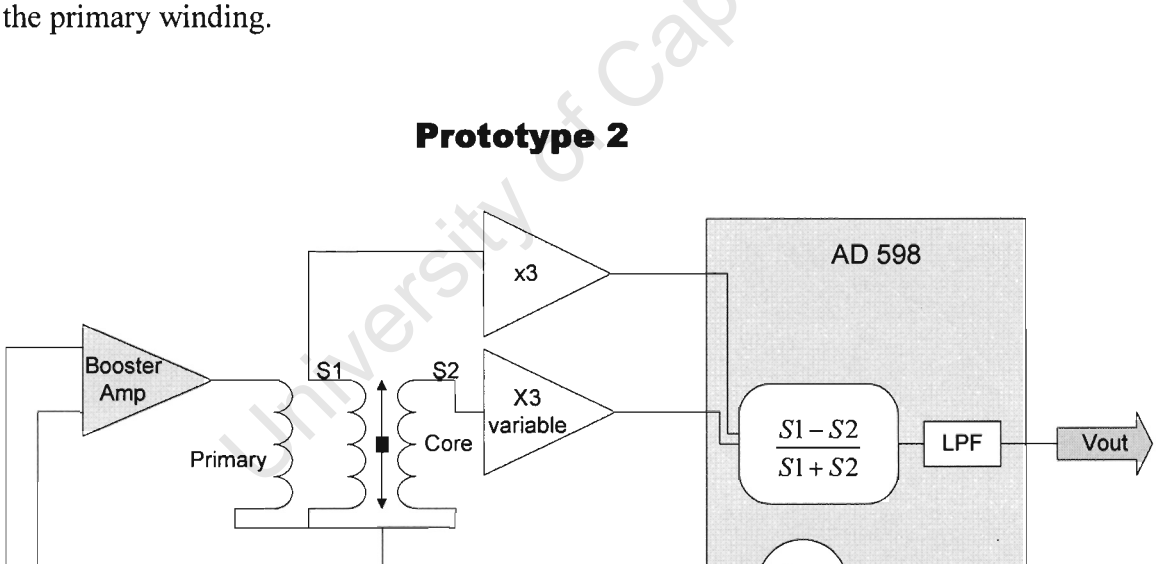

Figure 28 Functional block diagram of P2.

9.5.1 Pre-amp for secondary signals

A pre-amp was added to each of the secondary windings. These amplifiers serve two purposes. The first is to amplify the secondary signals, approximately 3 times amplification, to get them into the optimum operating range of the AD598 device. The input signals to the AD598 should be between 1 and 3 Vrms for optimum linearity and minimum noise susceptibility.

The second purpose that the pre-amps serve is to allow for null-point adjustment. One pre-amp has fixed gain whilst the other has adjustable gain. When the amplification of one secondary signal is changed, the position where the core causes identical secondary signals (the null point) changes. This null point adjustment function is particularly useful when a non-symmetrical core is used.

9.5.2 Excitation booster amplifier

The output stage from the AD598 is designed to drive the primary side of an LVDT with up to 30mA of primary current. LVDTs typically have thousands of turns on their primary winding, resulting in relatively large inductance. The windings of the PCLT are planar; they are printed concentrically on a PCB plane. This means that the maximum number of windings depends on the track thickness and spacing. The version 2 PCLT layout consists of a total of 30 turns, 15 each on 2 layers, and thus has a much lower inductance than an LVDT. This load appears as a short circuit to the AD 598 output amplifier, and thus a more powerfull booster amplifier was required to drive the PCLT primary winding.

9.5.3 Prototype 2 circuit diagram

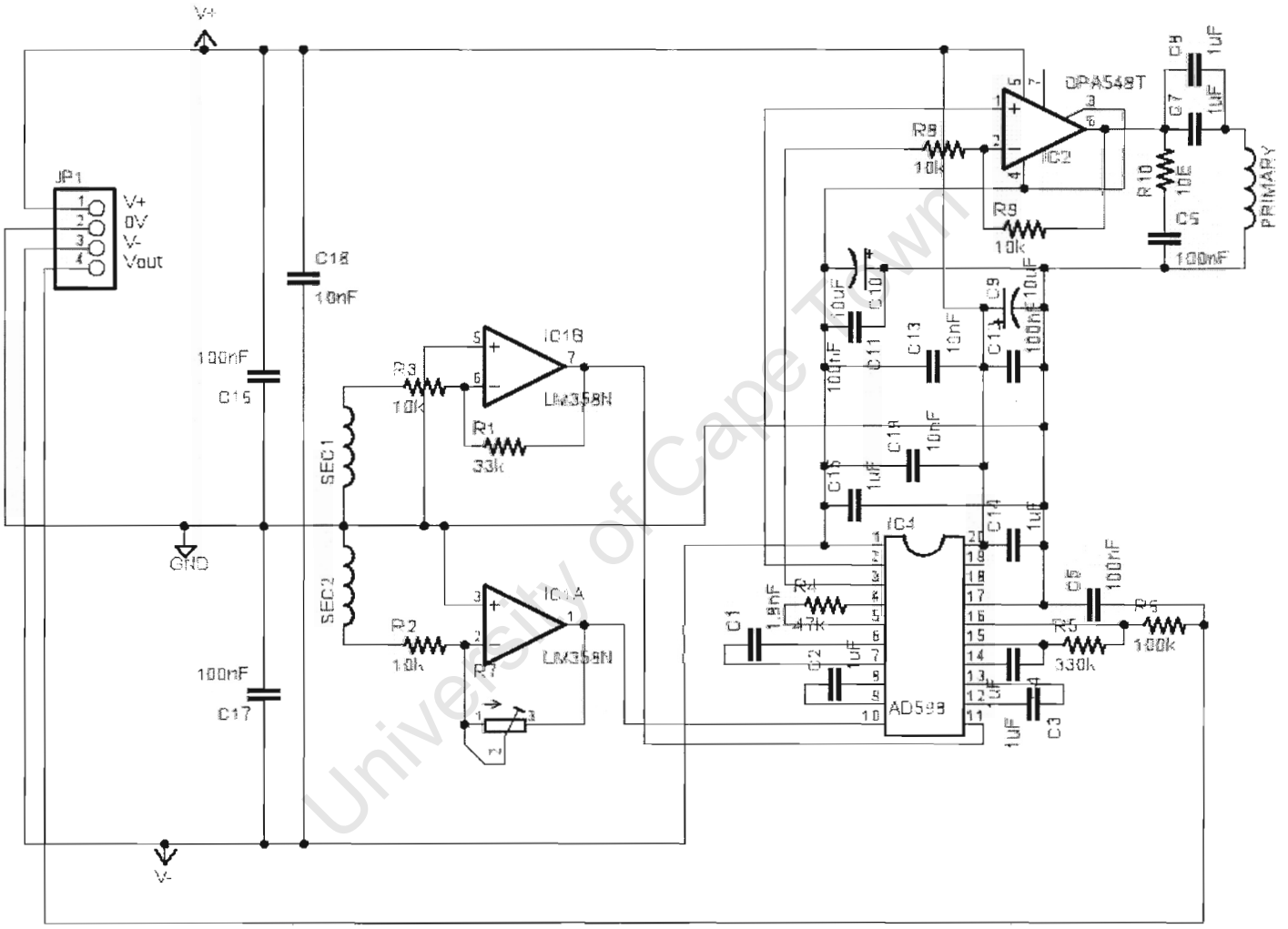

Figure 29 Prototype 2 circuit diagram.

9.6. Prototype 3 – discrete component self-synchronous demodulation

Prototype 3 uses the same primary excitation elements as Prototype 1; a sine wave oscillator and power amplifier. The difference of the two AC secondary waveforms is calculated with an AD620 instrumentation amplifier (ideal for its high CMRR), and then synchronously demodulated with an AD630 balanced demodulator and low pass filtered with a Sallen-Key 4 pole Butterworth filter. An adjustable gain output amplifier allows for full scale output adjustments.

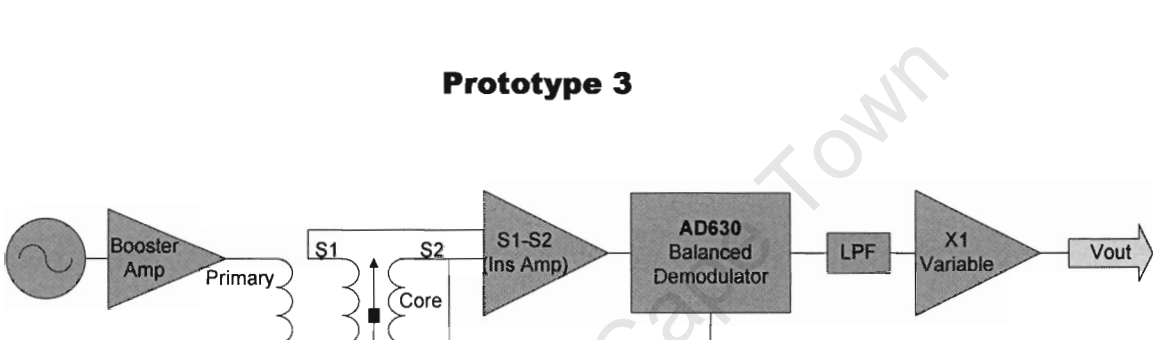

Figure 30 Functional block diagram of P3.

9.6.1. Self-synchronous demodulation

Normally, synchronous detection uses the primary waveform, phase shifted until it is in synch with the secondary waveforms, to demodulate the secondary signal. A simple RC filter network can shift phase by a fixed amount, but when the phase difference between the primary and secondary signals varies, a more complex phase shifting mechanism is required to actively track the phase.

As shown in Figure 30, Prototype 3 does not use the primary signal for demodulation; it uses one of the secondary signals. This technique is referred to as self-synchronous detection [20], and has the major advantage that the carrier signal is always perfectly in synch with itself, so no phase shifting is required. This method can only be utilized

when the magnitude of the demodulating signal is not important to the demodulation process. The AD630 is configured so that the demodulating carrier signal is connected to zero crossing comparator so that only the magnitude of the difference of the secondary signals is considered in the demodulation calculation.

9.6.2. Prototype 3 circuit diagram

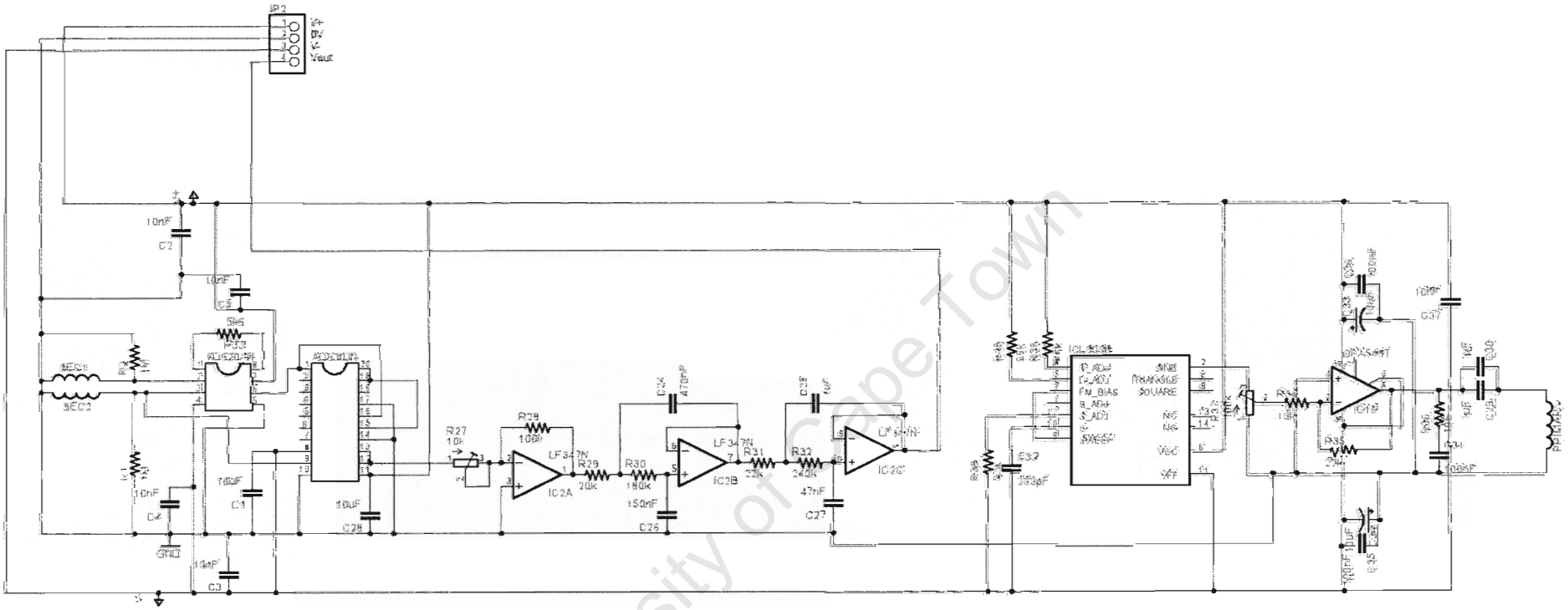

Figure 31 Prototype 3 circuit diagram.

9.7. Prototype 4 – LVDT synchronous demodulating AD698

The circuitry for Prototype 4 is built around the AD698 signal conditioning subsystem. This subsystem uses synchronous demodulation to determine core position and is specifically designed for use with LVDTs. It calculates the ratio of the difference in the secondaries divided by the excitation signal. The ratio-metric stage helps to improve temperature stability and immunity from fluctuations in the excitation waveform. As with Prototype 2, an additional booster amplifier was necessary to drive the low impedance primary winding.

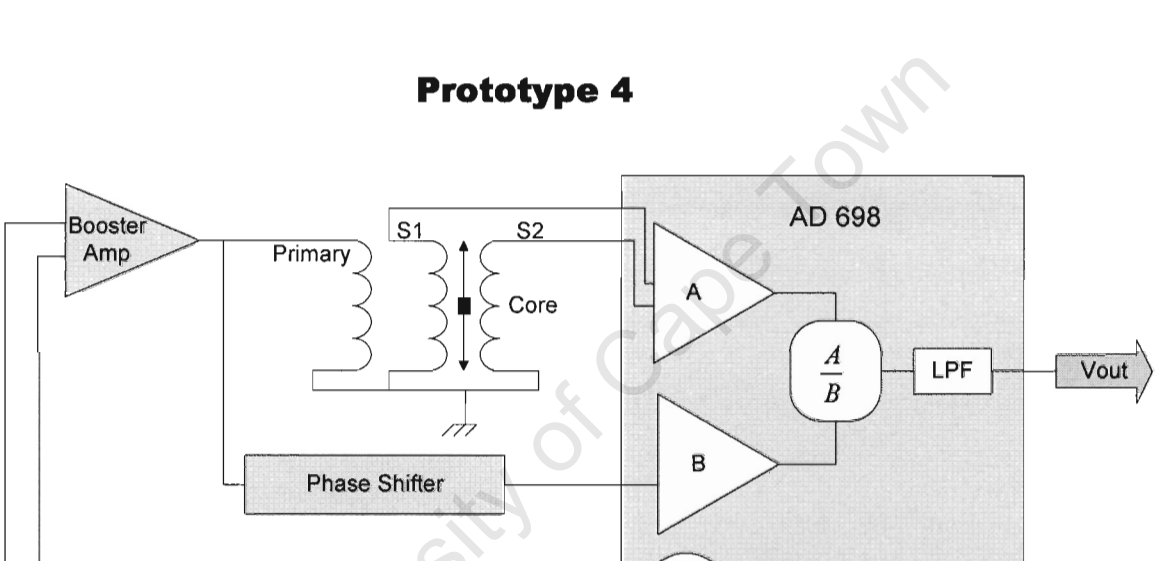

Figure 32 Functional Diagram of P4.

An RC filter is used to shift the frequency of the primary signal so that it is 'normally' in phase with the secondary signals. This is a condition required for accurate synchronous demodulation. However, the phase difference between the primary and secondary signals is not perfectly constant over the full range of core position. There is a shift of up to 3 degrees as the core approaches either end of the sensor when they are configured to be perfectly in phase over the central region of the sensor. Thus this phase shift causes a slight inaccuracy in the demodulation process when the core is near the end points of the sensor. This problem can be overcome with the added complexity of a phase locking system that adjusts the phase shift as necessary.

9.7.1. Prototype 4 circuit diagram

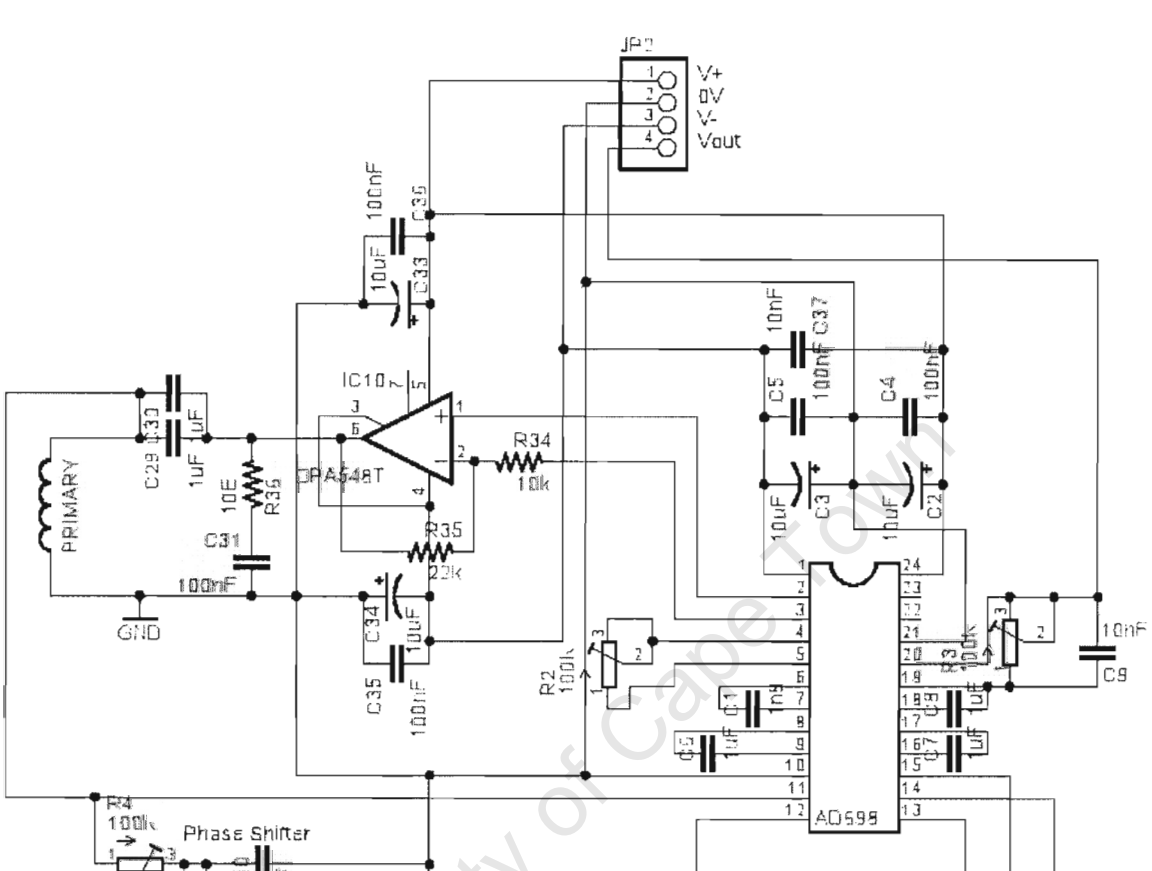

Figure 33 Prototype 4 circuit diagram.

10. Test Rig

Once the prototypes were functioning, their performance needed to be tested. Accurate measurements of sensor properties such as linearity, accuracy, dynamic response, repeatability and sensitivity require precise control of the core position. A test rig based on the design of a lathe was built, with a platform moved by a rotating threaded rod.

10.1. The mechanical structure

Three support rods guide the moving platform, with Teflon bushes that allow it to slide smoothly. The platform is moved by a rotating threaded rod driven by a bidirectional geared DC motor. A shaft (sensor rod) is used to connect the moving platform to the core of the sensor being tested. The advantages of this are that multiple sensors can be connected in-line, and the sensors can be positioned far away from the motor and threaded rod, two likely causes of interference.

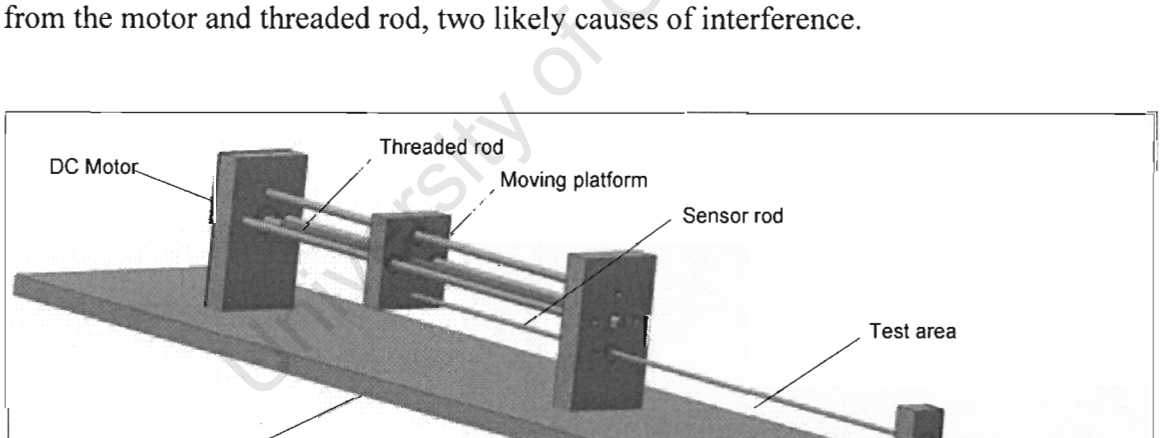

Figure 34 Test Rig Assembly. Overall length 1550mm, width 300mm. The DC motor turns the threaded rod, which in turn shifts the moving platform and the sensor rod that is joined to it.

The entire rig was constructed using non-ferrous metal, with the exception of the threaded rod and the base plate. Non-ferrous metals were used to ensure that the rig would not interfere with the sensors' magnetic fields. The base plate was made out of

mild steel so that it could be used to help shield the sensors from external EMI. The threaded rod was made from steel for cost and availability reasons.

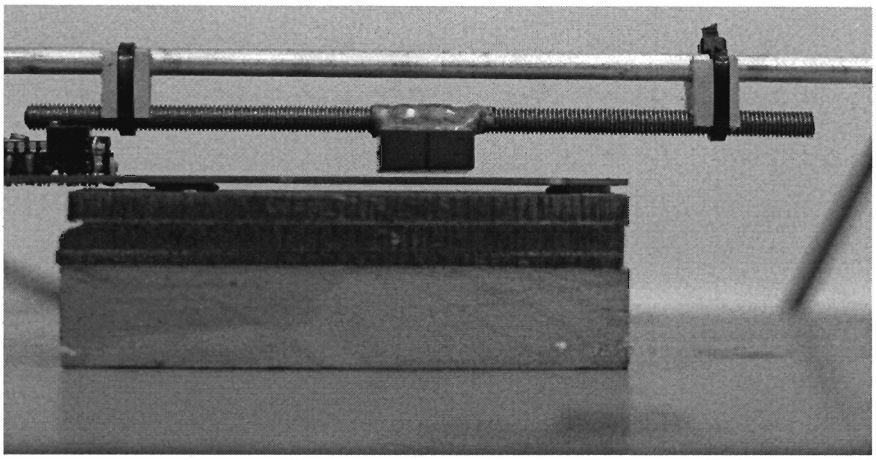

Figure 35 Photograph of PCLT with core mounted on test rig sensor rod.

10.2. Speed control

Unfortunately, the threaded rod was not perfectly straight, so movement was cyclically non-constant. Constant speed of core position change was required for dynamic linearity testing. In an attempt to overcome the non-constant speed problem, a rotational speed sensor was added, and used in a feedback circuit to control the voltage applied to the motor.

A 36 toothed slotted wheel mounted onto the test rig threaded rod was used to interrupt an infra-red beam which triggered a fixed width pulse one-shot with every 10 degrees of rotation of the threaded rod. Low pass filtering the one-shot pulse train produced a DC voltage proportional to the speed of the moving platform.

The speed controller reduced fluctuations in rotational speed, but did not eliminate the problem. An improvement to the rig was called for.

10.3. Modifications to the rig

The threaded rod came from a 6 m length, and its straightness was compromised by storage and handling. A new threaded rod was machined from a thicker 20mm rod. A 50mm long nut was fitted into the moving platform to make the joint more sturdy. This helped to make the movement more constant; however cyclical movement was still observed in some of the test results.

10.4. Accurate reference position measurement

In order to test the PCLT, an independent position measurement system was necessary, so that the PCLT's position output could be compared to the "actual" position of the core. This measurement system had to be more accurate and have better resolution than the PCLT, otherwise the tests results would be compromised by the reference measurements.

A standard 20mm stroke LVDT offers an accuracy of 10μm [21]. This figure was used as an estimate for the required resolution of the reference position measurement. A shaft encoder was mounted onto the free end of the threaded rod, as this would achieve the required resolution without obstructing the PCLT test area. The threaded rod acted as a worm gear, so that one full revolution corresponded to 1.5 mm (the pitch of the thread) of linear movement. The encoder was configured to give 180 rising edge triggers for every full revolution, and was thus able to measure discrete step intervals of 8.3 μm (1.5mm/180). The encoder's pulse train output was counted using a DM302 PC interface card. A data logging program was created using DT Measure Foundry, to count encoder pulses and read in PCLT V_{out}, and synchronously log these values to an Excel workbook.

11. Magnetic Field Around the PCLT

The magnetic flux that is produced in the primary winding and proportionally coupled to the secondary windings is a fundamental component of PCLT operation. This chapter investigates the density and distribution of the magnetic flux that is produced by the primary winding.

11.1. Method of magnetic field detection

A KMZ10A 'Magnetic Field Sensor' made by Phillips was used to measure the magnetic flux density of the field around the PCLT windings. This is a magnetoresistive type sensor that uses a thin-film ferromagnetic material whose electrical resistance is influenced by an external magnetic field [22]. The sensor utilizes a 'Barber pole' configuration to ensure linear response to the magnetic field strength. It is capable of operation up to 1 MHz, more than adequate for measuring the 20 KHz field generated by the PCLT.

11.1.1. Initial circuit configuration

Initially, the magnetic field sensor was connected to an instrumentation amplifier and the output was rectified and low pass filtered to obtain a DC voltage proportional to the magnetic field density.

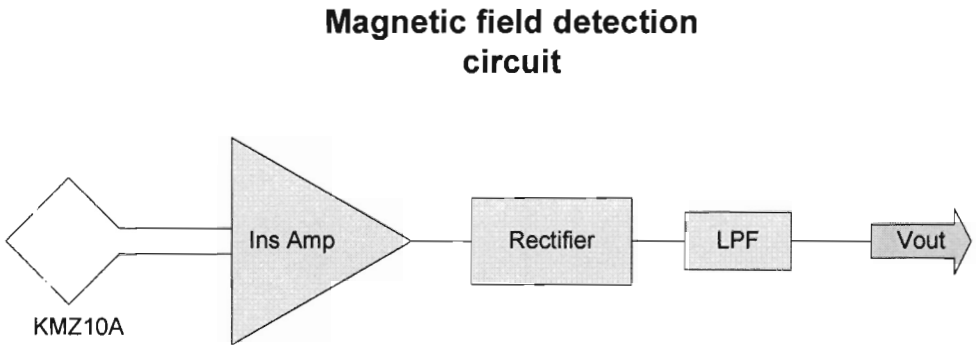

Figure 36 Circuit to measure the magnetic flux density of the field generated by the primary winding.

This circuit was effective at detecting the magnetic field strength. A shortcoming was that it also detected a background field generated not by the PCLT, but rather by one of the steel support beams of the test rig that had become magnetized.

11.1.2. Improved circuit configuration

Introducing a 4 pole Chebychev band pass filter between the instrumentation amp and the rectifier allowed for all non-20 KHz background fields to be eliminated.

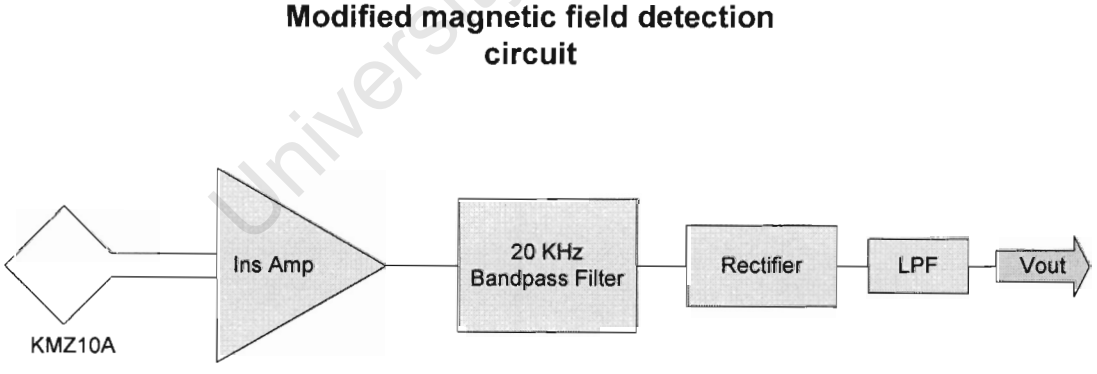

Figure 37 Modified circuit to eliminate magnetic field effects at all but 20 KHz.

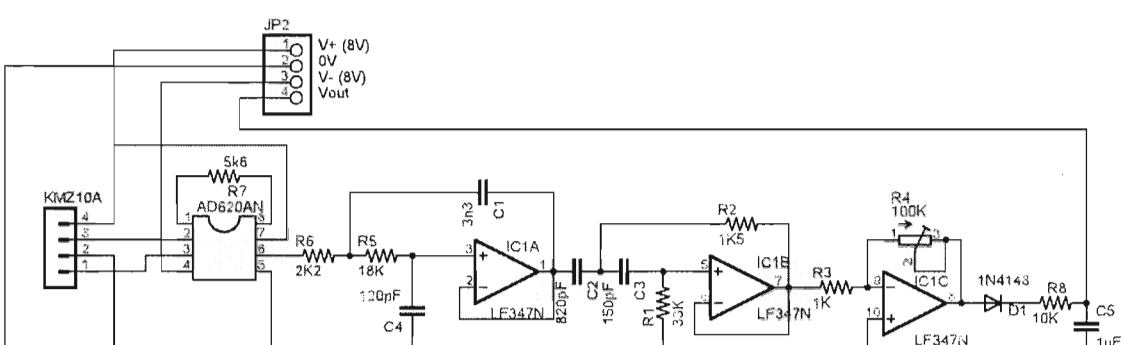

Figure 38 Magnetic field sensor circuit diagram.

The sensor was not calibrated to measure actual field intensity; it was used to give an indication of the relative field intensity over the test area.

11.2. Magnetic field results – measured lengthways

The magnetic field sensor was mounted onto the test rig such that the detecting face was 2mm away from, and parallel to, the PCLT PCB and therefore perpendicular to the magnetic field lines. The test rig was used to run the field sensor along the full length of the PCLT primary winding. The field sensor detecting face is approximately 5mm by 5mm, and was positioned at various y co-ordinates across the PCLT sensor area.

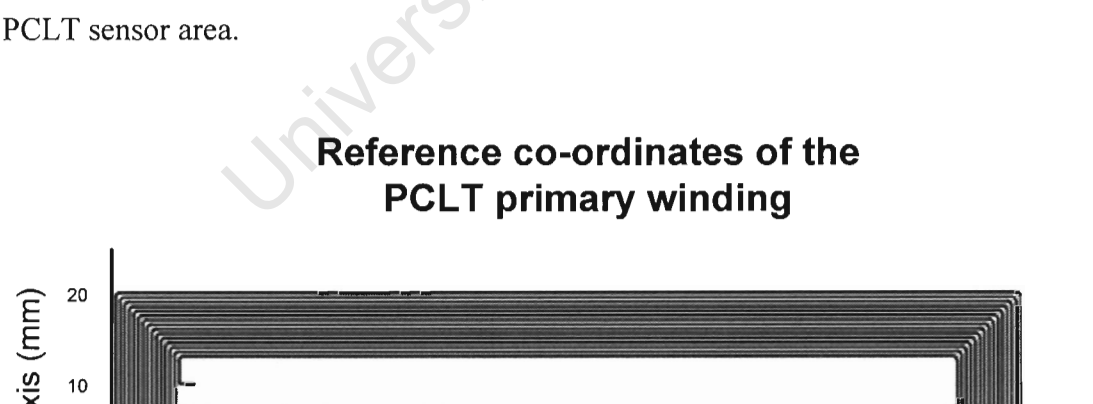

Figure 39 PCLT primary winding with reference axis and dimensions in mm.

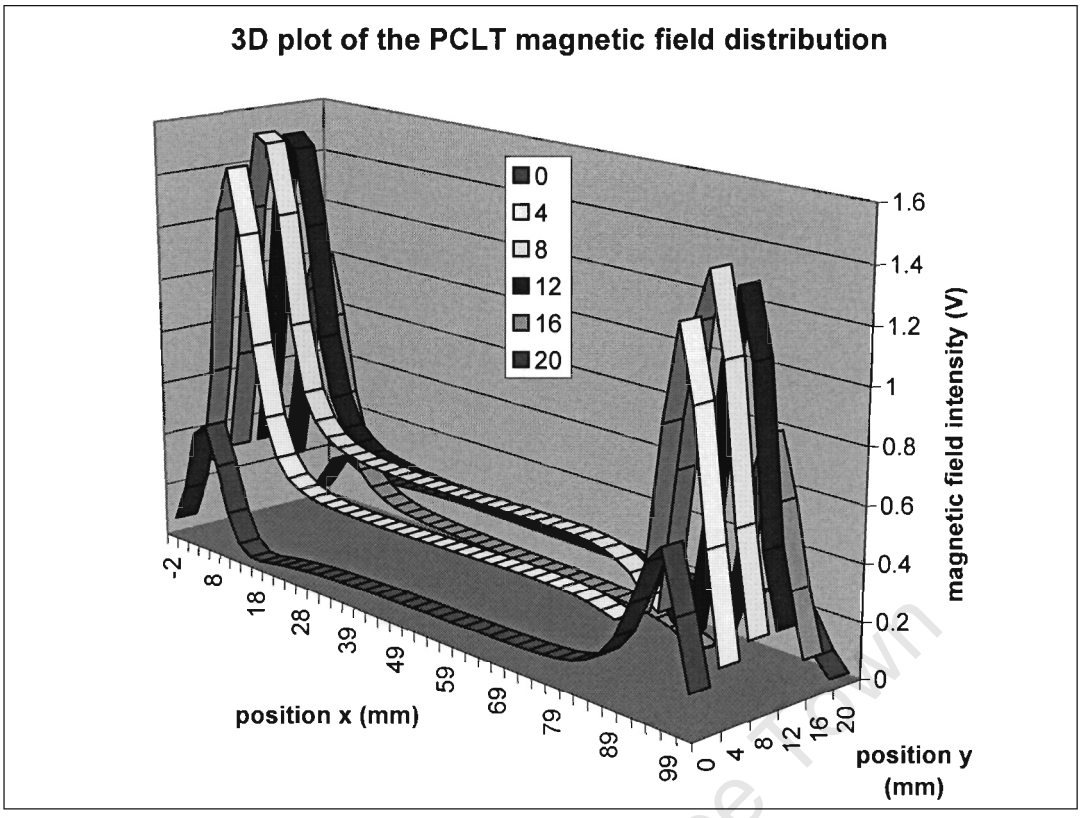

Figure 40 Plot of flux density in volts. Each strip represents a single run at the y co-ordinate indicated in the legend.

The results show a constant intensity along most of the length of the primary winding. This is a positive sign as it indicates a consistent magnetic field strength over most of the PCLT sensing area. The end points of the primary winding, where the coils turn, cause large peaks in the magnetic field strength. These magnetic hot-spots could cause non-linearity in the PCLT near the end points. Two other 3D graphs of the results from different perspectives are included in Figure 41 and Figure 42.

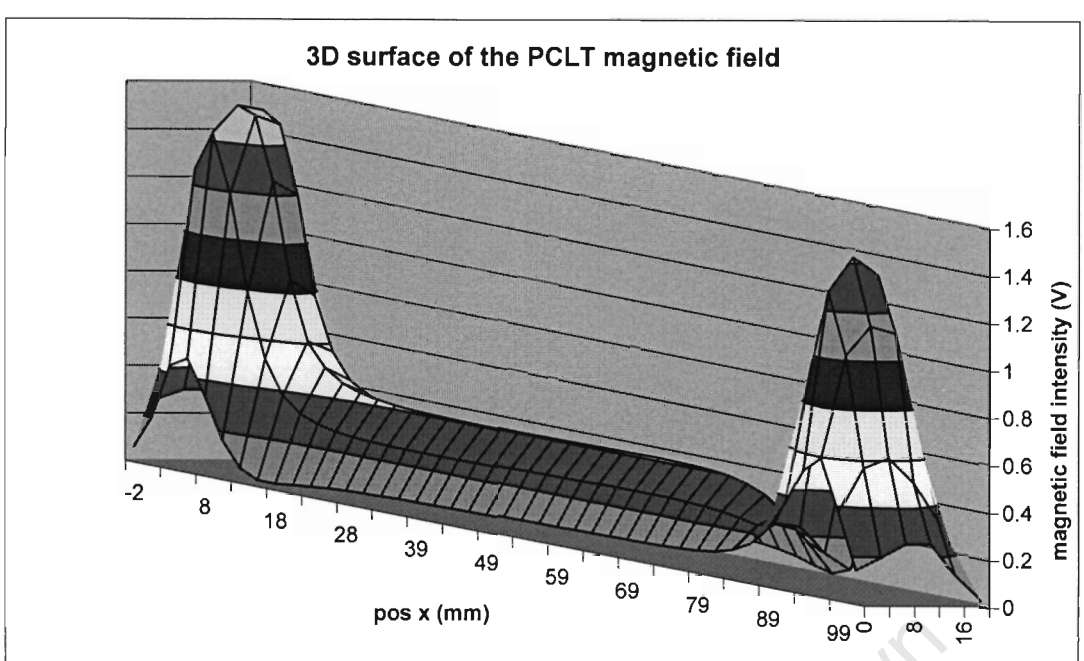

Figure 41 An elevated, oblique view of the 3D surface of the magnetic field above the PCLT primary winding.

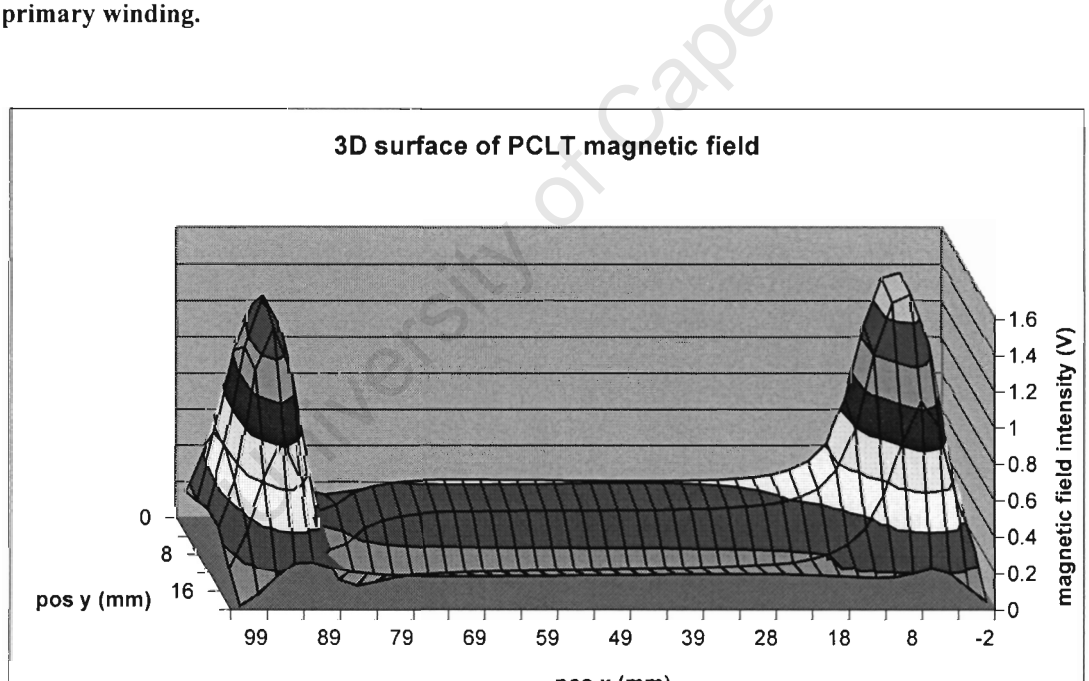

Figure 42 The 3D surface viewed from another angle.

11.3. Magnetic field results – measured crossways

The intensity of the generated magnetic field was also observed with the magnetic field sensor probe moved *across* the windings of the PCLT, along the y axis at different x co-ordinates.

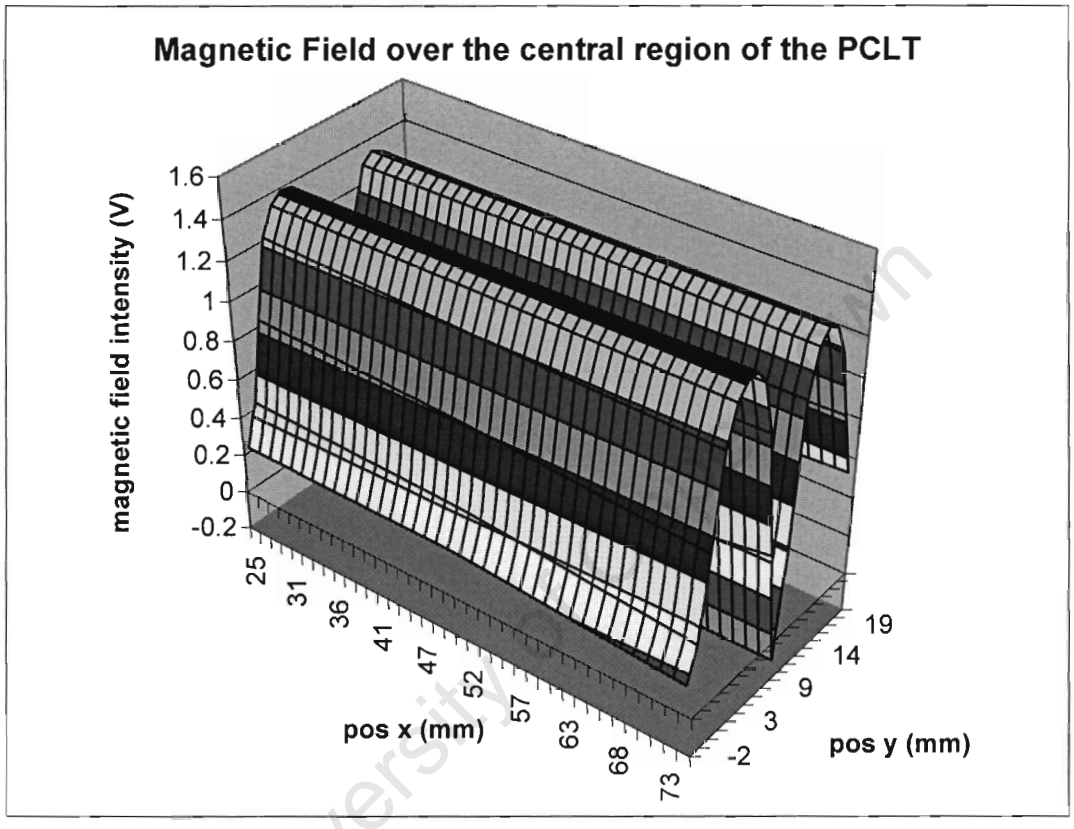

Figure 43 Magnetic field strength results over the x co-ordinate range of 25mm to 75mm, the region where end effects are negligible. The magnetic sensor probe was moved parallel to the y axis.

This result shows an interesting phenomenon. The magnetic flux density drops extremely quickly away from the actual tracks of the primary coil, so much so that at the centre of the narrow gap between the primary tracks, specifically 5mm from the inner track of the primary winding, the magnetic flux intensity is close to zero.

The varying of field strength across the windings should not adversely affect PCLT operation, as the core is the width of the windings, and so the differing magnetic flux densities should be averaged out. Figure 43 confirms the consistency of the magnetic field density in the direction of the x axis.

11.4 Summary of the magnetic field distribution

The magnetic field intensity over most of the sensor area, in the direction of the x axis, is constant. The end effects of the windings cause a large increase in magnetic flux, which will likely affect the primary to secondary coupling of the PCLT near the end points, ultimately resulting in non-linear performance. The magnetic flux density decreases rapidly with separation distance from the physical turns of the primary winding. The difference in field shape between Figures 41/42 and 43 is due to the different orientations of the vector type magnetic field sensor in the different tests.

12. PCLT Test Results

A test routine consisting of 10 tests was carried out on each of the 4 prototypes. These tests investigate the linearity, steady state stability (noise and drift over 2 minutes, 10 minutes and 12 hours), resolution, sensitivity and repeatability. The results are presented as a comparison of prototype performance for each test; the complete test data is included on the Data CD. All tests were carried out at 20 KHz, with Version 2 windings, with the ferrite slab core. The sensor output voltage was logged using a PC data acquisition card. No shielding was used.

The ferrite surround core should produce better results than those recorded in this chapter, but was not used because of a problem with mounting the PCLT and surround core on the test rig. Findings in the previous chapters indicate that improved performance should come with a higher operating frequency, but all the prototypes were operated at the same frequency to ensure accuracy in comparison of the different circuit approaches of the prototypes.

12.1. Linearity

The linearity of the sensor was tested by moving the core at a constant rate from one end of the sensor to the other, and the actual core position was recorded along with the sensor output (measured core position) at 250 ms intervals. The relationship between the measured and actual position readings indicates how linear the sensor is. The linearity was tested for the "full range" of the sensor and the "over range". Calculations are made on the data to determine the linearity as a quantifiable amount for comparison between prototypes, and with existing sensors.

12.1.1. Full range linearity test

The full range is defined as the entire region which is fully encapsulated by the primary windings.

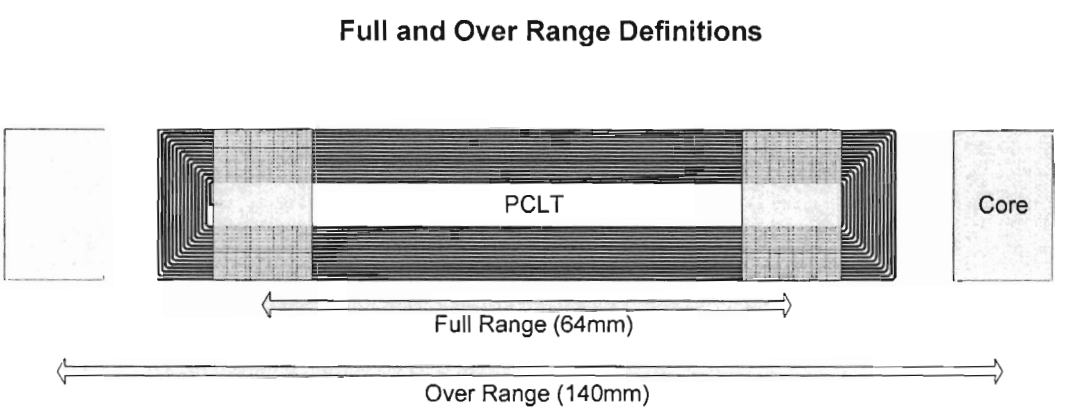

Figure 44 Range definitions. The full range is until the core touches the innermost turn of the primary winding, 64mm. The over range goes past the ends of the sensor, 140mm.

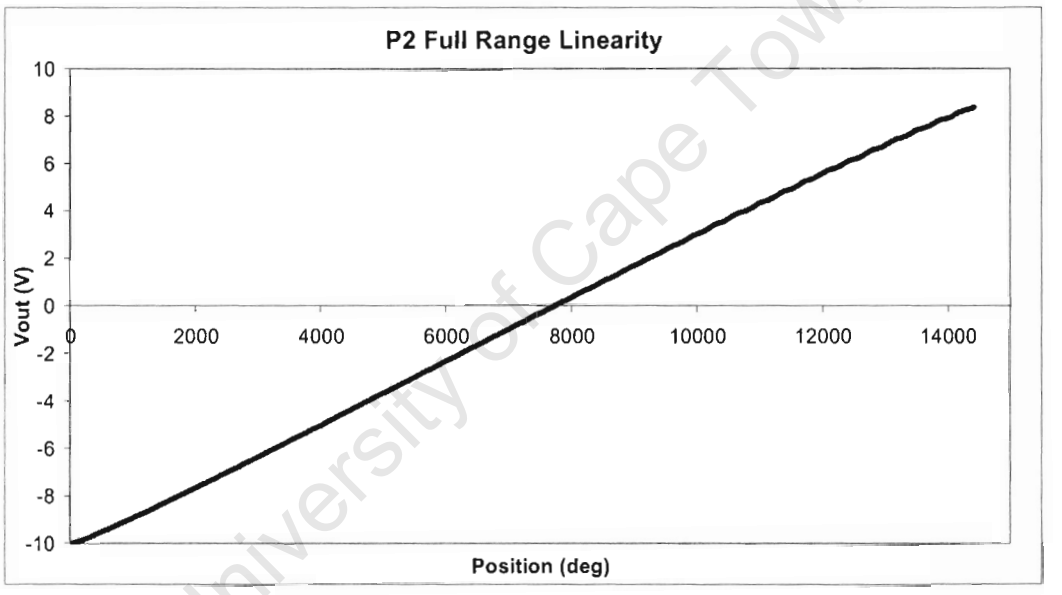

Figure 45 Full range linearity test for Prototype 2. The result shows good overall linearity with a slight 's' shaped curve around the quarter and three quarter regions.

The graph in Figure 45 exhibits a linear trend over the full range. The full range results from the other 3 prototypes show a very similar shape, and can be found on the Data CD. The stroke-to-length ratio of PCLT (operating on its full range) was 64%. The total length of the windings was 100mm, and the linear stroke length was 64mm. The core used was 20mm wide. If a narrower core were used, the linear stroke length could be increased.

12.1.2. Over range linearity test

The over range test differs from the full range test in that here the core is moved from outside the field of effect of the sensor, across the full length and past the other end. This is a useful test in that it gives an idea of what happens as the core moves beyond the limits of the sensor.

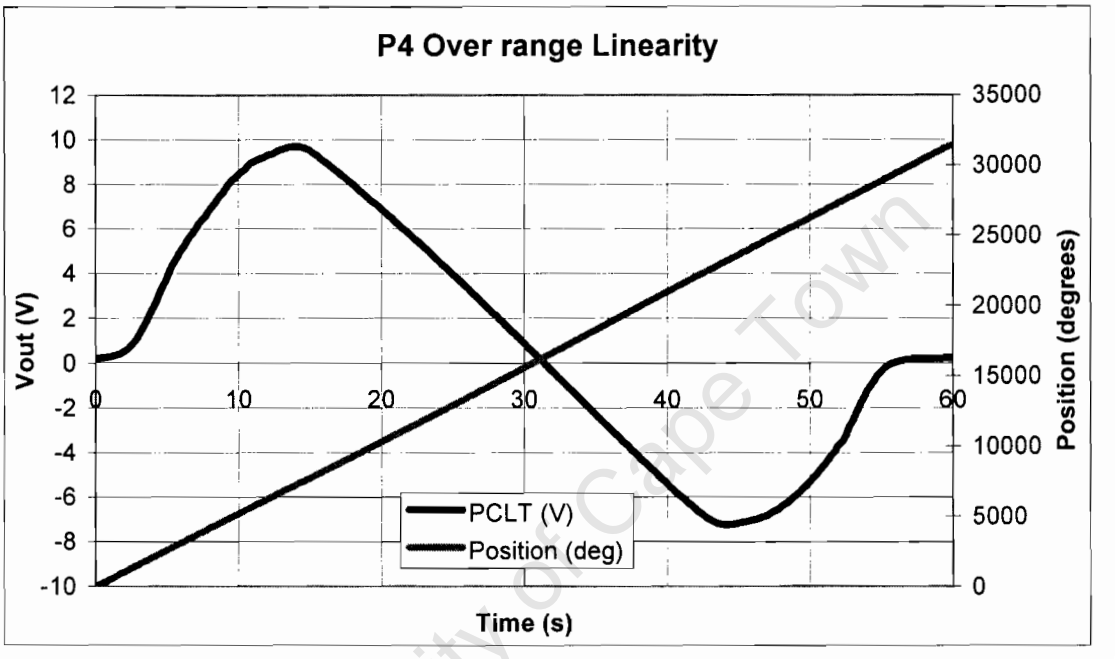

Figure 46 P4 V_{out} and actual core position plotted vs. time. The slight fluctuations in the position line illustrate how the test rig's movement was not perfectly constant. As the core moved out of the field of influence of the sensor, the output voltage went to zero.

In Figure 46 the actual and measured core position was logged with time. The position curve is a straight line, indicating the constant speed of the core. The darker V_{out} curve shows that at the end positions the core had no effect on the windings and the voltage was zero.

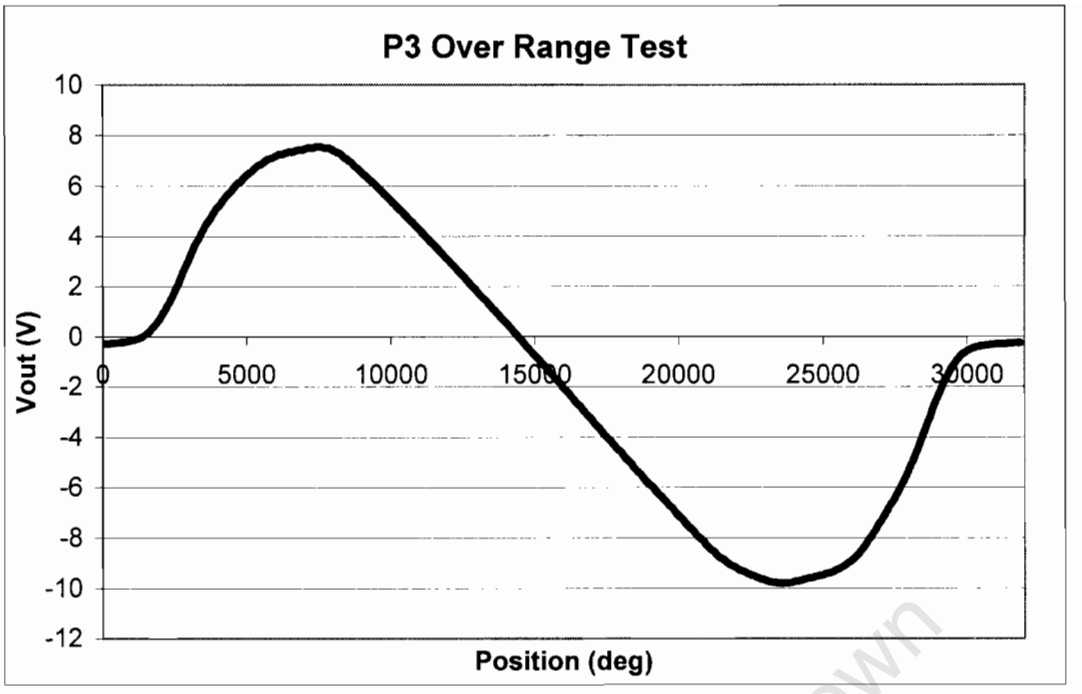

Figure 47 P3 over range test, V_{out} vs. position. The output is linear over the central region of the sensor, and there is good symmetry in the voltage drop off at both ends of the sensor.

When V_{out} is plotted against the actual position, as in Figure 47, the curve shape is similar to that of V_{out} versus time, as in Figure 46, because the test was carried out at close to constant speed.

The precise and repeatable shape of the response past the sensor end points suggests that the PCLT could be used to measure displacement over a range longer than the full range, if linearization techniques were applied to the output voltage. The sensor can detect the core position and produce an output signal beyond the full range, up to the turning points of V_{out} in Figure 47. This is a sensible range of 16200 degrees, or 68mm. The maximum stroke-to-length ratio of the sensor is thus 68%, but includes the non-linear turning points. The stroke-to-length ratio of the PCLT could be increased by using narrower core. However, this reduction in core size may affect the sensor's performance.

12.1.3. Quantifying the linearity

The graphs offer a visual indication of how linear each prototype is, but this is not enough for accurate comparisons between the different sensors. It was thus necessary to develop a quantifiable measure of the linearity.

12.1.4. Rate of change of voltage with position

The range over which the derivative of the output voltage is constant is the range over which the sensor is linear. Data from the over range test was used to calculate the derivative of the voltage with respect to position (dV/dp) at each point.

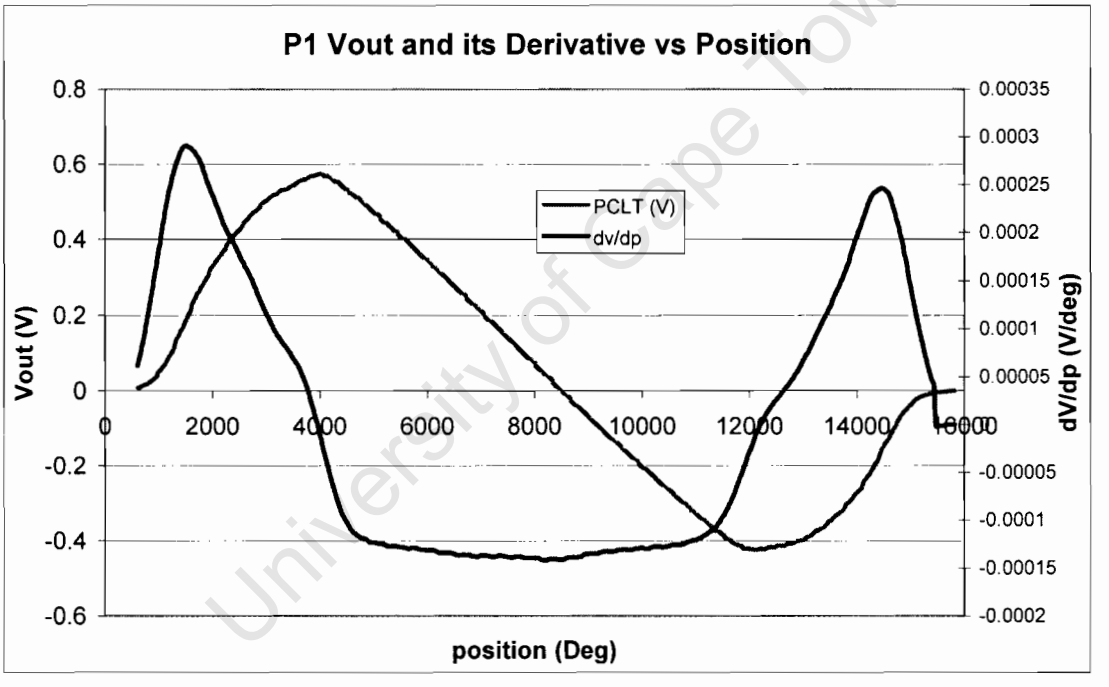

Figure 48 Derivative of V_{out} with respect to position. The linear region shows an almost constant gradient that decreases slightly towards the center and increases slightly as the core moves away from the center.

The derivative in Figure 48 was calculated using upper and lower 11 point averaging windows separated by 11 data points. The result illustrates that the sensor is reasonably linear almost all the way to the V_{out} turning points at the ends of the sensor.

The shape of the derivative curve illustrates that the gradient of the PCLT Prototype 1 output voltage is decreasing as it approaches the centre (null position), and is

increasing as it passes the centre, thus indicating a symmetrical nonlinearity in this sensor.

12.1.5. Maximum deviation from best fit

A convention for quoting the linearity of a displacement sensor is as the maximum deviation of the output from its best fit (least squares method) line. This can be expressed as a percentage of full scale (% FS) output or as a distance. This means that if a sensor is quoted as having a linearity of 10 μm, then *at worst* over the whole range, there is a 10 μm error due to non-linearity.

The best fit line is found using linear regression. The vertical displacement between the actual curve and the best fit line is called the deviation; the maximum deviation is quoted as the worst case linearity. The linearity was calculated for full range and for two reduced ranges, as the most non-linear behavior was expected to occur at the extremes of the full range where the end effects of the primary winding and the change in primary inductance are most prominent.

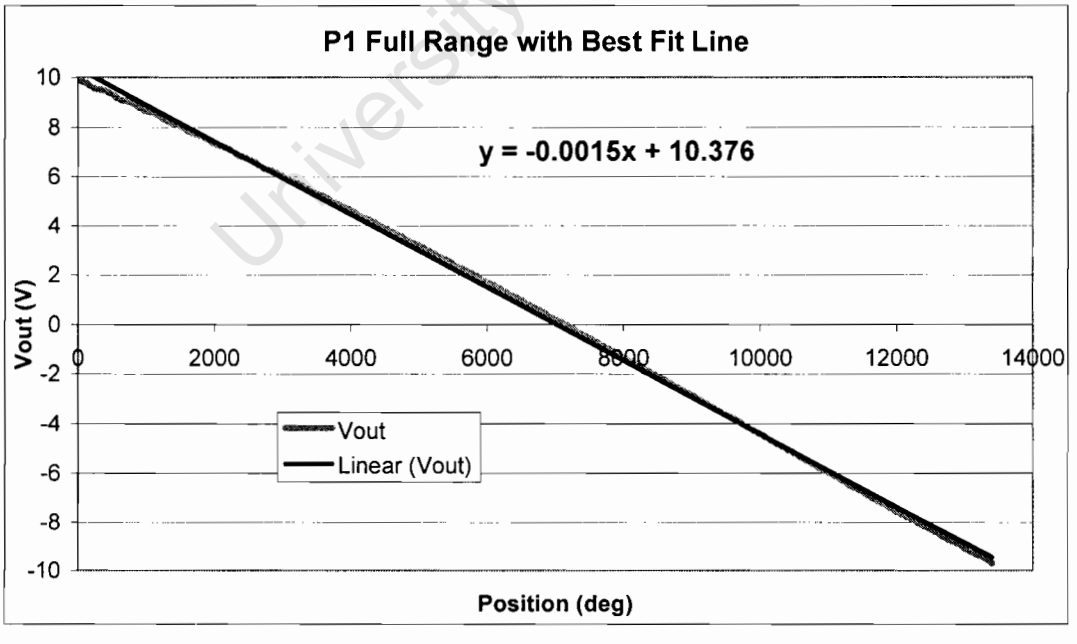

Figure 49 P1 Full range with best fit straight line. The sensor output and the best fit straight line lie almost on top of each other. Towards the sensor ends the output is slightly lower than best fit, and at the center, slightly higher.

	Full Range		90% of Full Range		50% of Full Range	
	% FS	Distance (μm)	% FS	Distance (μm)	% FS	Distance (μm)
P1	2.38	1522	1.688	1080	0.584	374
P2	1.72	1098	1.323	847	0.347	222
P3	2.204	1411	1.248	799	0.396	253
P4	0.979	627	0.919	588	0.178	114

Table 3 Record of linearity of each prototype over different ranges. Prototypes 2 and 4 show superior linearity.

Prototypes 2 and 4 show the best linearity over the full range and the 50% range. Prototype 3 shows the second best linearity performance over the 90% range. The linearity over the 50% range was markedly better than over the 90% range, which was markedly better than the linearity of the full range. This confirms that the sensor is most linear at the center, and the linearity degrades as the range increases.

12.2. Steady state stability

Steady state stability refers to how steady the output signal from the sensor is with the core not moving. Ideally a sensor would give an unvarying output for a fixed core position. However, actual sensors experience both noise (high frequency random fluctuations) and drift (low frequency output variance often with a trend in one direction, caused, for example, by temperature change).

12.2.1. Altering the duration and sample rate

Three different tests were carried out to determine the stability of the prototypes. In all three tests, the core remained at a fixed position, and the output voltage was logged with time. The duration of the first test was 2 minutes and data was logged at 250 ms intervals. The second was 10 minutes logged at 1 second intervals, and the third was 12 hours logged at 1 minute intervals.

These 3 tests were used to identify the noise and drift as separate elements. Here, the results from Prototype 1 are used to illustrate how the summarized results in Table 4 were calculated. The graphs and data for the other prototypes are included on the Data CD.

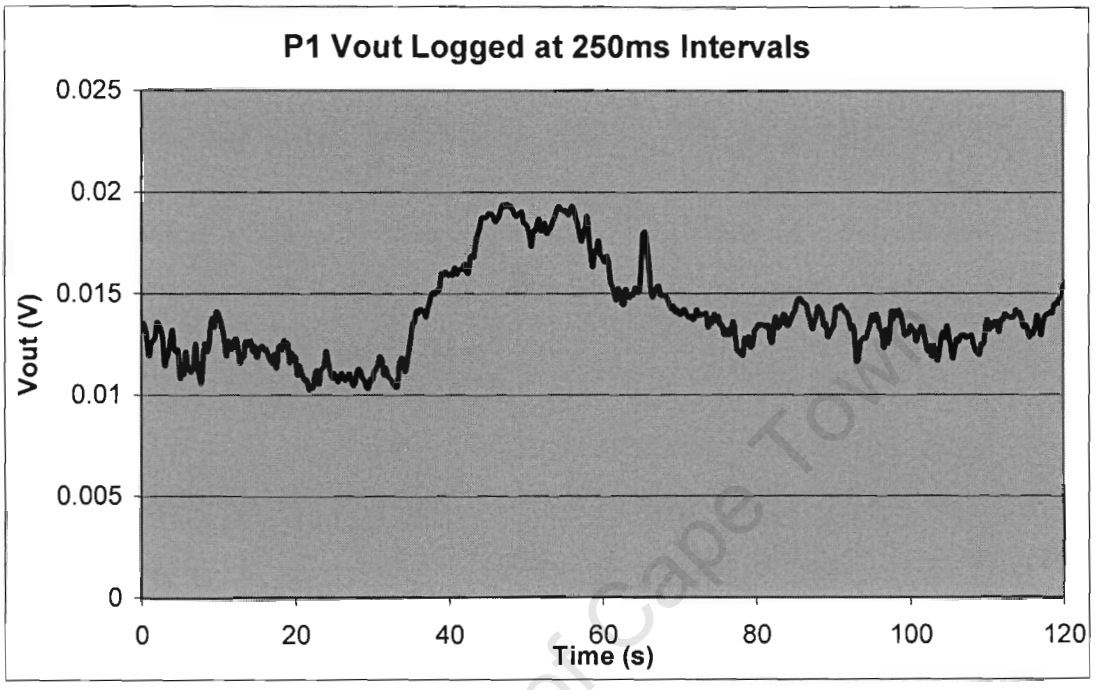

Figure 50 P1 steady state test over 2 minutes. The output shows a maximum change of just less than 10 mV.

In Figure 50 the output voltage of Prototype 1 is shown, and can be seen to vary over a range of just less than 10 mV.

$$MaximumSignalVariation = V_{max} - V_{min} \qquad (10)$$

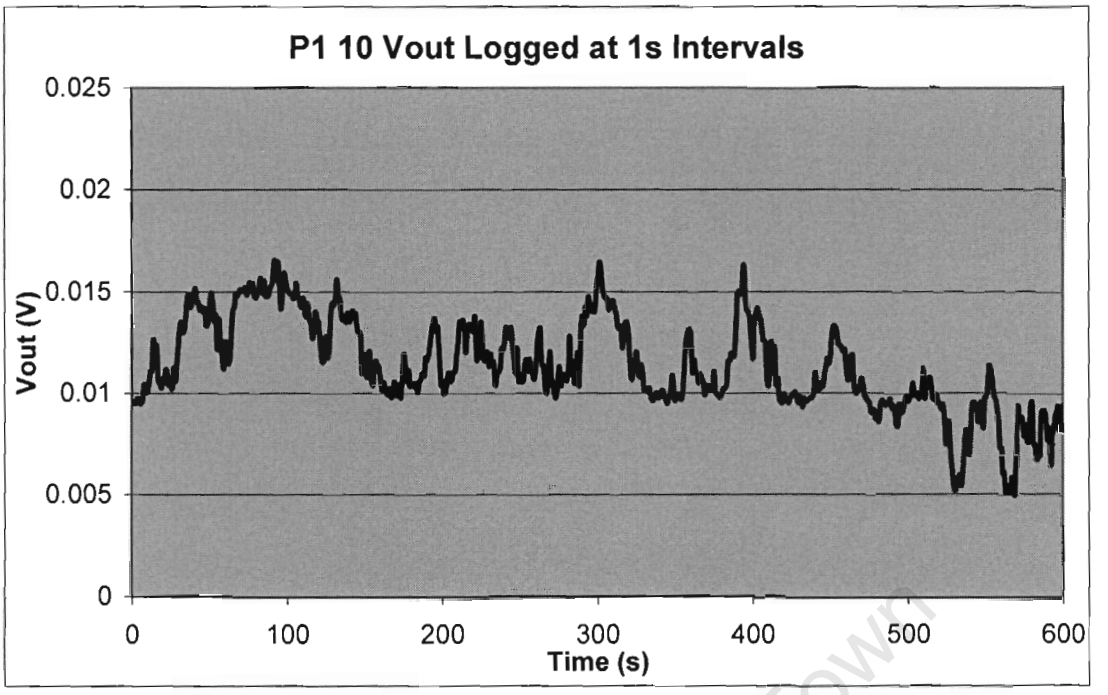

Figure 51 P1 10 minute stability test, showing a maximum signal variation of 12 mV.

When the test time was increased to 10 minutes (shown in Figure 51), the signal variation increased slightly to about 12 mV.

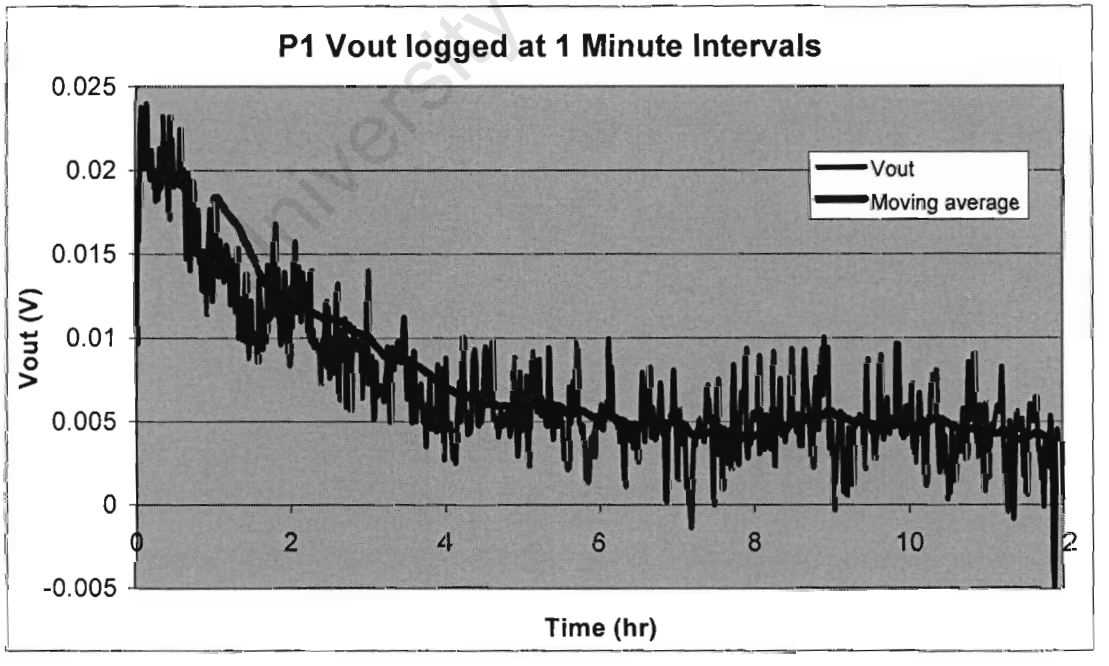

Figure 52 P1 12 hour stability test. There is 10 mV of noise and a general decreasing trend in the average of the output, most likely a temperature related drift.

In Figure 52 the moving average line represents the recorded data without noise (assuming that noise is random and therefore on average zero). The maximum signal variation is 30 mV, yet the noise is 10 mV peak to peak, and the drift is 15 mV. The drift is taken to be the maximum change in the average value over the test period.

12.2.2. Summary of stability test results

Below is a table which lists the critical values concerning signal stability for each of the four prototypes, which were extracted from the test data included on the Data CD.

	Total Signal Variation			**Noise**	**12 hr Drift**
	2 min	***10 min***	***12 hr***	**(pk-pk)**	
Prototype 1	9 mV	12 mV	30 mV	10 mV	15 mV
Prototype 2	4 mV	8 mV	50 mV	10 mV	45 mV
Prototype 3	1 mV	1.5 mV	9 mV	2 mV	8 mV
Prototype 4	0.75 mV	2 mV	2 mV	2 mV	0.5 mV

Table 4 Summary of stability test results for all four prototypes. Prototypes 3 and 4 show superior steady state behavior in all of the steady state tests.

Prototype 4 had the best steady state stability, with 2 mV of noise on the output signal and 0.5 mV of drift over 12 hours. Prototype 3 also had 2 mV of noise, but 8 mV of drift.

12.3. Resolution and sensitivity

The resolution is a measure of the minimum core position change that will produce a detectable change in the sensor output. For this test, the core was moved 10 discrete steps by the minimum detectable amount possible with the test rig, two degrees of rotation or 8.3 μm.

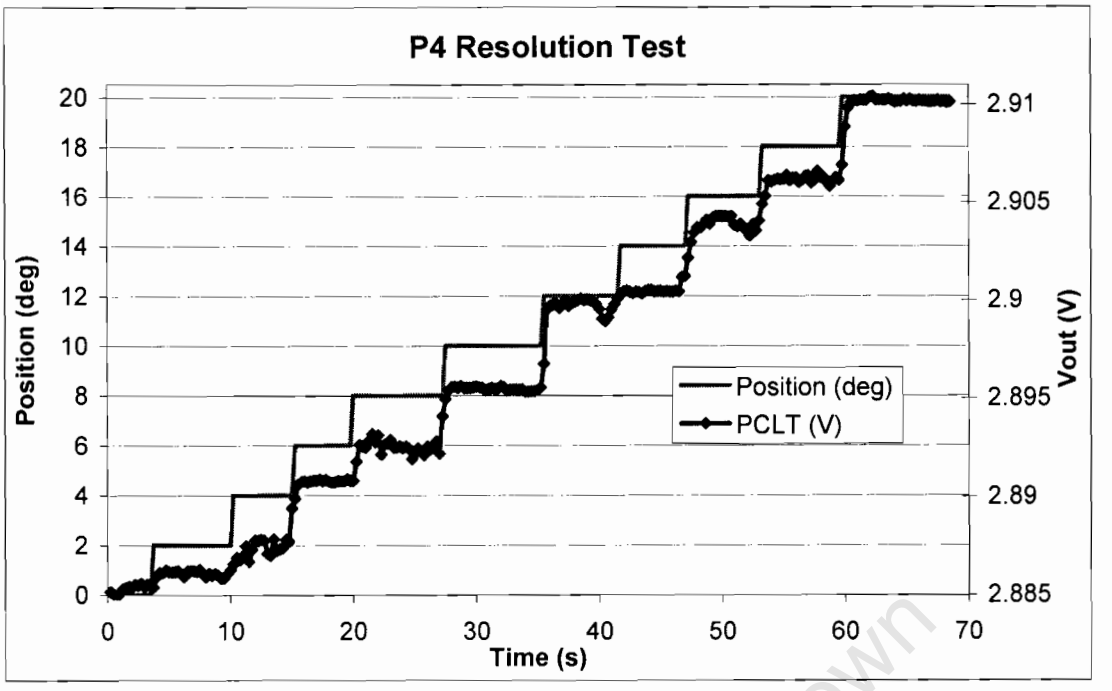

Figure 53 P4 Resolution test, core moved in two degree step increments. With each position step, the PCLT voltage changed, indicating a resolution of at least the position step size, in this case 8.3 µm.

The output voltage changes as the core position is stepped, indicating that P4 has a resolution of 8.3 µm or better. The resolution could not be determined exactly because the maximum resolution of the test rig had been reached. The first position change did not cause much of a change in voltage; this was likely due to limiting factors in the test rig such as friction and backlash or slack in the thread. The same pattern of an undetected first step is apparent in the other prototype results, included on the Data CD.

The resolution test was also done with position changes in 4 degree steps, as the 8.3 µm position change was too small for Prototype 1 to respond to.

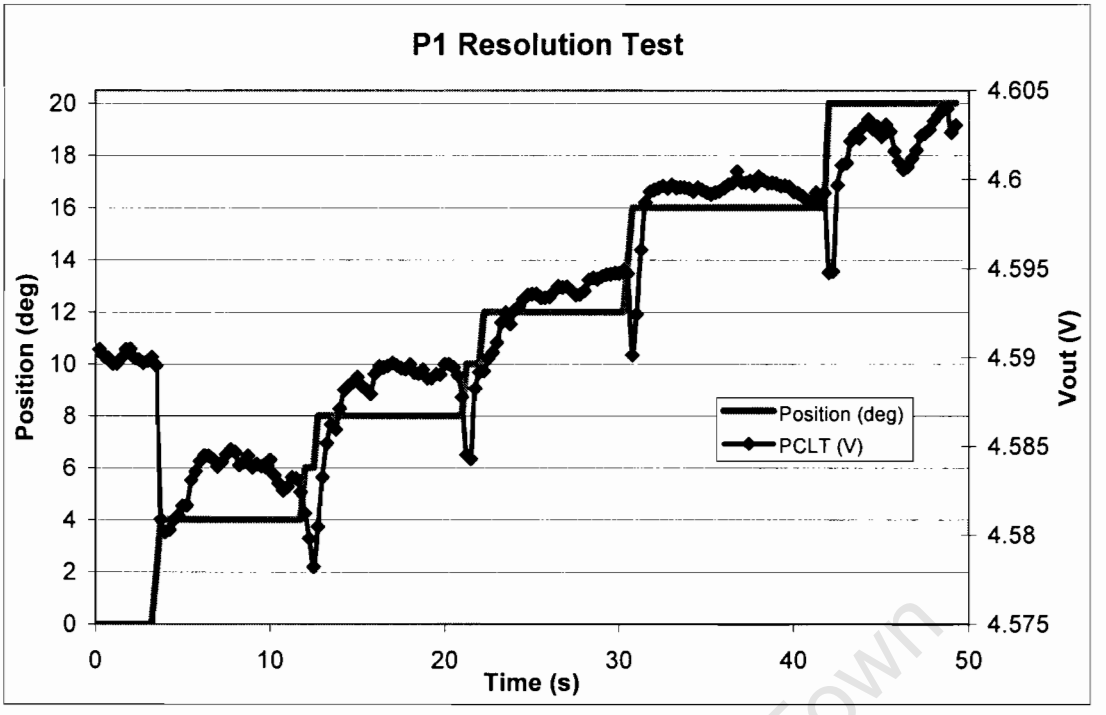

Figure 54 P1 resolution test, core moved in 4 degree steps. The output voltage of P1 changed with core position steps, but a curious downward spike occurred each time the core was moved.

Figure 54 shows the response of P1 to 16.6 μm position changes. As the core was moved, the voltage spiked downwards before rising to its new value. This is unexpected and undesirable behaviour. There appears to be a derivative effect as the core starts to move. A possible reason for this spike is that the circuitry responds to the rate of change of the core position. It is apparent that the downward spikes are a result of the signal conditioning method, namely passive demodulation, for the spikes appear in the P1 and P2 results, but not in the P3 and P4 results.

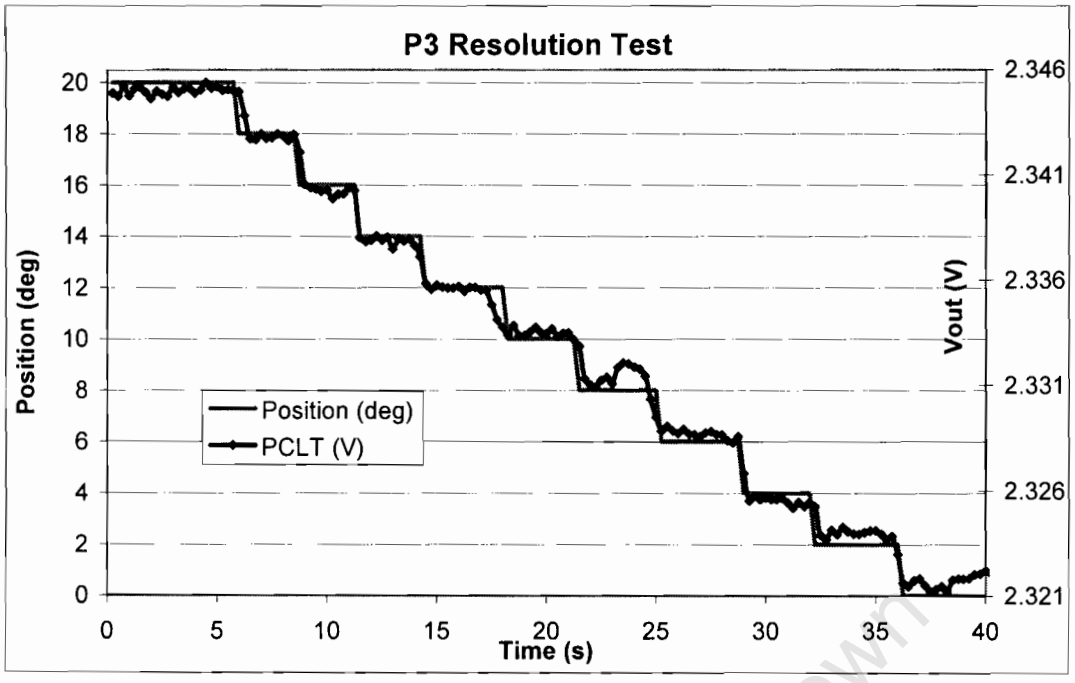

Figure 55 P3 Resolution test, core moved in 2 degree steps. The output shows clear stepping with position changes, indicating that it is capable of even greater resolution.

P3 exhibits reasonably even and well shaped voltage steps in synch with the position changes.

	Resolution	
	(% FS)	(µm)
P1	0.013-0.026	8.3-16.6
P2	0.013	8.3
P3	< 0.013	< 8.3
P4	< 0.013	< 8.3

Table 5 Summary of the resolution of the different prototypes. Prototypes 3 and 4 show the best resolution, better than could be measured by the test rig.

12.3.1. Sensitivity

Sensitivity is a measure of how much the output voltage changes by per unit of displacement. Figure 55 shows that with P3 8.3 µm corresponds to a 3mV output signal change. This is a sensitivity of 0.3125 V/mm. All the prototypes have the same range and output signal of -10 to 10 V, and thus have the same sensitivity. With

the PCLT reconfigured to operate only over its most linear range (stroke of 32mm), the sensitivity is 0.625 V/mm.

12.4. Repeatability

The repeatability is one of the most important performance indicators for displacement sensors. It is a measure of how accurately the sensor can detect a particular position, after having been moved away from and then back to the same position.

To test the repeatability, the core was moved by 2000 degrees of rotation (approx 8.3mm), and then returned to the original position, and this motion was repeated 3 times. The sensor output was compared at the end points of the movement path, namely the 0 degree and 2000 degree positions. The maximum difference between 'same position' readings was given as the worst case repeatability. The test was also done over a 200 degree (0.83 mm) movement cycle.

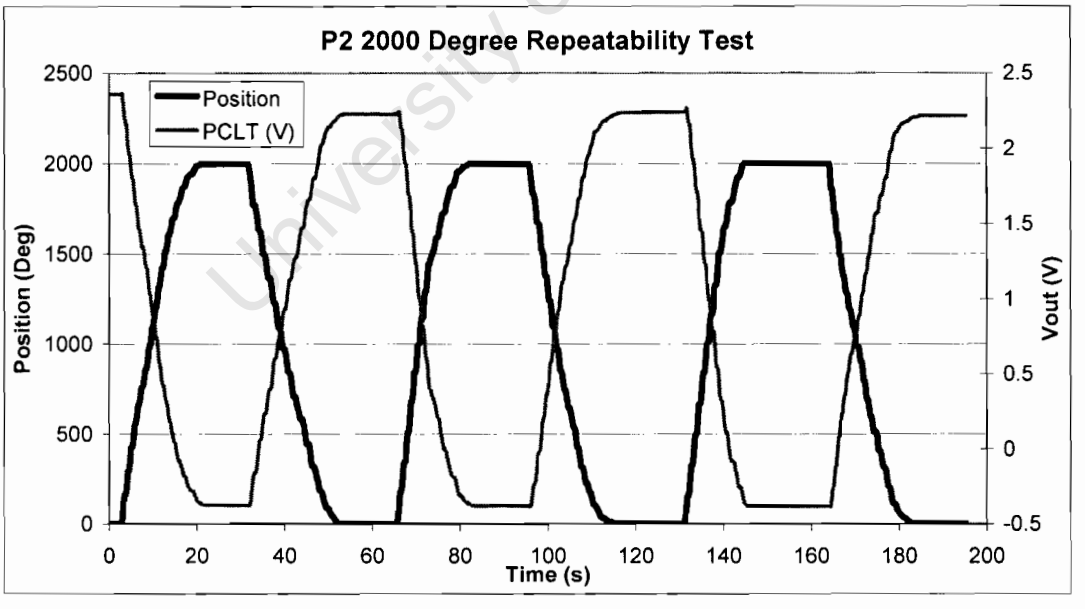

Figure 56 P2 repeatability test showing 3 sweeps of a 2000 degree movement cycle.

The position line in Figure 56 is jagged as the core was moved by hand, instead of by motor, to ensure that the core stopped at the exact end points of the movement cycle.

The maximum difference between the 3 lower turning points was 6.1 mV, and between the higher turning points was 24mV. The larger difference, or worst case, was used to calculate the repeatability as a percentage of full scale and as a distance.

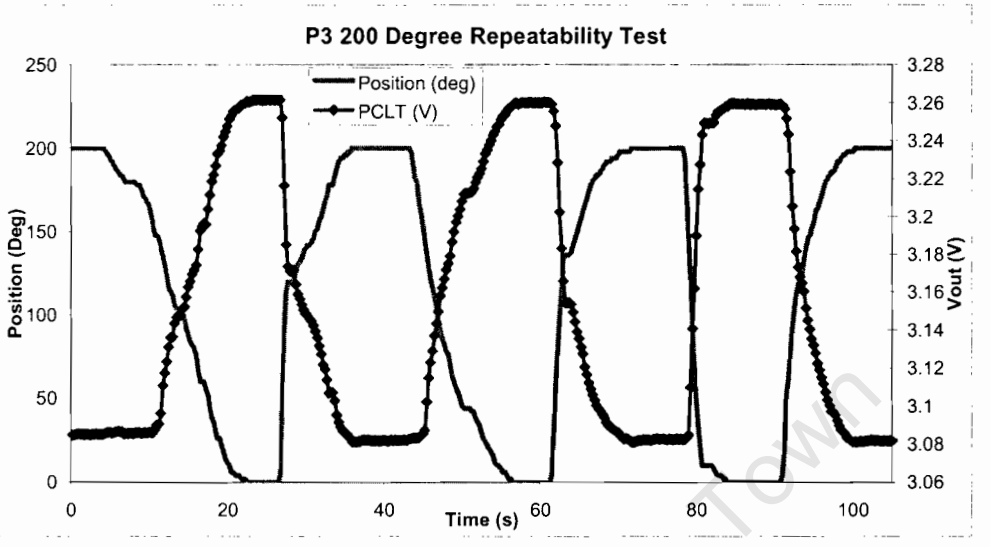

Figure 57 200 degree movement cycle repeatability test result for P3. P3 shows excellent repeatability.

	2000-Degree Repeatability		200-Degree Repeatability	
	(% FS)	(um)	(% FS)	(um)
P1	0.106306	68.09877	0.045495	29.17148
P2	0.120533	76.34634	0.032687	21.24644
P3	0.050138	32.08990	0.010527	6.842278
P4	0.047996	31.11738	0.004974	3.232946

Table 6 Summary of the repeatability results. Again, Prototypes 3 and 4 exhibited the best results.

The repeatability results from the 200 degree movement cycle tests were better (ten times better with P4) than those from the 2000 degree tests. This may be due, completely or in part, to inaccuracy in the test rig.

P4 had a worst case repeatability of 0.005% FS and P3 of 0.01 % FS, with the 200 degree test.

13. Conclusions

The use of a ferrite material doubled the primary to secondary coupling achieved with a soft iron core. The use of a surround ferrite core as opposed to a flat ferrite slab increased the coupling by a factor of ten. Use of the surround core comes at the cost of increased weight and increased complexity of sensor mounting.

The Version 2 windings layout produced excellent symmetry in secondary signals response and an increase in coupling over the Version 1 layout. The single multilayered PCB increased robustness by keeping the separation gap between all of the windings identical. The Version 2 windings of the PCLT produced an excellently constant magnetic field distribution over the length of the windings, up to the turning points of the primary winding.

Excitation of the primary winding required an amplifier with good reactive load stability, because of the very low resistance and low inductance of the primary winding.

Frequency is an important factor in PCLT operation, with higher frequencies offering increased efficiency, coupling, and temperature stability. Although all of the prototypes were operated at the same frequency of 20 KHz, the findings in this report indicate that a higher operating frequency will improve PCLT performance.

An investigation into the performance of the PCLT at resonance revealed both advantages and disadvantages of operating at the resonant frequency. The resonant frequency can be controlled by the amount of series or parallel capacitance introduced to the primary winding. The findings are concluded in Appendix A.

An un-calibrated test rig was used to test the prototypes. The resolution of the rig was not small enough to test the prototypes to their limits, and the accuracy of the rig was unknown. The test rig served well for inter-prototype comparisons, but failed to give results that can be accurately compared to other sensors.

Prototypes 2 and 4 had the most linear performance, due to the on-board ratio-metric calculations of the dedicated LVDT signal conditioning subsystems. The ratio-metric calculation serves to eliminate the effects of variance in the excitation signal, caused by the change in inductance of the primary winding with core position movement.

In all of the tests except those for linearity, P3 and P4 showed the best results, identifying synchronous demodulation as the better method of secondary signal conditioning. In the linearity tests, of the two prototypes using ratio-metric division, the synchronously demodulating version performed best, and of the two prototypes not using ratio-metric division, the synchronously demodulating version also performed best.

With the resolution tests, both of the prototypes using passive demodulation had downward voltage spikes on core position changes, whereas the synchronous demodulating prototypes did not. P3 and P4 are capable of greater resolution than the test rig was capable of measuring, this being 8.3 µm.

Prototype 4 showed the best results, achieving:

Linearity of 1%FS over the full range and 0.18%FS over the 32mm stroke
Output noise of 2 mV (peak-peak) and 0.5mV of **drift** over 12 hours
Resolution of at least 8.3µm or 0.013% FS
Repeatability of 3.2µm or 0.005% FS

14. Recommendations

The PCLT should use ratio-metric division of the primary and secondary signals to achieve maximum linearity.

Future versions of the PCLT should exploit the performance enhancing factors identified in this project. These factors include:

- High operating frequency (as high as possible without distortion)
- A surround ferrite core
- Synchronous demodulation
- Ratio-metric division of primary and secondary voltages
- Capacitance to create resonance at the operating frequency.

Further research into the implications of operating the PCLT at resonance needs to be done before an optimum capacitance configuration and operating frequency can be identified.

Even though P4 achieved the best results, it is recommended that future versions of the PCLT be built around the P3 circuit design, as P4 is limited to a maximum operating frequency of 20 KHz, whereas P3 is limited to 100 KHz, and this could be pushed further with the use of a higher speed instrumentation amplifier than the AD620.

The stroke-to-length ratio of the PCLT can be increased by using a narrower core.

The PCLT must be tested on a calibrated rig in order for accurate comparison to other sensors to be made.

15. References

[1] M. Walton, '*Ball on beam balance using a point coupled induction sensor.*' Bsc. Thesis. University of Cape Town. 2002.

[2] J. Tapson, '*Point Coupled Linear Transformer*' US Provisional Patent number 60/496,554. University of Cape Town. 2003.

[3] S. Tabrizi *et al*, '*Linear variable differential transformer assembly with nulling adjustment and process for nulling adjustment.*' US Patent 6,605,940 B1. Aug 2003.

[4] M. Thompson, 'Inductance Calculation Techniques—Part 1: Classical Methods.' *Power Control and Intelligent Motion*, vol. 25, no. 2, Dec1999, pp. 40-50.

[5] J. Szczyrbak, E. Schmidt, '*LVDT Signal Conditioning Techniques.*' 1997. Available at www.msiusa.com/schaevitz/products/LVDT/**signal**.pdf (accessed 20/4/2005).

[6] E. E. Herceg, '*Handbook of measurement and control'.* Pennsauken, NJ : Schaevitz Engineering, 1976.

[7] M. Iles, 'Penny & Giles transducers help launch Ariane 5.' *Aircraft Engineering and Aerospace Technology*, vol. 70, no. 5, 1998, pp. 352-355.

[8] Y. Kano *et al*, 'New Linear Variable Transformer with Square Coils.' *IEEE Trans. Magnetics*, vol. 26, no. 5, Sept 1990.

[9] Y. Kano *et al*, 'New Type Linear Variable Differential Transformer Position Transducer.' *IEEE Trans. Instrumentation and Measurement*, vol. 38, no. 2, 1989.

[10] P. H. Sydenham *et al*, 'Low-cost, Precision, Flat Inductive Sensor.' *Measurement* vol. 15, 1995, pp. 179-188.

[11] '*Low Cost/High Volume OEM Linear Displacement Sensor*'. Schaevitz Engineering. Available at http://www.msiusa.com/schaevitz/pdf/displacement/lvit-z.pdf (accessed 20/4/2005).

[12] A. Madni *et al*, 'The Next Generation of Position Sensing'. *Sensors*, vol. 18, no. 3 & 4, 2001.

[13] S.Y. Hui, S.C. Tang, and H. Chung, 'Optimal Operation of Coreless PCB Transformer-Isolated Gate Drive Circuits with Wide Switching Frequency Range,' *IEEE Trans. Power Electronics*, vol. 14, no. 3, 1999, pp. 506-514.

[14] E. E. Herceg, '*Handbook of measurement and control'*. Pennsauken, NJ : Schaevitz Engineering, 1976. p. 3-10

[15] D. Halliday, R. Resnik, J. Walker, '*Fundamentals of physics'*. New York: John Wiley and Sons, 1997. pp. 739-774.

[16] E. E. Herceg, '*Handbook of measurement and control'*. Pennsauken, NJ : Schaevitz Engineering, 1976. p. 4-6.

[17] E. E. Herceg, '*Handbook of measurement and control'*. Pennsauken, NJ : Schaevitz Engineering, 1976. p. 7-6.

[18] Apex Microtechnology, '*Loop Stability with Reactive Loads*'. Application Note 38, rev. B, 2001. Available at http://eportal.apexmicrotech.com/mainsite/support/pages/app_notes.asp (accessed 20/4/2005).

[19] D. Halliday, R. Resnik, J. Walker, '*Fundamentals of physics'*. New York: John Wiley and Sons, 1997. pp. 823-826.

[20] Trans-Tek inc. '*Synchronous vs. Asynchronous Demodulation'*, 2002. Available at www.transtekinc.com/TekNotes/SYN_ASYN_DEMOD.PDF (accessed 20/04/2005).

[21] Solartron Metrology, '*2002 catalogue'*. pp. 52-53. Available at www.solartronmetrology.com (accessed 20/04/2005).

[22] Phillips semiconductors, '*SC17 datasheet'*. 1997. Available at http://www.semiconductors.philips.com/acrobat_download/various/SC17_GENERAL_APP_1996_1.pdf (accessed 20/04/2005).

[23] E. Mombello *et al*, 'Impedances for the calculation of electromagnetic transient phenomena and resonance in transformer windings'. *Electric Power Systems Research*, vol. 54, 2000, pp. 131-138.

[24] J. B. Calvert, '*Coils and Inductance*'. Aug 2001. Available at http://www.du.edu/~etuttle/electron/elect20.htm (accessed 20/4/2005).

[25] S. Graaff, '*A two-dimensional ball position controller using point coupled linear transformer*' Bsc. Thesis. University of Cape Town, 2003.

Appendix A - The PCLT in Resonance

Driving the PCLT at resonance offers a major increase in the coupling between the primary and secondary windings [23]. This means an increase in the overall sensitivity of the sensor and ultimately increased resolution of the sensor, as smaller position changes will still give detectable voltage changes. This chapter is an investigation into the resonant properties of the PCLT, and the effects of resonance on PCLT performance. It introduces some important trends and lays the groundwork for further investigation into this vast topic.

A.1 Effect of core and series capacitance

The shape of the frequency response profile was observed with the windings directly coupled to a frequency generator, and 2μF decoupled from the signal generator, with and without a ferrite core present.

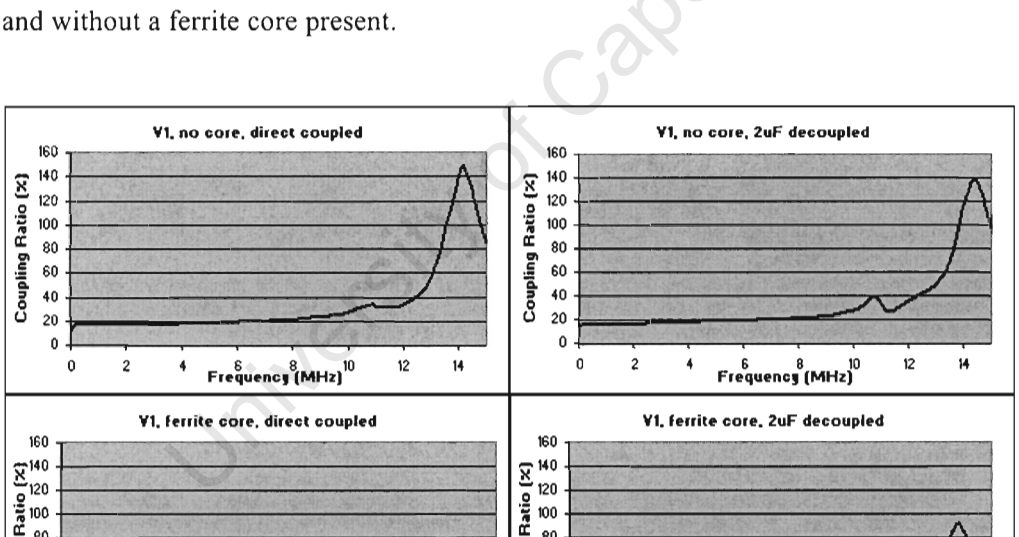

Figure 58 Frequency response of the Version 1 primary winding. On the left, direct coupled to signal generator, on the right decoupled with a 2μF series capacitor. On top, without any core, on the bottom with a ferrite core. Secondary windings open circuit.

The frequency range of the tests was from 10 KHz to 15 MHz. Both versions of PCLT windings were tested.

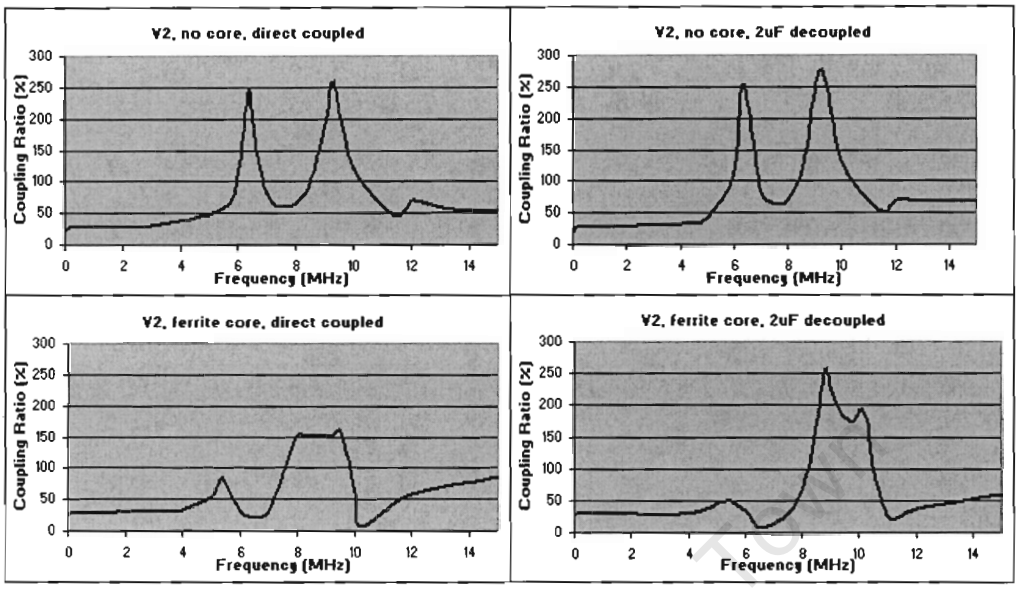

Figure 59 Frequency response of Version 2 windings. On the left, direct coupled to signal generator, on the right decoupled with a 2μF series capacitor. On top, without any core, on the bottom with a ferrite core. Secondary windings open circuit.

Some trends were noticed in the changes in frequency response as a ferrite core and series capacitance were added in different combinations.

The introduction of the ferrite core had the following effects on the coupling ratio:

1) Increased coupling at frequencies below 4 MHz,
2) Decreased coupling at the high frequency resonant points,
3) Decreased the resonant frequency by about 1 MHz,
4) Changed the shape of the frequency response profile (especially with V2).

The introduction of the core changed the mutual inductance of the secondary windings, thus affecting the apparent inductance of the primary winding and consequently the resonant characteristics.

The introduction of a 2μF decoupling capacitor (labeled C_{series} in Figure 61) made almost no change to the coupling when no core was used. With the core, the addition of series capacitance caused:

1) Coupling at frequencies below 4 MHz to stay the same,
2) Coupling at the high frequency resonant points to increase,
3) No change in the frequencies at which the resonant peaks occurred.

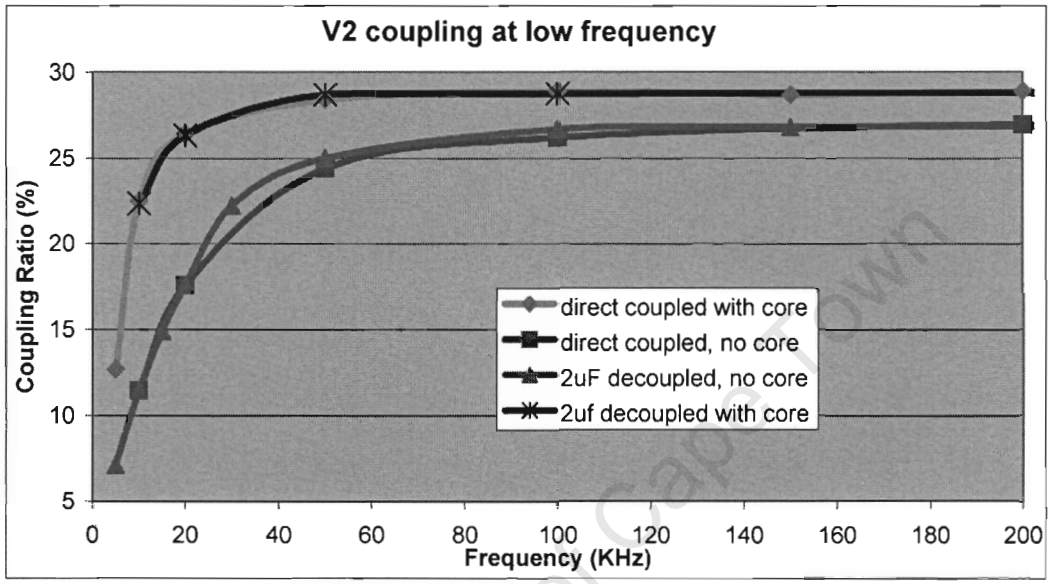

Figure 60 A look at the coupling ratio over a limited frequency range, 10 KHz to 200 KHz, with and without a core and decoupling capacitance.

Figure 60 confirms that the core causes an increase in the coupling, and series capacitance has no effect on the coupling, at low frequencies.

A.2 Effect of varying the series capacitance

Various value capacitors were put in series with the primary winding, and the voltages across the windings were monitored over a range of frequencies. A signal generator was used to produce the excitation sine wave, which was boosted by an OPA 548 power amplifier. A ferrite core was fixed at the null point of the windings in each test.

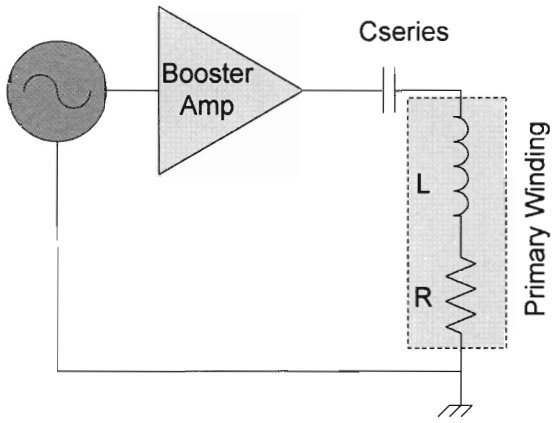

Figure 61 Capacitor connected in series with the PCLT primary winding. The primary winding is equivalent to an inductor and resistor in series.

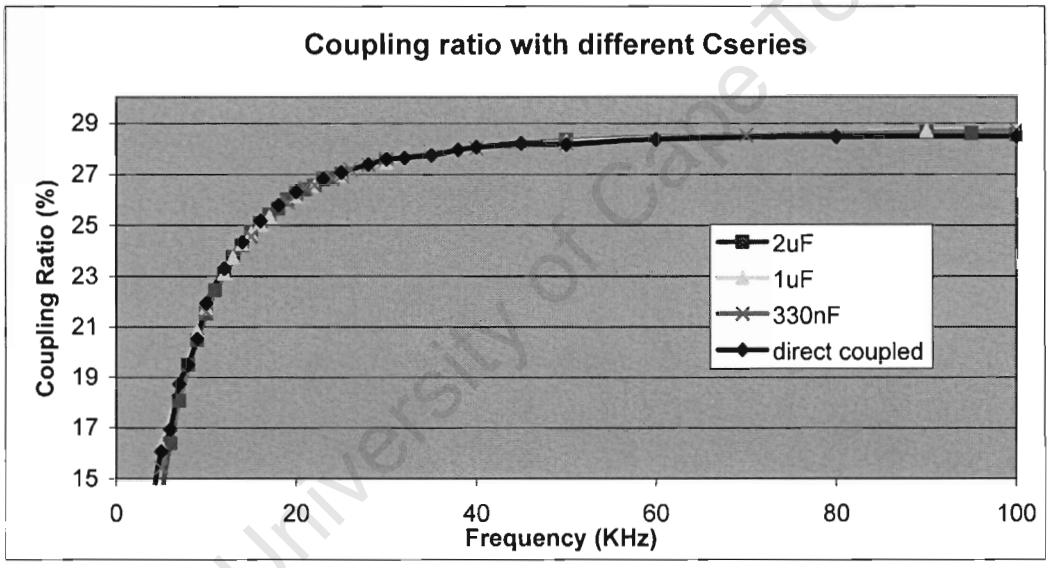

Figure 62 The ratio of the coupling between the primary and secondary windings is identical regardless of capacitance.

Again, the results show that primary to secondary coupling is not influenced by the series capacitance. However, the primary and secondary voltages are influenced by the amount of capacitance, as illustrated in Figure 63 and Figure 64.

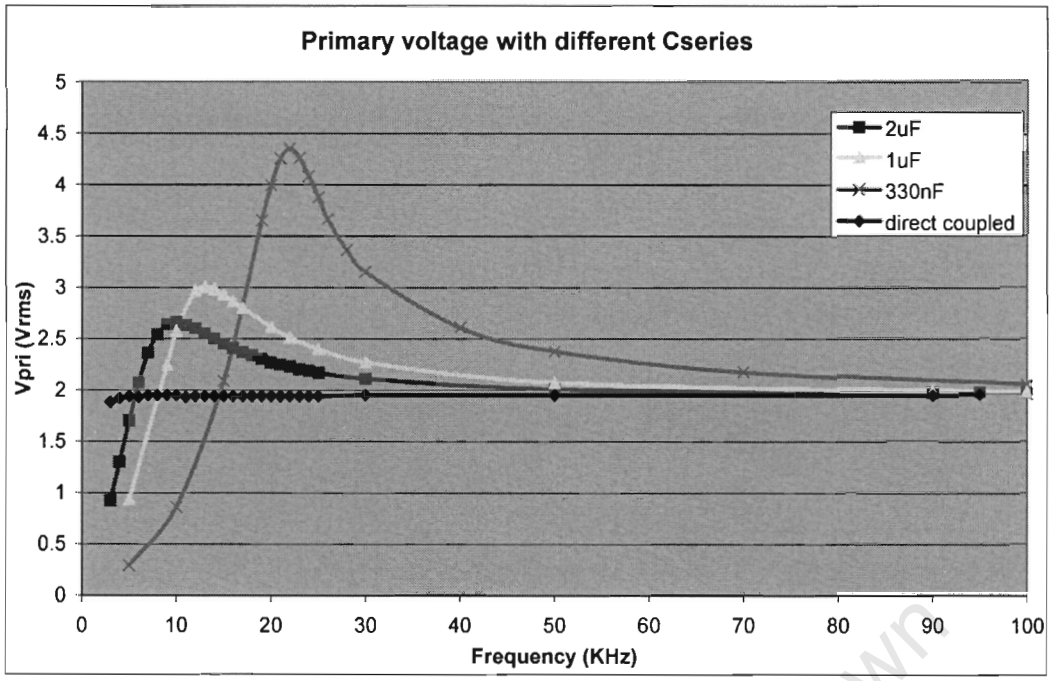

Figure 63 The primary voltage shows peaking of different amounts and at different frequencies depending on the amount of series capacitance. No peaking occurred when the primary was direct coupled to the signal generator.

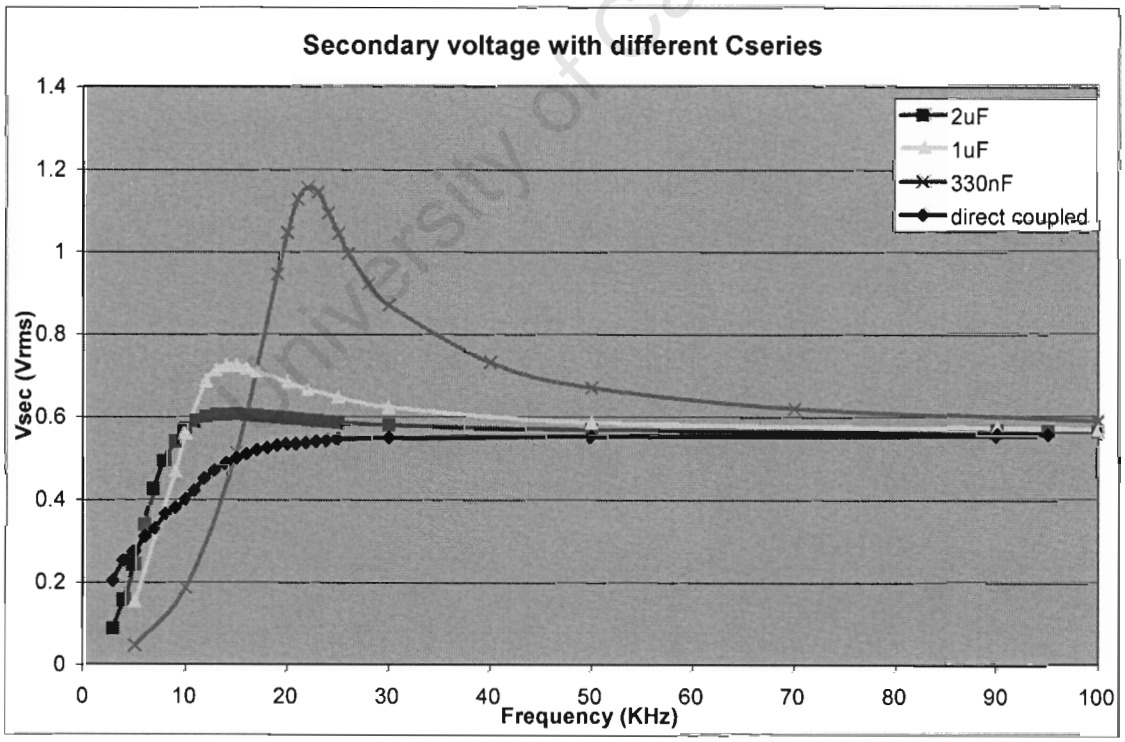

Figure 64 the secondary voltage shows peaking similar to that of the primary voltage in Figure 63.

The primary and secondary voltages show resonant peaks at frequencies approximately predicted by (9). This is however not reflected as a peak in the coupling ratio because the peaks are matched in magnitude and frequency.

A.2.1. The apparent coupling ratio

During these tests, the excitation voltage remained constant. This meant that for a constant magnitude excitation voltage applied, the secondary voltage peaked at the resonant frequency. Consider the ratio between the voltage applied by the power amplifier and the secondary voltage, the apparent coupling ratio (ACR). The ACR is a measure of how much of the voltage *applied by the booster amplifier* appears across the secondary windings, it is effectively the coupling ratio of the transformer with the series capacitor included as part of the primary winding (see Figure 10).

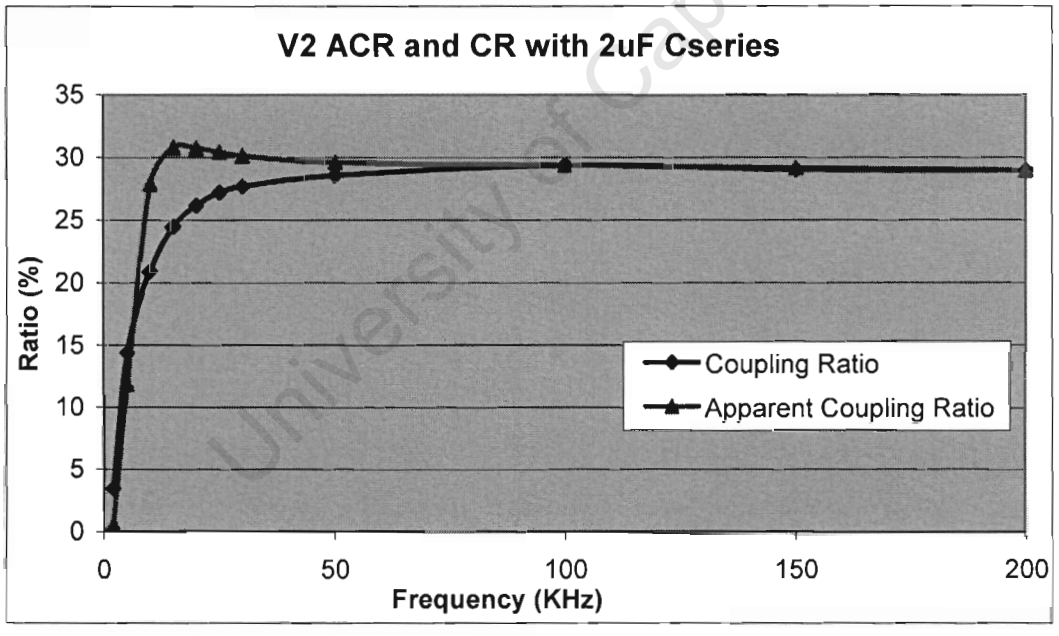

Figure 65 Comparison between the apparent and actual coupling ratio of the Version 2 PCLT windings with 2μF series capacitance. The ACR shows 32% coupling at the 17 KHz peak, as opposed to the 25% CR.

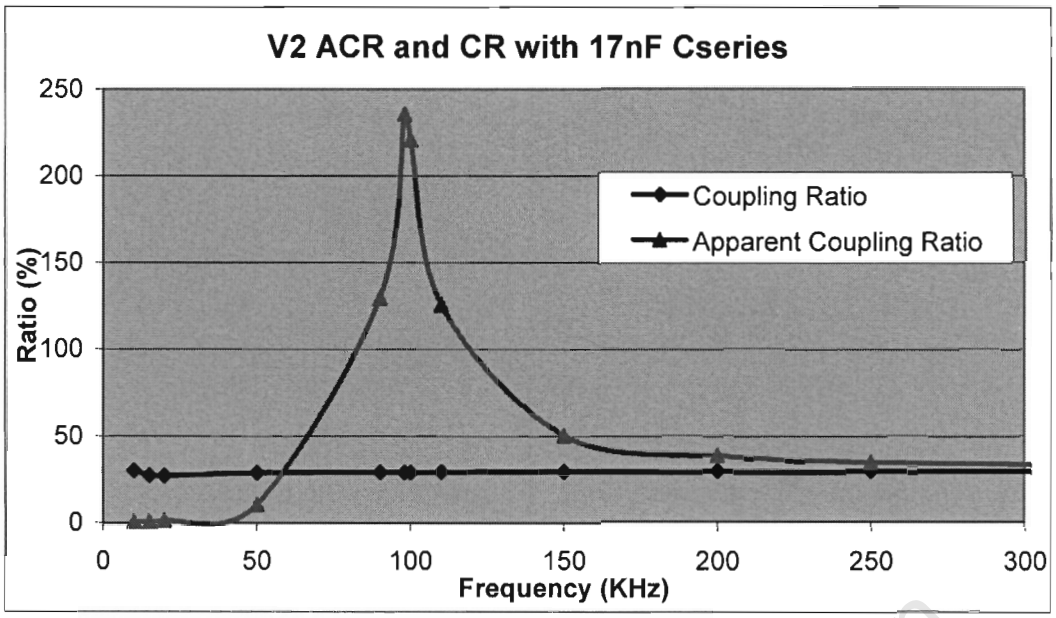

Figure 66 Comparison between the apparent and actual coupling ratio of the Version 2 PCLT windings with 17nF series capacitance. The ACR shows 235% coupling at the 100 KHz peak as opposed the 30% CR.

The series capacitance directly influences the frequency at which the apparent coupling ratio peaks, and also determines how high and wide that peak is. Reducing the capacitance causes the resonant peak to occur at a higher frequency, and causes an increase in the magnitude and sharpness (height to width ratio, or Q) of the peak. Use of a 2μF capacitor yields 35 % coupling at 17 KHz, and a 17nF capacitor yields 235 % coupling at 100 KHz. Thus, the higher the operating frequency of the PCLT, assuming the correct value of capacitor is used to make the resonant peak occur at this frequency, the larger the secondary waveforms induced for detection, and consequently, the better the sensitivity of the sensor.

A.2.2. Current consumption

The total current consumption of the excitation circuit was monitored around the resonant frequency for different series capacitances.

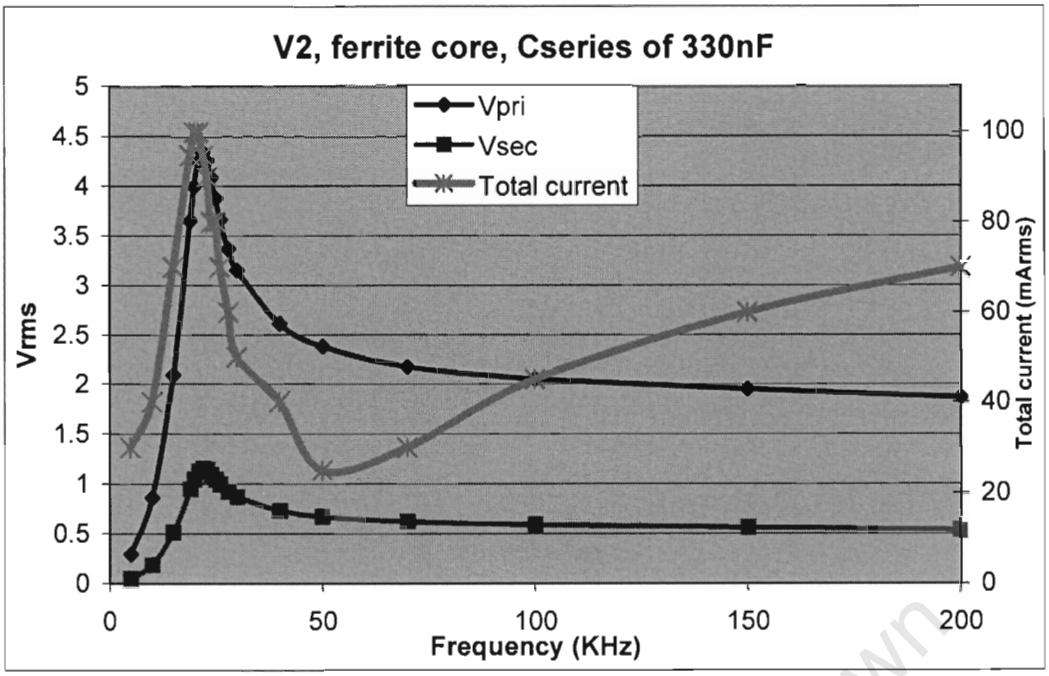

Figure 67 The total current consumption of the booster amplifier and primary winding around the resonant point. The current peaks with the voltages at 20 KHz, then subsides to its lowest value at 50 KHz.

Figure 67 shows the current peak occurring at the same frequency as the voltage peaks, with a 330 nF capacitor. This result shows a similar pattern to that observed with the other capacitor values, specifically that the current peaks at the resonant frequency, so results from the other tests are included on the Data CD.

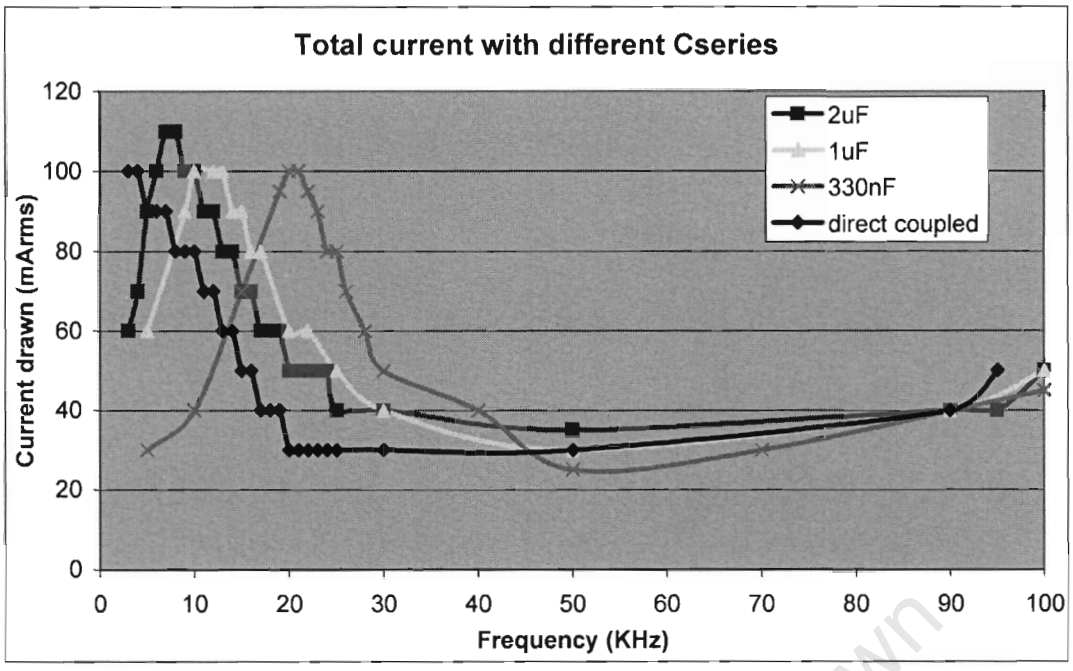

Figure 68 Current peaks with different series caps. Smaller caps have current peaks at higher frequencies. High and low values of current drawn are similar for all cases.

The current peaks with the primary and secondary voltages. This was expected, as a resonating series RCL combination load appears purely resistive, so the current must be directly proportional to the voltage across the load [19].

The large increase in current at resonance is an undesirable characteristic, as it means that the power consumption of the sensor will rise if it operates at resonance. Also, the increase in the primary current leads to increased heating in the coils.

It may be useful to operate the PCLT at the frequency above the resonance, where the current is lowest, for the advantage of drastically improved power efficiency and less heating in the windings, but at the cost of decreased sensitivity. This hypothesis is outside the scope of this investigation, but could be investigated further in future work.

A.3 Effect of parallel capacitance

An alternative method of manipulating the resonant frequency is to introduce a "tank" capacitor in parallel with the primary winding.

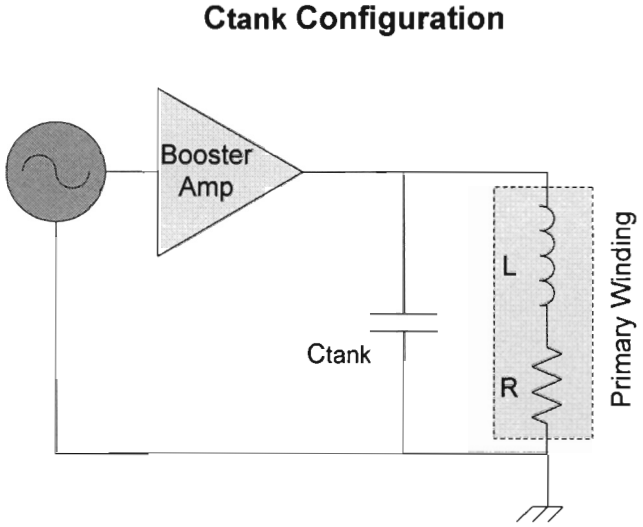

Figure 69 Capacitor connected in parallel with the PCLT primary winding.

The resonant frequency of the LC combination in parallel can be calculated with (11).

$$f_{resonance} = \frac{1}{2\pi\sqrt{LC}} \qquad (11)$$

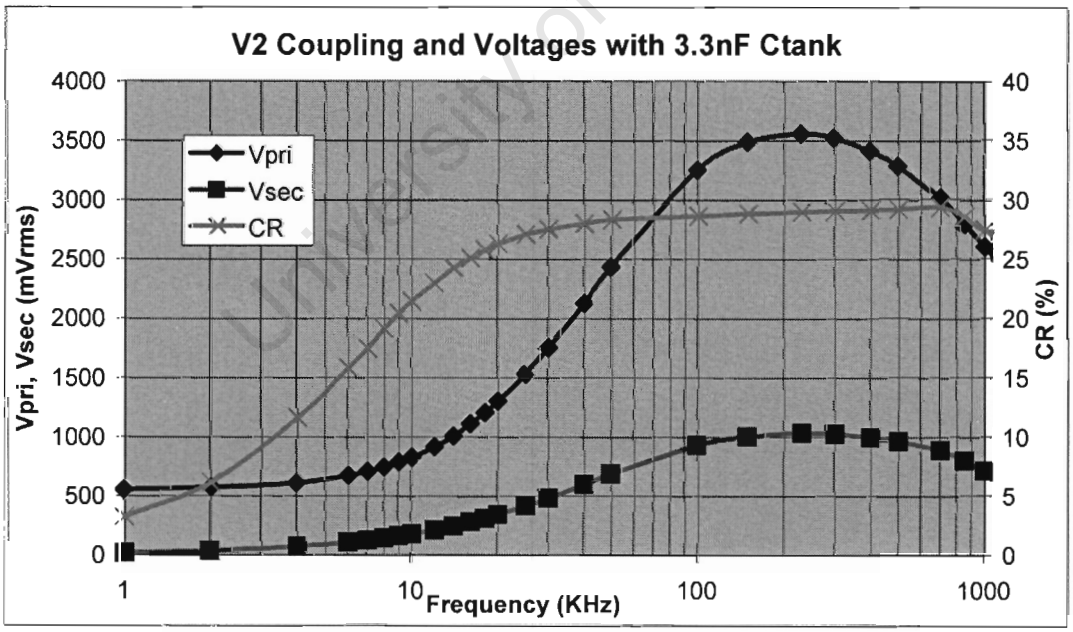

Figure 70 The primary and secondary voltages clearly show peaking around 230 KHz, the resonant frequency calculated with (11).

Figure 70 confirms that the PCLT primary winding in parallel with C_{tank} acts as a parallel resonant load, and resonates at the frequency calculated with (11).

A.3.1. Primary and secondary voltages

Observation of the voltages across the V2 PCLT windings with parallel capacitance revealed a very different shape to that with either series capacitance or direct coupling (no capacitance).

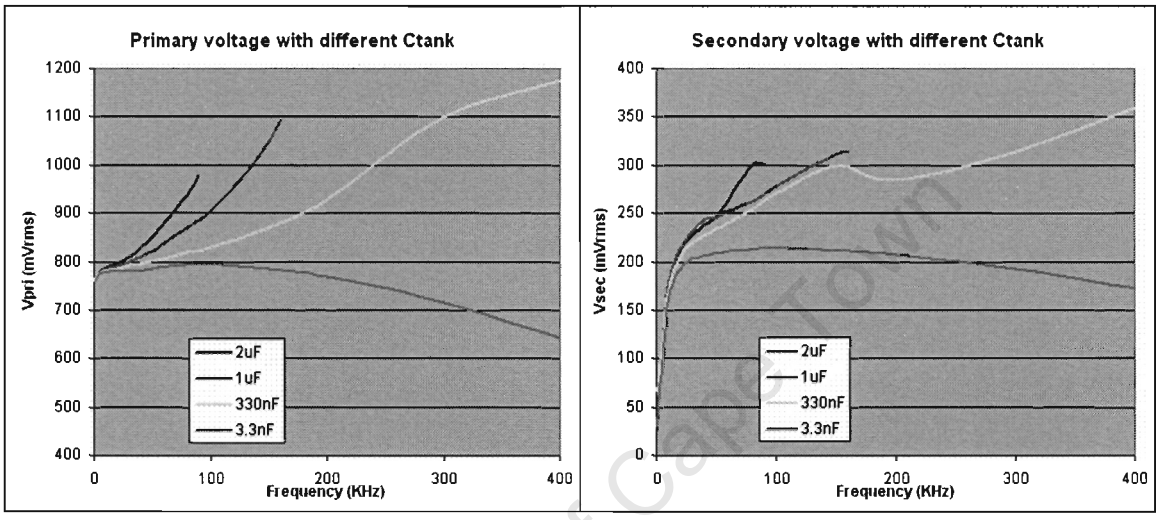

Figure 71 Primary and secondary voltages with different value tank capacitors. Results for the 1 µF and 2 µF tests stop when the PSU 0.5Amp current limit was reached.

The current drawn in these test was very large, and increased with frequency and capacitance. With a 2 µF tank capacitor, the current drawn was half an amp at 90 KHz, preventing the test to be carried on to higher frequencies without risk to the booster amplifier or PCLT windings.

A.3.2. Coupling Ratio

The coupling ratio (which is exactly the same as the ACR as no series capacitor was used) was measured over a low frequency range for different value tank capacitors.

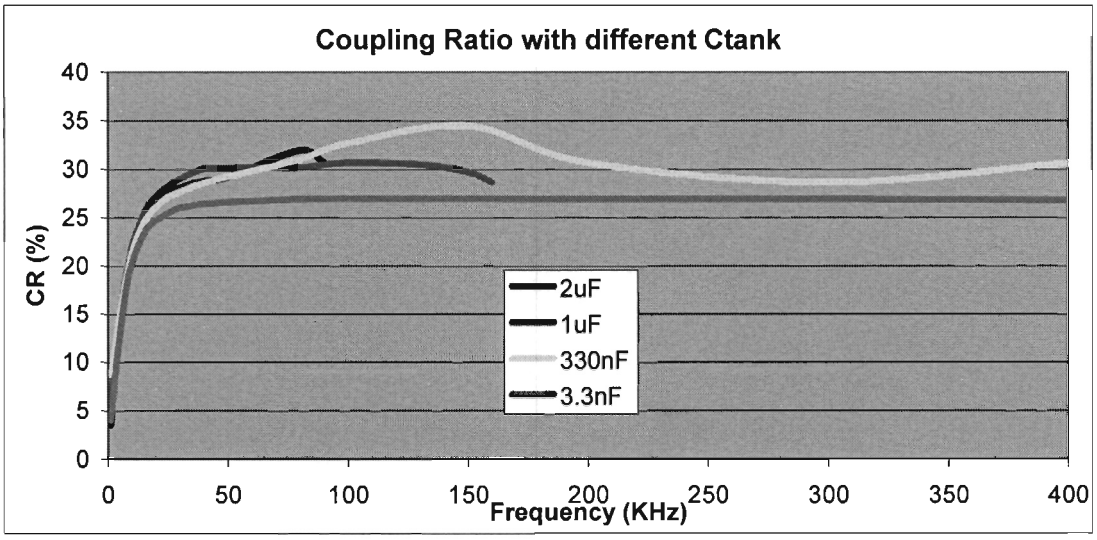

Figure 72 Coupling ratio measured with different value tank capacitors. Results for the 1 µF and 2 µF tests ended when the current drawn reached 500mA.

The coupling ratio does not change significantly with different amounts of parallel capacitance. A closer look at the response when using a 2µF tank cap, as in Figure 73, reveals a coupling ratio very similar to that obtained without any parallel capacitance.

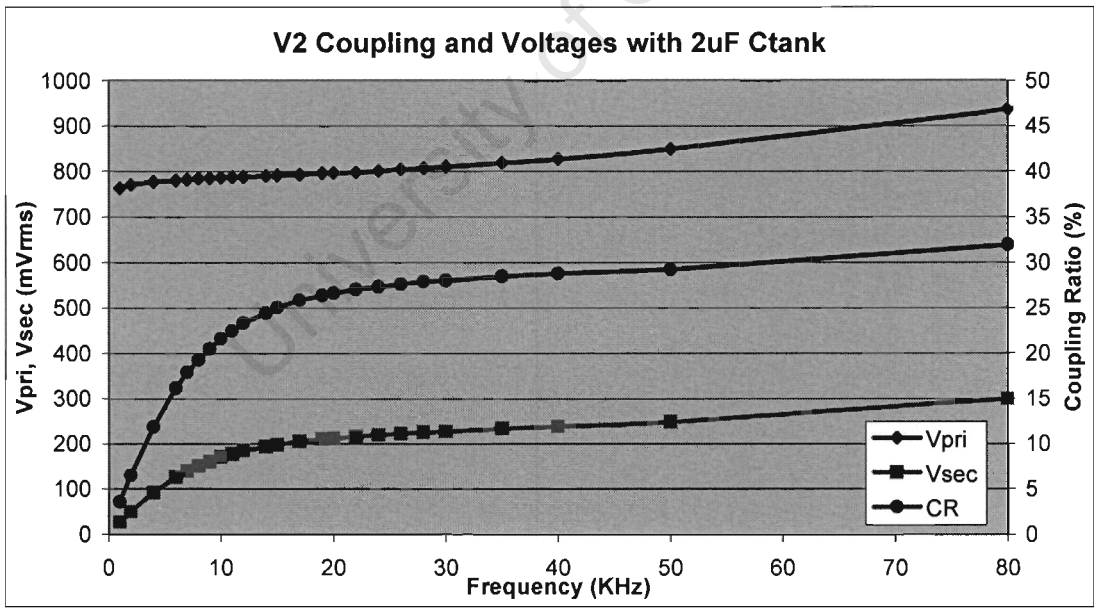

Figure 73 Coupling ratio and voltages with a 2µF capacitor connected in parallel with the Version 2 primary winding.

There appears to be no increase in the coupling ratio of the PCLT when parallel capacitance is introduced.

A.3.3. Current consumption

It is expected that the current consumption of a parallel resonance configuration will be very small. With a parallel LC circuit, the current and voltage are in antiphase, resulting in the current cycling between the capacitor and the inductor, and thus very little current needs to be added by the booster amplifier to maintain the resonant oscillations [24].

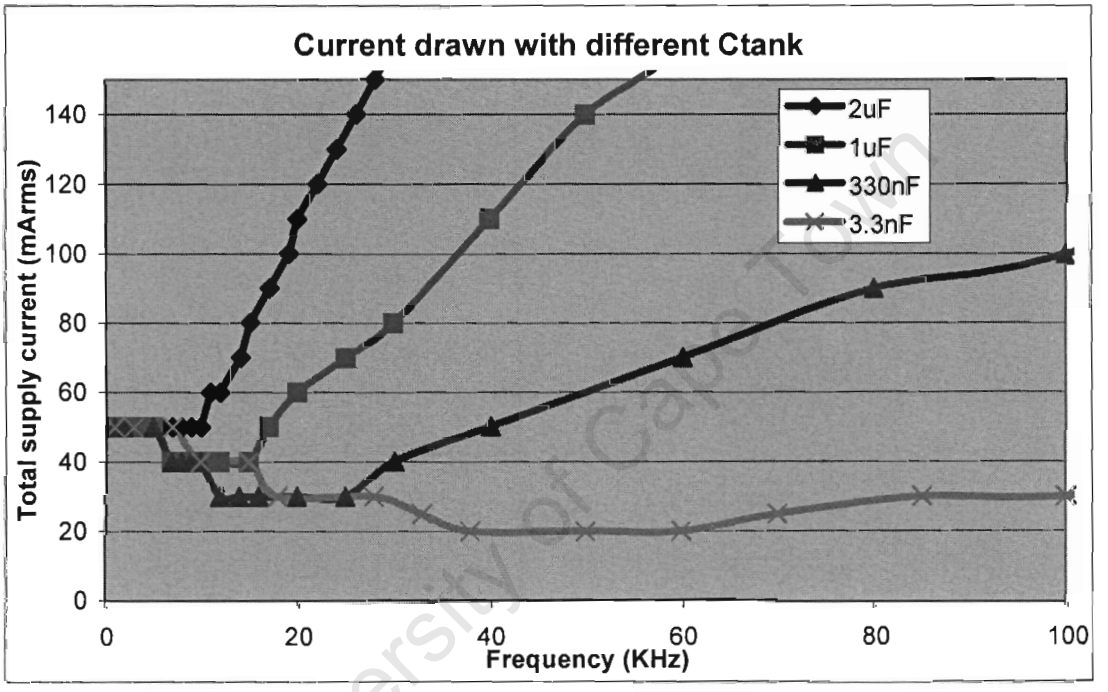

Figure 74 Current drawn with different sized tank capacitors. Smaller value caps result in lower supply current and higher frequency minimum-current points.

The capacitance affects the frequency at which the current is a minimum, indicating that as the resonant frequency increases, so does the minimum-current frequency.

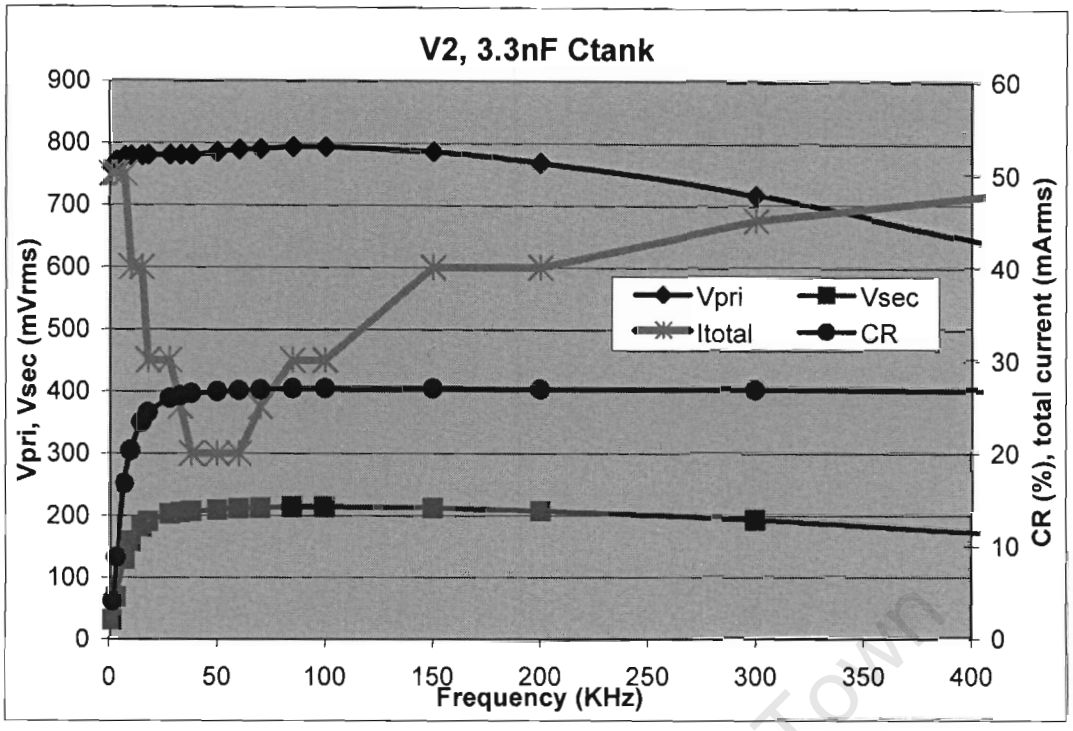

Figure 75 Total current drawn in context with the position of the primary and secondary voltage peaks.

The shape of the current curves in the parallel capacitance configuration is opposite to that of the series capacitance configuration current curves. Where, in series, the current is low but peaks sharply at the resonant frequency, in parallel, the current is normally high but drops sharply at the resonant frequency.

A.3.4. Distortion of the primary and secondary waveforms

There was a noticeable decrease in the quality of the primary and, consequently, secondary waveforms when a tank capacitor was used, as opposed to when the primary was directly or series coupled to the booster amplifier. Operating at 20 KHz, THD was 10 % with C_{tank} and less than 1 % with C_{series}.

A.4 Summary of the resonance characteristics

Series capacitance can be used to greatly increase the coupling of the PCLT at a desired frequency. Decreasing the series capacitance causes an increase in the amount of coupling at the resonant point. The resonant points occur at higher frequencies for small capacitors, in accordance with the relationship expressed in (9). The higher the frequency of the resonant point, the sharper the peak in coupling is. The frequency of the resonant peak is also a function of the inductance of the primary winding.

As shown in Chapter 6, the inductance of the primary winding changes with core position. This change in inductance will have a negative effect on the performance of the PCLT if it operates at one of the sharply peaking resonant points, because as the inductance changes with core position, the resonant frequency will change, but the frequency of operation of the circuit will not, resulting in a large change in the coupling, and consequently, a large change in the magnitude of the secondary signals. This problem can be avoided by; 1) operating the PCLT at a resonant point that is not sharp, such that a small change in the inductance will cause an insignificant change in the coupling, 2) not operating the PCLT at resonance, 3) modifying the PCLT windings and core structure or layout to ensure that core position changes do not affect primary winding inductance.

Operating at a series resonant point causes a large increase in the current consumption of the drive circuit.

Using parallel capacitance to control the resonant frequency has the advantage of decreasing the current required by the drive circuit, however is not suitable because of the large distortion it causes in the primary waveform. It may be possible to improve on the distortion by using a combination of series and parallel capacitance.

There is room for further investigation into the resonance characteristics of the PCLT, which is outside the scope of this project.

Appendix B - 2 Dimensional PCLT

B.1 Introduction

The idea for a two dimension position sensor was developed by J. Tapson in 2003 [2]. Simon Graaff used this concept in an attempt to build a two-dimensional ball position sensor as part of a B.Sc. undergraduate thesis submitted in October 2003 [25].

B.1.1. Aim

The aim of this section was to develop further, and improve upon, the existing design of the 2D PCLT, using the improved methods and circuitry developed for the one dimension PCLT detailed earlier in this report.

B.1.2. Scope

This section of the investigation is limited to minor physical changes to the sensor layout, a redesign of the circuitry, and testing.

B.2 Principal of operation

The 2D PCLT is simply an extension of the 1D PCLT. It is in effect two square 1D sensors placed perpendicularly to each other that share a common core and excitation field. A pair of secondary windings with tapers opposing compose one axis of detection, a second pair make up the other axis of detection. Figure 76 shows an exploded view of the four secondary windings required for 2D displacement sensing. Windings A and B are paired for detection along the x axis, and C and D along the y axis. The arrows on the diagram indicate the direction of taper of the windings.

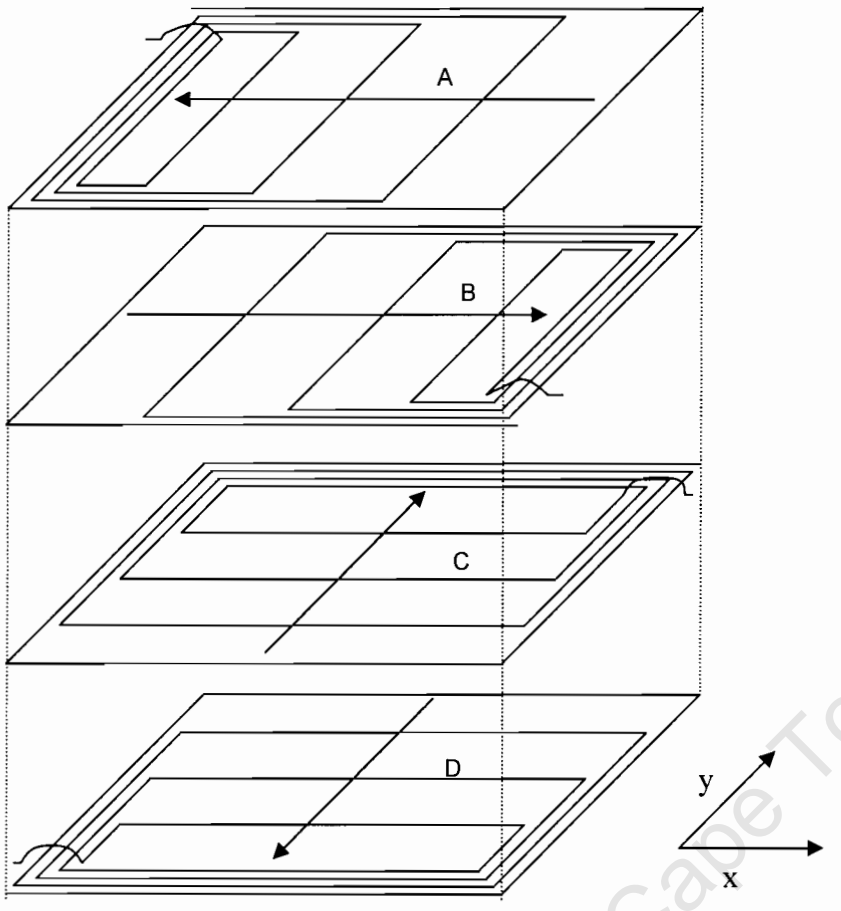

Figure 76 Exploded view of the four secondary windings of 2-D PCLT showing direction of taper of the windings. [2]

The primary winding is a square coil placed at the bottom of the stack; the core is placed on the top of the stack.

B.3 Windings layout

The sensor is made up of six layers printed onto three double sided PCBs. The primary winding is on one board, with the windings laid on both sides in series. The primary winding consists of 40 turns, and has an inductance of 775uH, and resistance of 37Ω.

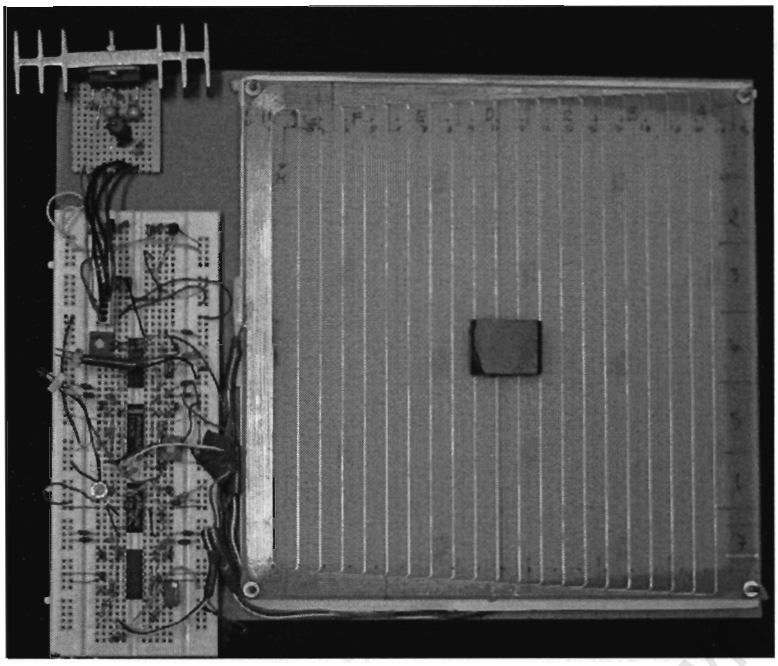

Figure 77 Photograph of the 2D PCLT windings with ferrite core and circuitry.

B.4 Magnetic field distribution over the sensor area

The magnetoresistive sensor used in Chapter 0 was modified to operate at 50 KHz, and used to map out the magnetic field produced by the primary winding. 10 runs were recorded with the magnetic probe moved parallel to the x axis.

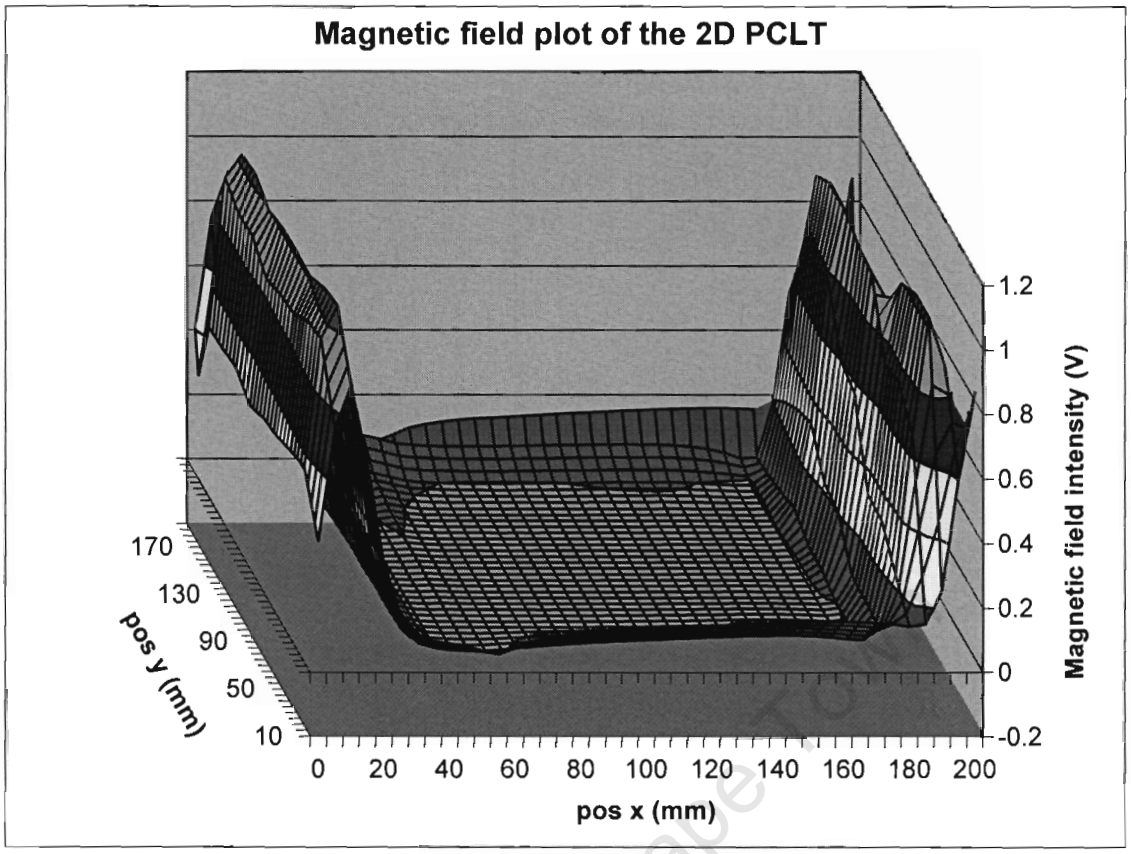

Figure 78 3D surface of the magnetic field above the 2D PCLT sensor area. The blue area (central square) has an intensity of close to zero, indicating that there is almost no magnetic flux present here.

The 2D PCLT exhibits a magnetic dead zone over most of the central sensing region. This is likely to seriously inhibit the sensors ability to detect the core position in this region. A possible counter-measure to solve this problem is to use a very large core in an attempt to 'pull in' some of the flux that is in abundance around the edges of the sensor region. However, this solution is likely to cause serious non-linearity in sensor response as the less flux will reach the centre of the sensor region than will reach the outer regions.

A more promising solution would be to redesign the layout of the primary winding such that the turns come all the way to the center, and thus create a more even flux distribution.

B.5 Signal conditioning circuitry

The circuitry for the 2D PCLT is based on that developed for the 1D PCLT. The excitation stage is identical, as the square primary has properties similar to the 1D PCLT primary winding. The 1D Prototype 3 PCLT exhibited excellent overall performance, and was thus chosen to perform the secondary signal conditioning for the 2D PCLT.

B.5.1. Sensor output format

The sensor measures position in two dimensions, a -10 to 10 V signal is used to describe position along one axis (x), and another -10 to 10 V signal describes the position in an orthogonal axis (y). This is achieved by duplicating the secondary signal conditioning components such that there are two synchronously demodulating stages (one operating on secondaries A and B, the other operating on C and D in Figure 76) that share the same excitation source.

B.5.2. The 2D self-synchronous PCLT

A 2D PLCT sensor was built using the demodulation stage from the 1D Prototype 3. A problem immediately became apparent – there was a large imbalance in the magnitudes of the secondary voltages. The design was modified to include adjustable gain stages before demodulation for balancing the signals and setting the null point.

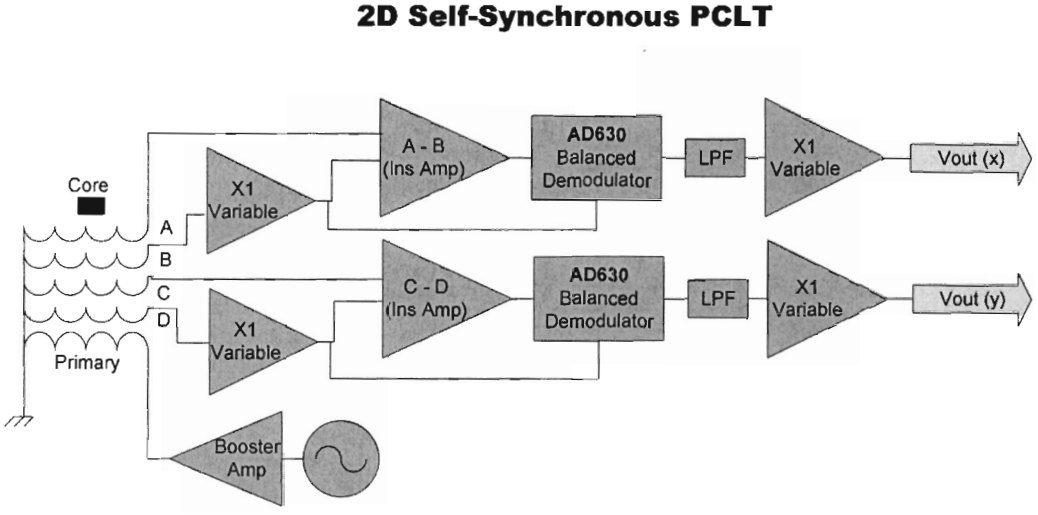

Figure 79 Functional diagram of 2D self synch PCLT with added offset null adjustment for balancing secondary signals.

The circuit operated correctly, and could be adjusted to give zero output when the core was placed in the centre of the windings. However, the output voltages did not respond as expected when the core was moved. Analysis of the secondary waveforms revealed that the phase difference between the secondaries changed hugely as the core was moved, such that with the core at the edge of the sensor, the secondary windings were 120 degrees out of phase.

This is a characteristic of the physical sensor, the combination of primary and secondary windings layout and the core position. This largely changing phase difference makes accurate synchronous demodulation impossible. The best solution without completely redesigning the sensor was to use phase insensitive or passive demodulation. It is possible that the change in phase with core position could be used to detect core position.

B.5.3. The 2D Passive Demodulation PCLT

The next generation of 2D PCLT was built using the secondary signal conditioning stage of the 1D prototype 1 PCLT, namely discrete component passive demodulation. Passive demodulation is phase insensitive as only the magnitude of secondary signals is used via half wave rectification.

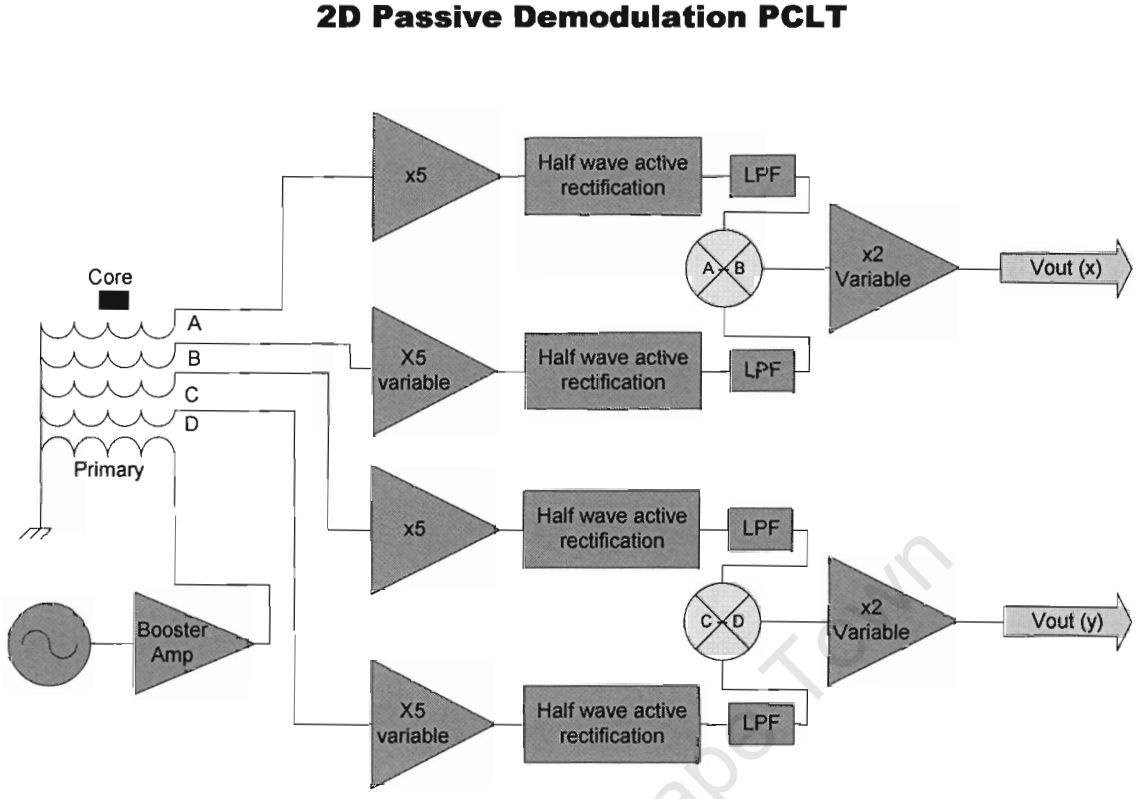

Figure 80 Functional diagram of phase insensitive version of the 2D PCLT, using circuits similar to the 1D Prototype 1.

This version of the 2D PCLT responded more as expected with core movements. The stability of the output signals with a steady state core was poor. The output signals are affected by any movement in the connecting wires or movement of the 3 deep PCB stack (e.g. by the weight of a core). This problem can be overcome by printing all the windings onto a composite 6 layer PCB, with the circuitry built into the board as well. This step was not taken during this project because of the expense of a 6-layer PCB.

B.6 2D PCLT Test Results

The x and y output voltages were logged every second as the core was moved over the sensing area of the 2D PCLT. Seven runs were done, labeled A through G.

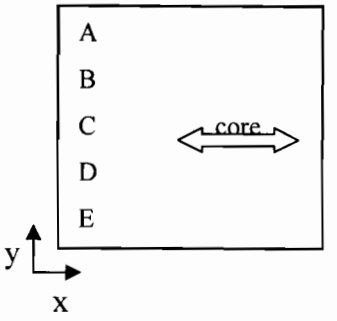

Figure 81 2D PCLT test setup. The core was moved along the x-axis at 7 different y co-ordinates.

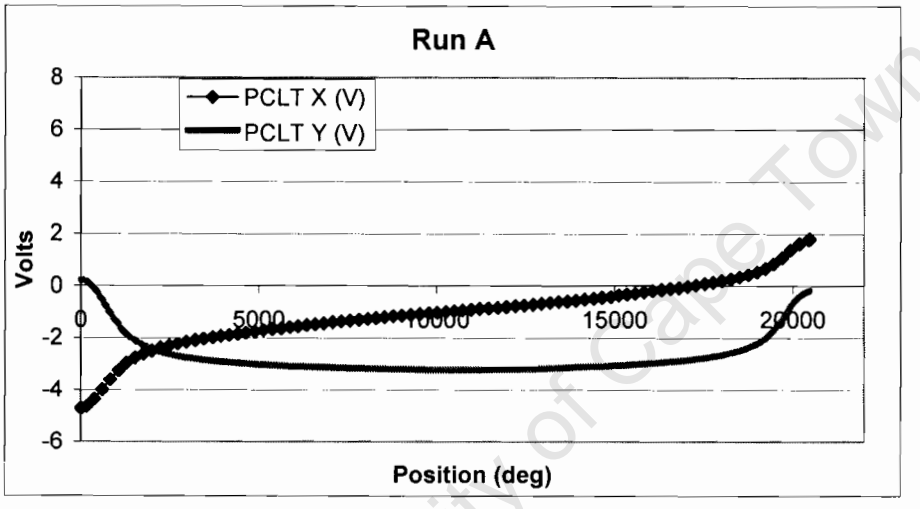

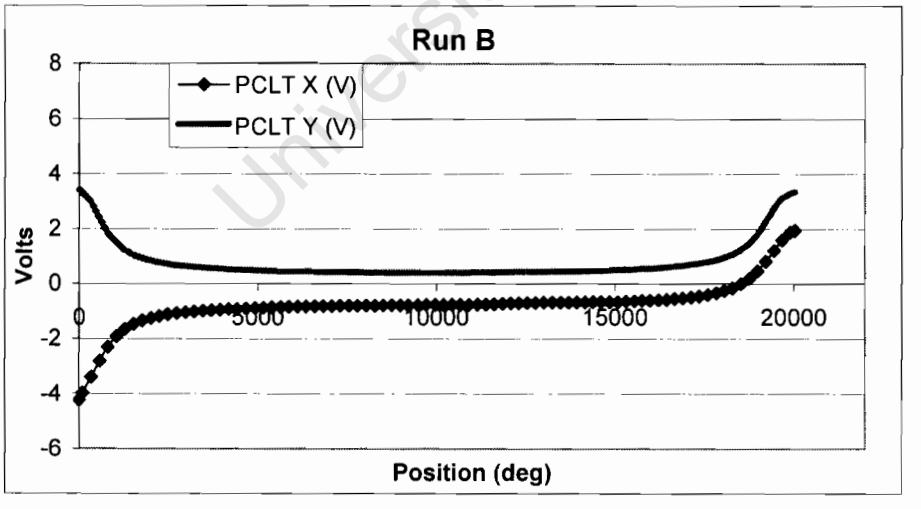

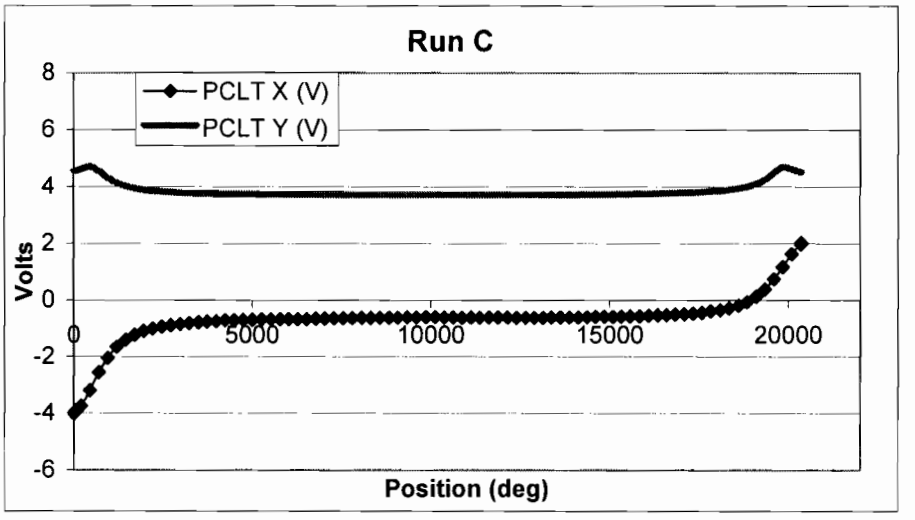

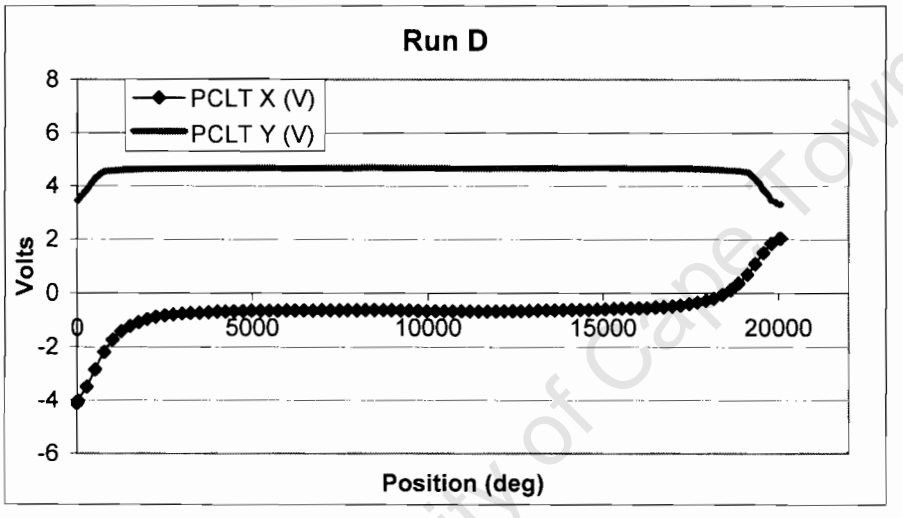

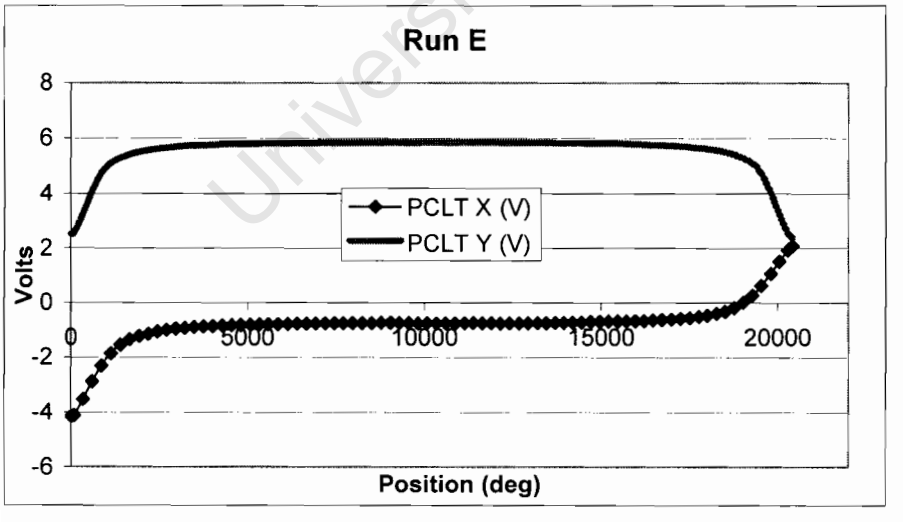

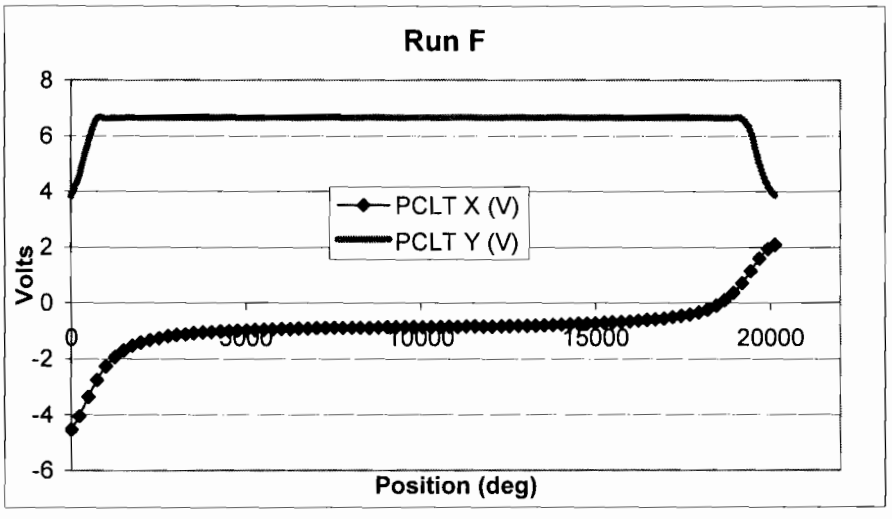

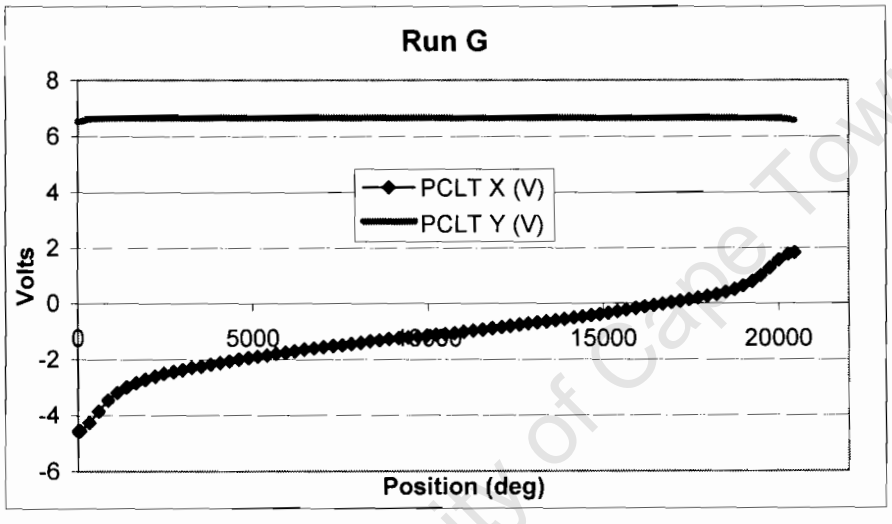

Figure 82 Plots of x and a y voltage over the seven test runs at y co-ordinates A through G.

The results show that there is most sensitivity in the x direction on runs A and G, these runs are directly above the coils of the primary windings, where the magnetic flux density is greatest. Figure 83 shows the x voltages superimposed in a 3D image for comparison. For the more central runs, the response over the central region is flat, showing very little sensitivity.

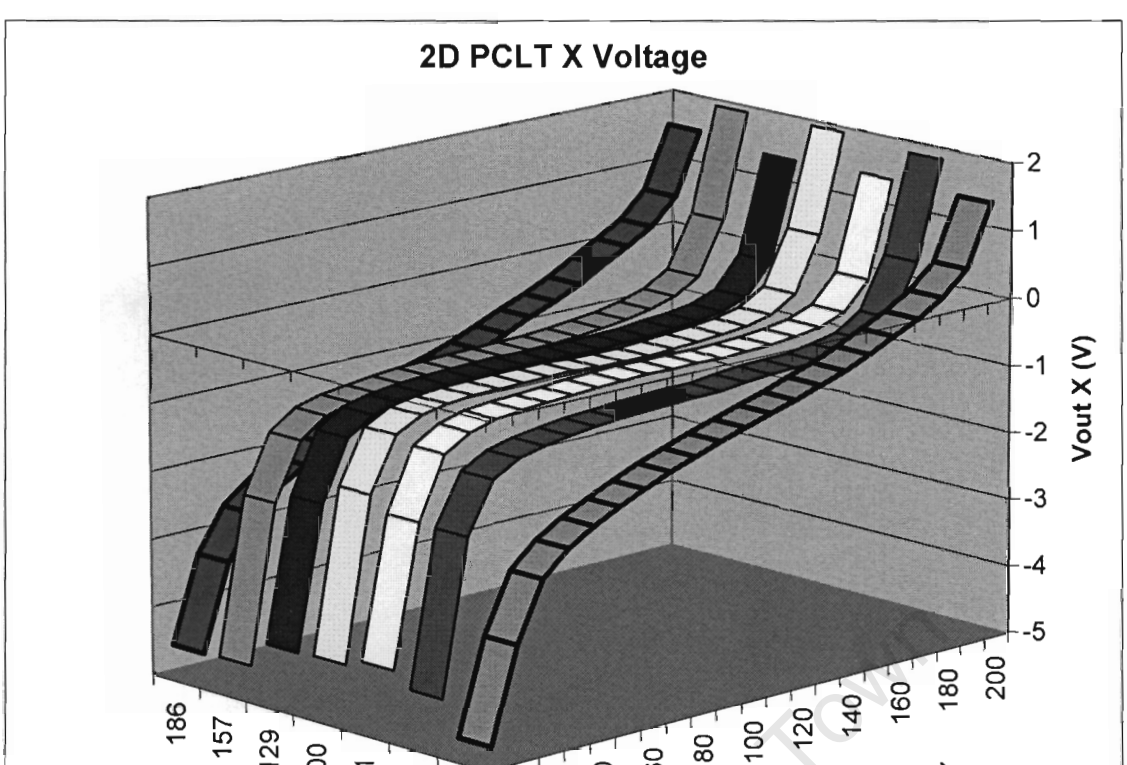

Figure 83 3D plot of the x voltage for all seven runs. Runs A (at y co-ordinate 14mm) and G (at y co-ordinate 186mm) show the largest sensitivity, the other runs are almost equally flat.

Ideally, the y-voltage should remain constant over the entire run, and it does over most of the central region, but not when the core moves directly over the primary turns at the start and end of each run. At these points, the y-voltage either rises or drops, depending on which y co-ordinate the core is on. Figure 84 shows the y voltages superimposed in a 3D image.

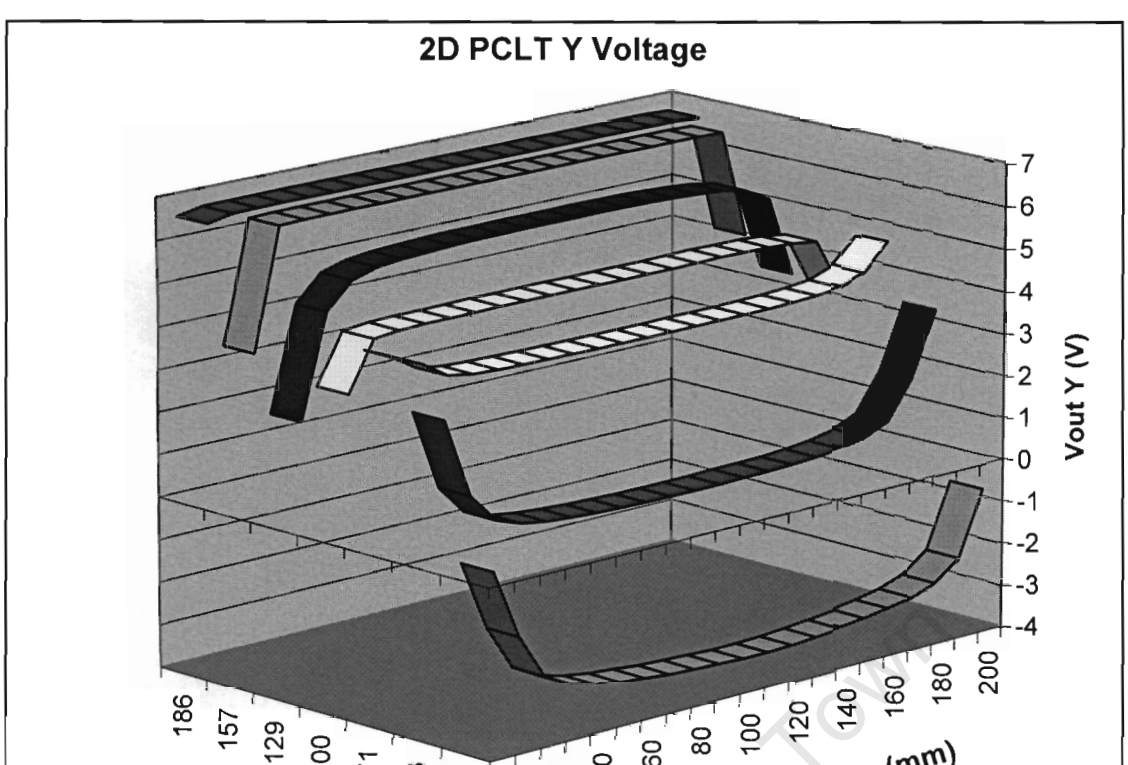

Figure 84 Plot of y voltages from all seven runs, showing good performance over the central region, but poor performance at the edges.

The level response of the y-voltage lines over the central region indicate that the y voltage remains constant with the unchanging y co-ordinate of the core, even though the x co-ordinate of the core is changing, which is the desired response from the sensor. However, as the core approaches the edges of the sensor, the y voltages are adversely affected.

B.7 Conclusions and Recommendations for the 2D PCLT

The large magnetic field dead-zone over the central region of the sensor area seriously impairs the sensor performance. A 'pancake' type spiral primary coil with windings reaching all the way to the center could be used to get an even distribution of

magnetic field over the entire detection area, and thus the sensitivity in the central area.

The large phase change of the secondary signals with core position change makes synchronous demodulation unsuitable for signal conditioning. Passive (rectifier) demodulation is phase insensitive, and is thus more suited for the signal conditioning of the 2D PCLT.

Combining all of the layers onto a single multilayered PCB should improve sensor stability and robustness, in a similar way that it did the case of the 1D PCLT.